Ph.D. in Physics - XXXIII$^{\text{rd}}$ Cycle

Ph.D. Thesis

Spin Hall effect and charge-to-spin conversion in graphene with proximity-spin-orbit coupling: the quasi-classical Green's function approach

Ph.D. candidate: Carmen Monaco

Adviser: prof. Roberto Raimondi

Declaration

I declare that this thesis is a presentation of original work and I am the author. My tutor Prof. Roberto Raimondi is the supervisor of the work of this thesis and contributed to it. This work has not previously been presented for an award at this, or any other, University. Furthermore, part of the work reported in this thesis has been used to write an article draft for publication, currently in the final stage of processing.

From Chapter 6, we are working on the following paper

- *Spin Hall Effect and spin-to-charge conversion in graphene with proximity-spin-orbit coupling: a quasi-classical Green's function approach.*

The last part of my research on the two-band regime (Chapter 7) could be also used to writing another paper. The innovative manipulation to bypass the problem of the quasiclassical Green's function definition is an interesting result. Furthermore, thanks to it we are able to include all vertex corrections to the physical response.

Contents

List of Figures **vii**

List of Tables **xiii**

Nomenclature **xv**

1 Introduction **1**

- 1.1 Spin-orbit phenomena 1
  - 1.1.1 Spintronics 1
  - 1.1.2 Origin of spin-orbit coupling 3
  - 1.1.3 Nonequilibrium effects 4
    - 1.1.3.1 The spin Hall effect 4
    - 1.1.3.2 The extrinsic spin Hall effect 8
    - 1.1.3.3 The Edelstein effect 10
    - 1.1.3.4 Other spin-orbit effects 13
- 1.2 2D material-based spintronics 14
  - 1.2.1 The advent of 2D materials 14
  - 1.2.2 Suitability of 2D materials for spintronics and van der Waals heterostructures 14
- 1.3 Graphene-based spintronics 15
  - 1.3.1 Spintronics with Dirac quasiparticles 15
  - 1.3.2 Enhancing spin-orbit coupling in carbon layers 19
- 1.4 Summary and outline 20
  - 1.4.1 Structure of this thesis 23

2 Theoretical tools **25**

- Overview 25
- 2.1 Semiclassical formalism 26

2.1.1 The 2D Boltzmann equation 26
2.2 Full quantum mechanical formalism 29
2.2.1 Kubo linear response theory 29
2.3 Out of equilibrium formalism 31
2.3.1 The Keldysh technique 31
2.3.2 Quasiclassical approximation 36

3 The 2D material Hamiltonian 41
Overview 41
3.1 The minimal clean Dirac-Rashba model 42
3.2 The generalised clean Dirac-Rashba model 47
Conclusions 50

4 The first steps: from Dirac fermions to graphene 51
Overview 51
4.1 The kinetic equations for Dirac fermions 52
4.1.1 The linearized BTE 53
4.1.2 The Eilenberger equation 55
4.2 Dirac-Rashba model with the density matrix 56
4.2.1 About the spin Hall conductivity 59
Conclusions 61

5 The disorder effects 63
Overview 63
5.1 The T-matrix approach 64
5.1.1 The detailed balance 66
5.2 The Born approximation 69
5.3 The one-band regime 70
Conclusions 75

6 Beyond the Born approximation and the skew-scattering mechanism 77
Overview 77
6.1 The skew-scattering mechanism 78
6.2 The kinetic equation for spin-valley Hamiltonian 79
6.3 The physical observables 81
Conclusions 86

7 The two-band regime **87**
Overview 87
7.1 The clean case 88
7.1.1 The density matrix evaluation 89
7.1.2 The quasiclassical Green's function evaluation 91
7.2 The disorder effect 93
7.2.1 About the ladder diagrams 97
Conclusion 99

Conclusions **101**

Appendix A The Dirac equation and the SOC **105**

Appendix B The Tight-Binding Low-Energy Model of Graphene **107**

Appendix C Symmetry Point Group of Graphene **111**

Appendix D From the Kubo to the Streda formula **115**

Appendix E The diagrammatic evaluation of skew-scattering **119**

Appendix F Calculation details in the regime II **123**
F.1 On the clean case 123
F.2 The disorder case 125

Bibliography **129**

List of Figures

1.1 *Schematic illustration of electron transport in a multilayer for parallel and antiparallel magnetisation of the successive ferromagnetic layers. The magnetization directions are indicated by the arrows. The solid lines are individual electron trajectories within the two spin channels. It is assumed that the mean free path is much longer than the layer thicknesses and the net electric current flows in the plane of the layers. Bottom panels show the resistor network within the two-current series resistor model. For the parallel-aligned multilayer, the up-spin electrons pass through the structure almost without scattering, whereas the down-spin electrons are scattered strongly within both ferromagnetic layers. Since conduction occurs in parallel for the two spin channels, the total resistivity of the multilayer is low. For the antiparallel-aligned multilayer, both the up-spin and down- spin electrons are scattered strongly within one of the ferromagnetic layers, and the total resistivity of the multilayer is high. Ref.[8].* 2

1.2 *Spin–orbit torque (SOT) as methods to exchange angular momentum between different elements. In a SOT configuration, the initial beam of electrons acquires spin angular momentum by passing through a material with SOC, therefore without the need of magnetization. After having gone through a normal metal (NM), spins exert a torque T on FM_2, similarly to what happens in a STT device. Ref.[15].* 3

1.3 *The direct spin Hall effect. The gray layer is a two-dimensional electron (hole) gas 2DEG (2DHG), to which an in-plane electric field is applied. Because of spin-orbit interaction in the system, spin-up and spin-down fermions are deflected in opposite directions, creating a pure spin current in the direction orthogonal to the driving field. Spin accumulation at the boundaries of the sample is the quantity usually observed in experiments and taken as a signature of the effect.* 5

1.4 *The ISGE due to the spin-momentum locking produced by the Rashba pseudomagnetic field (a.1), an out-of-equilibrium spin polarisation establishes orthogonally to the applied electric field* $\mathbf{E} = \mathcal{E}\hat{x}$*; the distorted Fermi surface is represented in (a.2) by the shaded circle. (b) Such a spin-current coupling cannot occur under preserved* $z \longrightarrow -z$ *symmetry conditions, since spin density and charge current transform differently under out-of-plane mirror reflection, the former (latter) being a axial (polar) vector. Breaking of this symmetry is hence required to have the ISGE.* 11

1.5 *a) Edge states in a 2D topological insulator (b) Schematics of the band structure of a 3D topological insulator with surface states within the band gap. Spin-splitted surface states exist due to the surface topology, independently from the Rashba effect. Topological insulators, indeed, display a spin-splitted linear dispersion relation on their surfaces (i.e. spin-polarized Dirac cones), while having a band gap in the bulk (this is why these materials are called insulators). Also in this case, spin and momentum are locked and, when a charge current flows in these spin-polarized surface states, a spin accumulation is produced and this effect is called Edelstein effect. A 2D charge-to-spin conversion mechanism occurs. Ref.[40].* 12

1.6 *A spin skyrmion. The spin texture is such that inversion of the out-of-plane component is realised by varying some parameter, e.g. the position (real-space skyrmion) or the momentum (momentum- space skyrmion).* 13

1.7 *By vertically stacking 2D materials with different properties, one can potentially obtain new platforms with enhanced properties. This Lego-like approach goes under the name of vdW epitaxy. The figure is taken from Ref.[69]* 16

1.8 *(a) The honeycomb lattice of graphene, with interpenetrating Bravais triangular sublattices A, B, respectively in red and blue. The first Brillouin zone is shown in dashed, with inequivalent corners* K, K'*. To describe electron dynamics in this particular crystal environment one adopts a massless Dirac 2D Hamiltonian. Carriers have here a spin-like DOF (pseudospin), stemming from the presence of two sublattices, which can be either parallel or antiparallel to the momentum vector, giving then a chiral characters to Dirac fermions (b). (c) The associated low-energy dispersion is linear, with two zero-energy points at the corners of the Brillouin zone* K, K'*. Carriers with positive energy at* K (K') *have positive (negative) chirality, conversely for negative. The chirality of Dirac particles is also responsible for the acquisition of a nonzero Berry phase upon adiabatic loops around the Dirac points, which might result in nontrivial topological phases when a bandgap is opened in the spectrum.* 17

1.9 *Transition metal dichalcogenides. a) A 3D visualisation of typical* MX_2 *layered compounds. b) Due to the structural inversion asymmetry, TMDs display spin-split bands at* K K' *points, with a large* $(0.1 - 0.5)eV$ *band gap. Time reversal symmetry guarantees that the spin polarisation is reversed at opposite valley, allowing selective spin excitation to the conduction bands by circularly polarised light (circular dichroism.)* 19

2.1 *The Keldysh contour in the complex* t*-plane. It starts at* $t = 0$*, proceeds to* $t = \infty$*, and then returns to* $t = 0$. 33

3.1 *Point-group symmetries of the honeycomb lattice. a) The bare hexagonal plaquette is characterised by the* D_{6h} *point symmetry group. b) Breaking of inversion symmetry about the 2D plane (e.g. by application of perpendicular electric field, or a substrate) reduces the point symmetry group* $D_{6h} \longrightarrow C_{6v}$*. c) If the sublattice symmetry is also broken, the symmetry group is further reduced* $C_{6v} \longrightarrow C_{3v}$*. The latter model is representative of graphene/TMD system we are interested in. Figure adapted from Ref.[5]* 42

3.2 *a) Energy dispersion of the Dirac-Rashba model around the* $\mathcal{K}$ *point. The splitting of the Dirac bands leads to a spin gap or* $pseudogap$ *of width* 2λ*. b) Tangential winding of the spin texture in regimes I and II.* 44

3.3 Energy bands and spin texture in systems with spin-valley coupling. As result a gap is opened and the Dirac spectrum at the Fermi energy, is splitted into 3 branches: regions I, II and III. For visualisation purposes, the bands are plotted along k_x (spins lie only in the yz plane). 49

4.1 Schematic diagram of the band structure and spin orientation for massive Dirac fermions. The presence of a massive term opens a gap between the valence and the conduction band. 53

5.1 Diagrammatic representation of the disordered Green's function and of self energy. In the first line, the disorder-average Green's function (blue arrow), which can be represented as a function of the self-energy Σ. The other lines contains the Gaussian and the T-matrix approximation respectively. In the first case one only consider the "triangle diagram" Σ_G with an impurity density cross n_i (red cross). While in the second one all diagrams to all powers in the scattering potential u_0 (dashed legs with dots) but with one impurity density insertion are taken into account. 65

6.1 Numerical color plots of a) $\tau_{\parallel}^{-1}$ and b) $\tau_{\perp}^{-1}$ as function of SOC variables in units of τ and skew-scattering coupling g_{ss}. The parallel component becomes more relevant for high values of SOC, while the perpendicular one increases with λ_{sv} for small values of the Rahsba one. In particular, the numerical results show an order of magnitude difference between the two rates. For both plots $\varepsilon\tau = 10$ with $\varepsilon = 1$. Furthermore, the Rashba and spin-valley parameters are in units of the Fermi energy. 81

6.2 Numerical color plots of the effective vertices for a) the charge, b) inverse-spin galvanic and c) spin Hall response. The plots show the coefficients of $\cos(\theta)$ and $\sin(\theta)$ in the Eqs.(6.14)-(6.16). The vertex $\overline{V}_{eff}$ decreases slowly and linearly with the spin-valley and Rashba variables. While $\overline{S}_{y,eff}$ and $\overline{J}^{z}_{y,eff}$ show a quite complementary behaviour in terms of the SOC values. For all the plots we fix $\varepsilon\tau = 10$ with $\varepsilon = 1$. Furthermore, the Rashba and spin-valley parameters are in units of the Fermi energy. 83

6.3 Numerical color plots show the behaviour of physical observables for the spin-valley and Dirac Rashba graphene system in regime II: a) the Spin Hall response increases slowly with the spin-valley coupling at small values of the Rahsba one; while b) the Edelstein effect becomes relevant for small values of SOC. For both graphs we fix $g^0_{ss} = 0.1$ and $\varepsilon = 1$ with $\varepsilon\tau = 10$. Furthermore, the Rashba and spin-valley parameters are in units of the Fermi energy. 84

6.4 SHE color plots for different values of the skew-scattering coupling $g^0_{ss} = n$ with $n = 1, ..6$. The spin Hall response is significant for high values of spin-valley coupling when the skew-scattering is small. On the contrary, when g^0_{ss} becomes high, the effect starts to be relevant also for small values of SOC. For all the graphs $\varepsilon\tau = 10$ with $\varepsilon = 1$. Furthermore, the Rashba and spin valley parameters in units of the Fermi energy. 85

B.1 *Lattice structure and band dispersion of bare graphene. (a) The honeycomb structure with penetrating inequivalent Bravais lattices made up of A, B carbon atoms (red and blue respectively) with lattice vectors* a_1 *and* a_2*. (b) In reciprocal space, two inequivalent corners* K, K' *appear, with the low-energy physics of this material being descried by excitations around those points. The Brillouin zone of graphene has the highest symmetry point* Γ*. (c) Visualisation of graphene band structure, where the linear dispersion (Dirac cone) in the vicinity of* K, K' *can be recognised. Ref.[15, 81].* 108

C.1 *Equation for the vertex renormalization. The empty dot represents the bare vertex while the black dots represent the scattering potential insertions. Ref.[127, 128].* 112

List of Tables

3.1 Clifford's algebra decomposition of projectors with $\hat{k}$ and $\hat{\theta}$ versor. A factor $1/4$ in front is omitted for the sake of simplicity. The columns represent the operators that appear in the Clifford's algebra decomposition. It is evident that all the columns sum up to zero except the one for the identity $\sigma_0 \otimes s_0$. . 46
3.2 Clifford's algebra decomposition of averaged projectors. Of course, also in this case, all the columns sum up to zero except the one for the identity $\sigma_0 \otimes s_0$. 47

5.1 Clifford's algebra decomposition of the retarded self-energy for all the bands in units of $-i/(4\tau) = -i\varepsilon u_0^2/4$. Σ_3 is the expression of the self-energy in the regime I reported in the Eq.(5.24), while the sum $\Sigma_3 + \Sigma_4$ is the regime II one given by the Eq.(5.23). 70

C.1 Symmetry operations of all the elements of Clifford's algebra. Four groups of four matrices transform in the same way, i.e. with same sign, under reflection transformation over $\hat{x}$ and $\hat{y}$ axis. 113

Nomenclature

$2DEG$	Two-dimensional electron gas
AHE	Anomalous Hall effect
BA	Born approximation
BSE	Bethe-Salpeter equation
BTE	Boltzmann transport equation
CSC	Charge-to-spin conversion
DOF	Degrees of freedom
DP	Dyakonov-Perel
DR	Dirac-Rashba
EE	Edelstein effect
FQM	Fully quantum mechanical
GMR	Giant magnetoresistance
$ISGE$	Inverse spin-galvanic effect
$ISHE$	Inverse spin Hall effect
LHS	Left-hand side
MEC	Magnetic exchange coupling
$NEGF$	Non-equilibrium Green's function
R/A	Retarded/Advanced

RHS	Right-hand side
SC	Semiclassical
$SCBA$	Self-consistent Born approximation
SGE	Spin-galvanic effect
SHE	Spin Hall effect
SOC	Spin-orbit coupling
SOT	Spin-orbit torque
SRT	Spin-relaxation time
STT	Spin-transfer torque
TB	Tight-binding
TI	Topological insulator
TMD	Transition metal dichalcogenide
WI	Ward identity
vdW	van der Waals

1

Introduction

1.1 Spin-orbit phenomena

1.1.1 Spintronics

Until forty years ago, the functionality of semiconductor devices relied only on the control of the electronic charge, whereas the spin degrees of freedom (DOF) of carriers did not play any role, and was not being utilized in any way. Recently, a technology has emerged called spintronics (spin transport electronics or spin-based electronics), which is centered on the manipulation of spin degrees of freedom in solid state systems [1–5]. One of the most important aims is to understand the relationship between the charge and the spin DOF. A good knowledge of this relationship provides the opportunity for a new generation of devices, combining standard electronic conduction with spin-dependent effects that arise from the interaction between the spin of the carriers and the magnetic properties of the material. The electrical control of spin population could be exploited by two different mechanisms, ferromagnetic interaction and spin-orbit coupling (SOC). Originally, the idea of spin-based electronic devices was based on ferromagnetic materials, used to inject a spin current in paramagnetic materials. One of the most studied effects caused by this type of injection is the famous giant magnetoresistance effect also known as GMR effect [6, 7]. The GMR [see Fig.1.1] is observed in hybrid thin-film materials composed of alternating ferromagnetic and nonmagnetic layers. The resistance of the system is lowest when the magnetic moments in ferromagnetic layers are aligned and highest when they are anti-aligned.

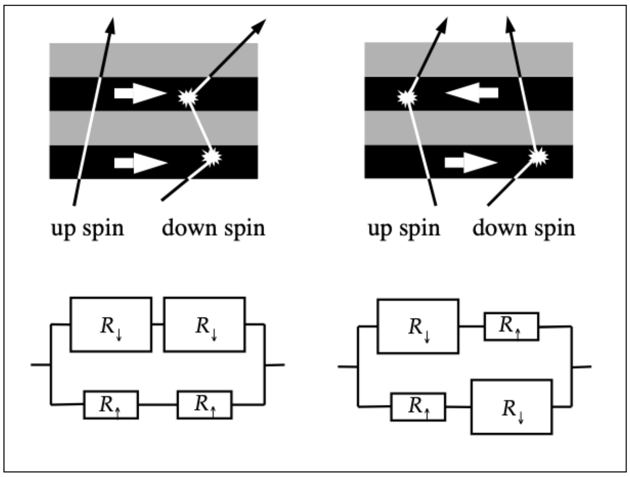

Figure 1.1: *Schematic illustration of electron transport in a multilayer for parallel and antiparallel magnetisation of the successive ferromagnetic layers. The magnetization directions are indicated by the arrows. The solid lines are individual electron trajectories within the two spin channels. It is assumed that the mean free path is much longer than the layer thicknesses and the net electric current flows in the plane of the layers. Bottom panels show the resistor network within the two-current series resistor model. For the parallel-aligned multilayer, the up-spin electrons pass through the structure almost without scattering, whereas the down-spin electrons are scattered strongly within both ferromagnetic layers. Since conduction occurs in parallel for the two spin channels, the total resistivity of the multilayer is low. For the antiparallel-aligned multilayer, both the up-spin and down-spin electrons are scattered strongly within one of the ferromagnetic layers, and the total resistivity of the multilayer is high. Ref.[8].*

The GMR effect is probably the best known spintronics effect, since its huge applications in hard disk storage led Albert Fert and Peter Grünberg to win the Nobel prize in 2007. Beside in its name, which was coined in the late nineties, the field is "new" mainly in the sense of its approach to the solid state problems it tackles, as it tries to establish novel connections between magnetism, superconductivity, the physics of semiconductors, information theory, optics, mesoscopic physics, electrical engineering. Typical spintronics issues are

1. how to polarize a system, be it a single object or an ensemble of many;
2. how to keep it in the desired spin configuration longer than the time required by device to make use of the information so encoded;
3. how to possibly transport such information across a device and, finally, accurately read it.

The principal advantage of promoting the spin DOF as the main carrier of information resides in its $non\text{-}volatile$ nature. For instance, non-volatile magnetic memories based on magnetic tunnel junctions, exploiting the spin-transfer torque (STT) effects, have offered lower power consumption and new paradigms for storage devices [9–12]. In a STT, an initially unpolarised

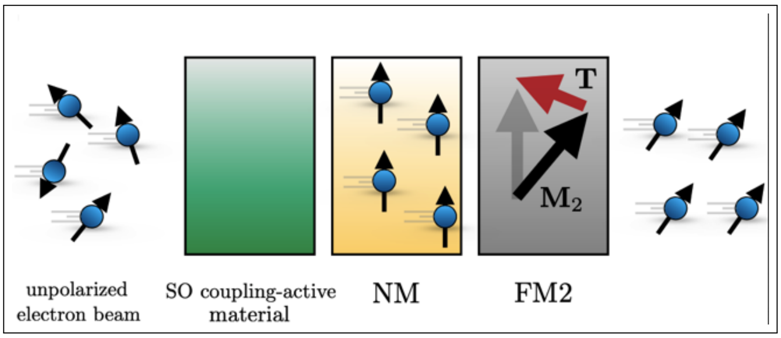

Figure 1.2: *Spin–orbit torque (SOT) as methods to exchange angular momentum between different elements. In a SOT configuration, the initial beam of electrons acquires spin angular momentum by passing through a material with SOC, therefore without the need of magnetization. After having gone through a normal metal (NM), spins exert a torque T on FM_2, similarly to what happens in a STT device. Ref.[15].*

electron beam is sent through a first ferromagnet with a certain magnetisation, where spins get polarised. After having gone through a normal metal, electrons with fixed spin polarisation pass through a second ferromagnet with a different magnetisation (not parallel to the first one). This results in the exertion of a "torque" on the second ferromagnet. The spin-orbit torque (SOT) is another important mechanism. In this case the initial beam of electrons acquires spin angular momentum by passing through a material with SOC (without magnetization). Successively spins exert a torque on a second ferromagnet, similarly to what happens in a STT device [see Fig.1.2]. The major limitation of these approaches is represented by their energy cost: typically for a single operation in a STT device, the required energy can potentially delete any non-volatile character of the spin DOF [13, 14]. In spintronics devices, information is encoded into the orientation of a collection of spins, this having being fixed at a local minimum in the energy landscape. Leakage of information would be represented by a change in this particular configuration [14]. In the present thesis we are interested in the study of spin transport electronic effects in graphene heterostructures, where the coupling between charge and spin degrees of freedom is due to the SOC. In the following we will see that in electronic devices this interaction allows us to control the spin current and spin polarization responses through an external electric field. In the next section, we start from the origin of SOC.

1.1.2 Origin of spin-orbit coupling

In atoms, the spin-orbit coupling is a $relativistic$ correction to the electrons' energy levels of atomic spectra. To illustrate its origin however, it suffices to adopt semiclassical (SC) electrodynamics and non-relativistic quantum mechanics arguments (see Appendix A for details). The spin-orbit interaction can be expressed

$$H_{SOC} = \frac{e\lambda_0^2}{4}\Big(\boldsymbol{\sigma} \times \nabla V(\mathbf{x})\Big) \cdot (-i\nabla), \tag{1.1}$$

with $\mathbf{k} = -i\hbar\nabla$ the momentum, $eV(\mathbf{x})$ a static electric field and $\boldsymbol{\sigma}$ the Pauli matrices linked to the electron spin $\boldsymbol{\sigma} = 2\mathrm{S}/\hbar$. Here $\lambda_0 = \hbar/(mc) \simeq 10^{-10}cm$ is the Compton wave length in a vacuum, which is very small compared with the characteristic lengths in solids. However, when considering the spin-orbit interaction in solids one must take into account that an effective Compton wave length λ may appear [16, 17]. In some cases this brings a big enhancement of the strength of the spin-orbit interaction. For example, in GaAs the effective Compton wave length λ is about three orders of magnitude larger than the vacuum value λ_0. In atoms, the potential eV in the Eq.(1.1) is the central field due to the nucleus and to the screening of electrons and the SOC term gives rise to the fine structure of the atomic spectra. In solids, the Eq.(1.1) applies to all potentials acting on the electrons. In this respect one may speak of different spin-orbit mechanisms depending on the origin of the potential. Those which, due to the potential from impurities and defects, break the translational symmetry of a periodic lattice, are called extrinsic mechanisms. On the other hand, those mechanisms arising from the potential of the host lattice or from the confining potential determining an electronic device, as in the case of a two-dimensional electron gas (2DEG), are called intrinsic. In the following, we discuss some effects out of equilibrium (spin Hall effect, etc) that define the observables which we are interested in for the rest of the work of this thesis.

1.1.3 Nonequilibrium effects

1.1.3.1 The spin Hall effect

The SOC manifests in materials via a category of effects allowing an efficient conversion between charge and spin signals. The most famous example is the spin Hall effect (SHE) [18–20]. It could allow for the manipulation of the spin DOF inside a device by means of electrical fields only. It is an eminent example of what Awschalom calls a “coherent spintronic property” [2], as opposed to the “non-coherent” ones on which older devices are based. Originally proposed in 2003 for a two-dimensional hole gas (2DHG) by Murakami et al. [21], and soon after for a two-dimensional electron gas by Sinova et al. [22], it has attracted much attention and is still being actively debated. In a spin analogy to its charge counterpart, i.e. the classical Hall effect [23], the SHE consists of a spin accumulation at the

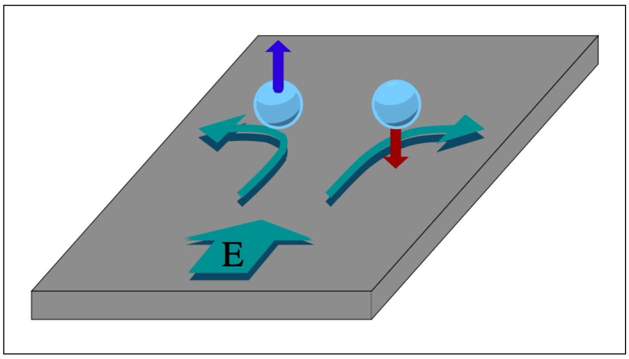

Figure 1.3: *The direct spin Hall effect. The gray layer is a two-dimensional electron (hole) gas 2DEG (2DHG), to which an in-plane electric field is applied. Because of spin-orbit interaction in the system, spin-up and spin-down fermions are deflected in opposite directions, creating a pure spin current in the direction orthogonal to the driving field. Spin accumulation at the boundaries of the sample is the quantity usually observed in experiments and taken as a signature of the effect.*

boundaries of a conductor, the “spin voltage” building up in the orthogonal direction [see Fig.1.3].

The SOC plays a similar role to the Lorentz field in the classical Hall effect, such that no magnetic field is required for the SHE to happen. In fact, similarly to Mott scattering in a vacuum [24], the "electron beam" is separated by the spin-orbit interaction present in the material into its spin components. Indeed this mechanism in normal metals was proposed by Dyakonov and Perel [18, 19] as a solid-state realisation of Mott scattering. The SHE was first measured in semiconductors, with the spin accumulation at the boundaries of the samples probed by optical means [25, 26]. Onsager reciprocity [27], allows also the inverse effect to exist, i.e. the conversion of a spin-polarised current into a charge voltage. Such inverse spin Hall effect (ISHE) was discovered in semiconductors and in metals shortly after the reports on the discovery of the SHE [28–30].

Now, we try to discuss briefly the spin-charge coupling in the diffusion equations. In a paramagnetic metal the diffusion equations for charge and spin are

$$\begin{aligned} j_i &= (-e)\mu n E_i - D\partial_i(-e)n, \\ j_{ij} &= \mu s_j E_i - D\partial_i s_j, \end{aligned} \tag{1.2}$$

where n is the total density, s_j the spin polarization measured in units such that the spin current j_{ij} has the same physical dimensions as the charge current. This means to multiply the usual s_j by $-e/\hbar$, $e > 0$ being the unit charge. In the Eq.(1.2), $\mu = -e\tau/m$ is the electron mobility, τ the spin conserving scattering time and m the effective electron mass. The spin-orbit interaction couples the spin and charge currents. The idea goes back to Mott [24] and yields a polarization of the diffused particles, assumed to be initially non polarized. Electrons transporting charge in a conductor undergo collisions with impurities and phonons and, as a result, there should be a coupling between charge and spin currents due to SOC. According to the theory of Dirac's equation, the spin-orbit interaction is given by the Eq.(1.1). Let us consider the Born approximation (BA), i.e. the lowest order scattering amplitude. This means that we take the matrix element of H_{SOC} between an initial plane wave with momentum $\mathbf{k}$ and a final wave with momentum $\mathbf{k}'$. We obtain

$$\langle \mathbf{k}|H_{SOC}|\mathbf{k}'\rangle = -i\frac{\lambda_0^2}{4}V(\mathbf{k}-\mathbf{k}')\mathbf{k}\times\mathbf{k}'\cdot\boldsymbol{\sigma}, \tag{1.3}$$

where $V(\mathbf{q}) = V(\mathbf{k}-\mathbf{k}')$ is the Fourier transform of $V(\mathbf{x})$. According to the above equation, the scattering amplitude reads

$$f = V(\mathbf{q})\left[1 - i\frac{\lambda_0^2}{4}\mathbf{k}\times\mathbf{k}'\cdot\boldsymbol{\sigma}\right], \tag{1.4}$$

where the first term represents the ordinary scattering. In general, beyond the Born approximation, we have

$$f = A + B\hat{\mathbf{k}}\times\hat{\mathbf{k}}'\cdot\boldsymbol{\sigma}. \tag{1.5}$$

The scattering probability is given by the amplitude square, i.e.

$$\mathcal{P} = |f^2| = |A|^2 + |B|^2 + 2Re(AB^*)\hat{\mathbf{k}}\times\hat{\mathbf{k}}'\cdot\boldsymbol{\sigma}, \tag{1.6}$$

where the last term is responsible for spin asymmetry in the scattering processes. If $Re(AB^*) \neq 0$, the skew-scattering mechanism appears (in the Section 1.1.3.2 we discuss in details the extrinsic effects). On the contrary, in the Born approximation one has $A = V(\mathbf{q})$ and $B = -i\frac{\lambda_0^2 k^2}{4}A$, so that $Re(AB^*) = 0$. The effect of the spin-orbit interaction in a conductor is more complicated then the process of a single scattering. First of all, one has to take into account multiple scattering which is responsible for the diffusive motion. Second, the source of SOC are due to different mechanisms. From a phenomenological point of view, we can consider electrons with an initial direction along the positive $x-$axis. We assume that spin up electrons are deflected along the positive $y-$axis, while the opposite occurs for down spin particles. In terms of currents we have

$$\delta j_{y\uparrow} = \eta j_{x\uparrow}, \qquad \delta j_{y\downarrow} = -\eta j_{x\downarrow}, \tag{1.7}$$

where η is a dimensionless parameter depending on the spin-orbit interaction. The spin-current in the $y-$direction reads

$$\delta(j_{y\uparrow} - j_{y\downarrow}) = \eta(\eta j_{x\uparrow} + \eta j_{x\downarrow}), \tag{1.8}$$

while the charge current in the $y-$direction is

$$\delta(j_{y\uparrow} + j_{y\downarrow}) = \eta(\eta j_{x\uparrow} - \eta j_{x\downarrow}). \tag{1.9}$$

Hence, a charge current along $x-$axis generates a transverse spin current along the $y-$axis, while a spin current along the $x-$axis generates a transverse charge current along $y-$axis. The first case is referred to as the SHE, while in the second case one speaks of the (ISHE) or anomalous Hall effect (AHE) depending on the nature of the spin current. If the latter has been originated by spin injection in a paramagnetic system, one deals with a pure spin current, i.e. a spin current in the absence on a charge current. This is the ISHE. If instead the spin current is due to a difference in spin population as in a ferromagnet, this is the AHE. In this latter case the driving spin current goes along with a driving charge current. Hence, one has a transverse charge current in response to a longitudinal charge current independent of the magnitude of the magnetic field. To make a contact with the Eq.(1.2), we rewrite the Eqs.(1.8) and (1.9) as

$$\delta j_{yz} = \eta j_x, \qquad \delta j_y = \eta j_x. \tag{1.10}$$

Hence the parameter η couples charge currents labelled by one index, the coordinate axis along which the current flowing, with spin currents labelled by two indices, indicating the flowing direction and the polarization axis. For arbitrary direction the coupling contain the Ricci tensor ε_{ijk}, i.e.

$$\delta j_{ij} = \varepsilon_{ijk}\eta j_k, \qquad \delta j_y = -\varepsilon_{ijk}\eta j_{jk}. \tag{1.11}$$

One can write the coupled equations for the currents as

$$\begin{aligned} j_i &= (-e)\mu n E_i - D\partial_i(-e)n - \varepsilon_{ijk}\eta j^0_{jk}, \\ j_{ij} &= \mu s_j E_i - D\partial_i s_j + \varepsilon_{ijk}\eta j^0_k, \end{aligned} \tag{1.12}$$

where the superscript 0 indicates the expression in the absence of η. The minus sign difference between the two above equations agrees with the general requirements due to the Onsager relations [27], based on the properties of the charge and spin currents under time reversal. We notice that, while the charge current is odd, the spin current is even under time reversal, since both spin polarization and velocity change sign. The Eqs.(1.12) must be used with the continuity equations for charge and spin that read

$$\partial_t \rho + \partial_i j_i = 0 \qquad \partial_t s_i + \partial_j j_{ji} + \frac{s_i}{\tau_s} = 0, \tag{1.13}$$

where τ_s is a phenomenologically introduced spin relaxation time, since spin conservation is not a general property in contrast with charge conservation. Let us now assume a paramagnetic conductor and imagine applying a uniform and constant electric field E_x along $x-$axis. Since in the absence of the electric field there is no spin polarization $s_i = 0$, to linear order in the field one has

$$j_{yz} = \eta j_x^0 = \eta \sigma E_x \equiv \sigma^{sH} E_x, \tag{1.14}$$

where σ^{sH} is called the spin Hall (SH) conductivity and the transverse spin current along the $y-$axis induced by the the electric field constitutes the spin Hall effect. In the following we discuss other spin-orbit effects, such as skew-scattering and side-jump mechanism.

1.1.3.2 The extrinsic spin Hall effect

In the previous section, we have discussed the SHE in a phenomenological way by assuming a coupling between the charge and spin currents in the diffusion equations. Here we want to analyze the microscopic mechanisms for the SHE. We focus on mechanisms based on the extrinsic spin-orbit coupling, i.e. that originating from the potential impurities and defects. This SOC gives rise to two different types of mechanisms: the skew-scattering and the side-jump. The first one is important for our work because in the Chapter 6 we go beyond the Born approximation and study the skew-scattering in a specific graphene-Hamiltonian.

The skew-scattering Here we report a short discussion about the skew-scattering mechanism, we suggest the reader to see other literature for more details [31, 32]. The idea goes back to Mott [24] and we start from the scattering probability Eq.(1.6). To take into account the skew-scattering mechanism, we must have $Re(AB^*) \neq 0$. Particles with spin parallel to $\hat{\mathbf{k}} \times \hat{\mathbf{k}}'$ are deflected by angle θ (depending on the transferred momentum $(\hat{\mathbf{k}} - \hat{\mathbf{k}}')$), while those with spin antiparallel by an angle $\pi + \theta$. Here, as a model, we consider a disordered Fermi gas with spin-orbit interaction as

$$H = \frac{\mathbf{k}^2}{2m} + V(\mathbf{x}) - \frac{\lambda_0^2}{4} \boldsymbol{\sigma} \times \nabla V(\mathbf{x}) \cdot \mathbf{k}. \tag{1.15}$$

As already mentioned, to have a finite skew-scattering, the scattering amplitude at the Born level Eq.(1.4) is not sufficient. We need to compute the scattering probability beyond the Born approximation. Since, the spin-orbit coupling λ_0^2 can be treated perturbatively, the spin-dependent amplitude B will be considered at the level of the Born approximation, whereas we consider higher order correction for the spin-independent amplitude. To this end, solving the Schrödinger equation, one can consider the solution at second order in the potential $V(\mathbf{x}) = u_0\delta(\mathbf{x})$ (i.e. a potential for a single impurity located at the origin of the coordinates) [17, 33]. So, the spin-independent scattering amplitude can be written in the form

$$A = -\frac{m}{2\pi}u_0(1+u_0G(0)), \tag{1.16}$$

where $G(0)$ is the Green's function associated to the Schrödinger equation in the absence of potential at $\mathbf{x} = 0$. In the scattering probability we need $Re(AB^*)$. Since B is purely imaginary, we have to consider

$$\delta A = -i\frac{m}{2\pi}u_0^2 ImG(0). \tag{1.17}$$

In this way, one can evaluate the correction to the scattering rate and uses it in the Boltzmann equation (BE) (see Chapter 2). This new term modifies the kernel of the kinetic equation and the spin current can be expressed in terms of the charge current as

$$\frac{j_{ia}}{\tau} = -\varepsilon_{ija}\mathcal{W}_a(\mathbf{k},\mathbf{k}')p_i^2 j_j, \tag{1.18}$$

where $\mathcal{W}$ is the kernel of the equation, j_i the charge current along $i-$direction while a is the spin polarization. We underline that the parameter η can be defined phenomenologically and is $\eta \propto -\lambda_0^2 k_F^2$, with k_F the momentum at the Fermi energy.

The side-jump We briefly discuss the origin of the side-jump mechanism. To understand it, let us consider the equation of motion at a semiclassical level

$$\begin{aligned} \dot{\mathbf{x}} &= \frac{\mathbf{k}}{m} - \frac{\lambda_0^2}{\boldsymbol{\sigma}} \times \nabla V(\mathbf{x}), \\ \dot{\mathbf{k}} &= -\nabla V(\mathbf{x}) + \frac{\lambda_0^2}{4}(\boldsymbol{\sigma} \times \mathbf{k} \cdot \nabla)\nabla V(\mathbf{x}). \end{aligned} \tag{1.19}$$

To first order in λ_0^2, the equation for $\mathbf{x}$ becomes

$$\dot{\mathbf{x}} = \frac{\mathbf{k}}{m} - \frac{\lambda_0^2}{\boldsymbol{\sigma}} \times \dot{\mathbf{k}}. \tag{1.20}$$

Integrating over time from $-\infty$ to $+\infty$ (before the scattering and after the scattering), the trajectory acquires an extra contribution proportional to the transferred momentum upon the scattering in the form

$$\delta\mathbf{x} = \frac{\lambda_0^2}{4}\boldsymbol{\sigma} \times \delta\mathbf{k}. \tag{1.21}$$

This $\delta\mathbf{x}$ is the so-called side-jump effect and may affect the spin current. If at each scattering event there is a side jump, the total number of side-jumps per unit time has the dimensions of a velocity. Such a velocity depends on the spin state and this dependence gives rise ultimately to a spin current. The side-jump contribution to the spin current can be written quite generally as

$$j_{ia} = -\varepsilon_{iak}\mathcal{W}_a k_k, \tag{1.22}$$

where of course $\mathcal{W}$ is a different kernel respect to the skew-scattering case. Identically one can phenomenologically find the coupling η and obtain $\eta \propto -m\lambda_0^2/2\tau$. What explained until now is not the end of the story. When an electric field is present, the side-jump modifies the energy of the scattered particles. In fact, the generated dipole-like term yields a correction to the collision integral of kinetic equation. In this case the parameter $\eta \propto -m\lambda_0^2/4\tau$. We stress that, in contrast to what happens in the skew-scattering mechanism, the coefficient η in the side-jump depends on the inverse scattering time. This means that in high-mobility system tends to be small.

1.1.3.3 The Edelstein effect

Despite its historical significance, the SHE is not the only possible charge-to-spin conversion (CSC) mechanism induced by SOC effects. Broken structural inversion symmetry allows for the appearance of a current-induced spin polarisation, commonly known as inverse spin-galvanic effect (ISGE) [see Fig.1.4]. Originally proposed by Ivchenko and Pikus [34], and observed by Vorobev et al. in Te [35], the ISGE was later theoretically studied by Lyanda-Geller, Aronov and Edelstein (from which the name *Edelstein effect*) in a 2DEG with SOC of the Bychkov-Rashba type[1] [36, 37], whose Hamiltonian is (see Chapter 3 for a deeper discussion)

---

[1] For brevity, in the following we will adopt the common choice of referring to the 'Bychkov-Rashba interaction' as simply 'Rashba interaction'.

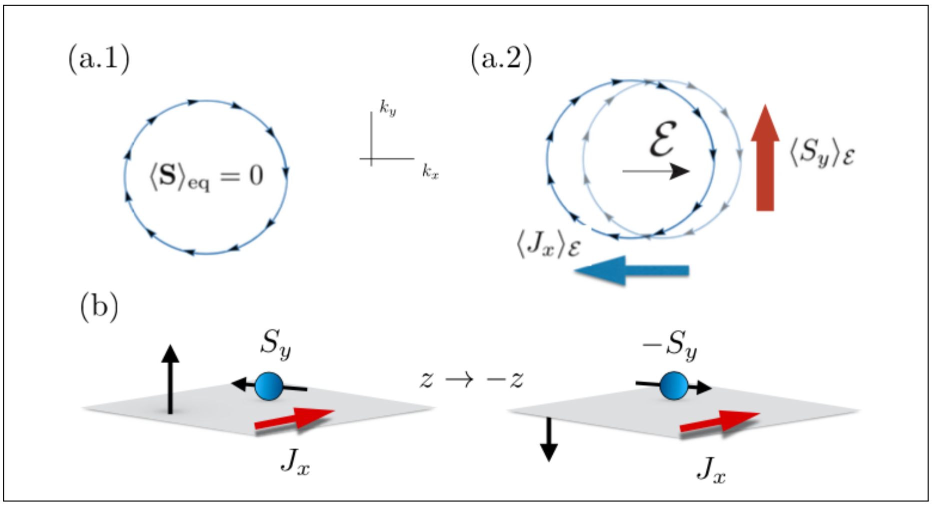
(a.1)
(a.2)
$\langle \mathbf{S} \rangle_{\text{eq}} = 0$
k_y
k_x
$\mathcal{E}$
$\langle S_y \rangle_{\mathcal{E}}$
$\langle J_x \rangle_{\mathcal{E}}$
(b)
S_y
$z \to -z$
$-S_y$
J_x
J_x

Figure 1.4: *The ISGE due to the spin-momentum locking produced by the Rashba pseudomagnetic field (a.1), an out-of-equilibrium spin polarisation establishes orthogonally to the applied electric field* $\mathbf{E} = \mathcal{E}\hat{x}$*; the distorted Fermi surface is represented in (a.2) by the shaded circle. (b) Such a spin-current coupling cannot occur under preserved* $z \longrightarrow -z$ *symmetry conditions, since spin density and charge current transform differently under out-of-plane mirror reflection, the former (latter) being a axial (polar) vector. Breaking of this symmetry is hence required to have the ISGE.*

$$H_0^{2DEG} = \frac{\mathbf{k}^2}{2m} + \lambda(\mathbf{k} \times \hat{z}) \cdot \boldsymbol{s}, \tag{1.23}$$

where $\boldsymbol{s} = (s_x, s_y)$ are Pauli matrices x, y acting on the spin DOF, m is the effective electron mass, and λ is the Rashba parameter. The spin-galvanic effect (SGE) has also been observed in GaAs semiconducting quantum wells [38].

The phenomenology of ISGE/SGE can be understood by symmetry arguments [39]. Electrical currents and spin polarisation are respectively polar and axial vectors. In centrosymmetric systems, where inversion symmetry is preserved, polar and axial vectors transform differently, hence no coupling between non-equilibrium spin density and charge current is allowed [see Fig.1.4(b)]. However, in reduced symmetry conditions, polar and axial vectors components may transform similarly. Consider, for instance, the case of electrons confined in the $x-y$ plane with mirror reflection about the $y-z$ plane ($\mathcal{R}_{yz}$) preserved but with broken $z \longrightarrow -z$ ($\mathcal{R}_{xy}$) symmetry–e.g. induced by the presence of a substrate. Under the vertical plane reflection $\mathcal{R}_{xy}$, the electrical current and spin polarisation transform as

$$\mathcal{R}_{xy} : J_x, J_y \longrightarrow -J_x, J_y, \tag{1.24}$$

$$\mathcal{R}_{xy} : S_x, S_y \longrightarrow S_x, -S_y. \tag{1.25}$$

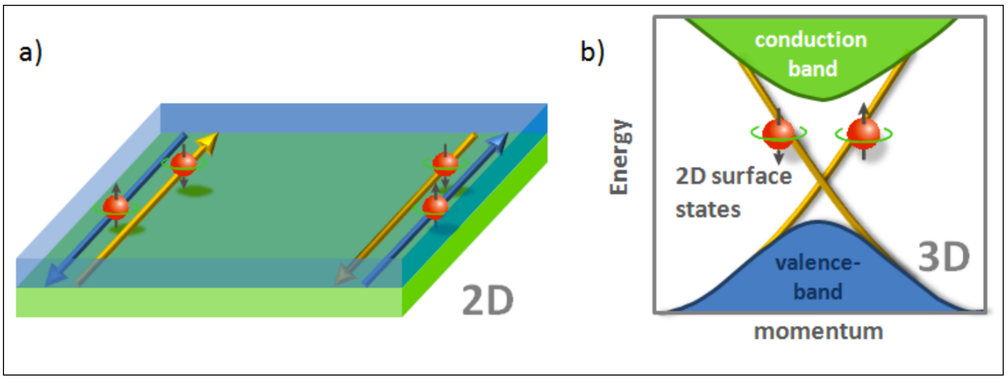

Figure 1.5: *a) Edge states in a 2D topological insulator (b) Schematics of the band structure of a 3D topological insulator with surface states within the band gap. Spin-splitted surface states exist due to the surface topology, independently from the Rashba effect. Topological insulators, indeed, display a spin-splitted linear dispersion relation on their surfaces (i.e. spin-polarized Dirac cones), while having a band gap in the bulk (this is why these materials are called insulators). Also in this case, spin and momentum are locked and, when a charge current flows in these spin-polarized surface states, a spin accumulation is produced and this effect is called Edelstein effect. A 2D charge-to-spin conversion mechanism occurs. Ref.[40].*

A coupling between $J_i - S_j$ with $i \perp j$ is therefore allowed for broken $\mathcal{R}_{xy}$ symmetry. Microscopically, such a coupling is mediated by the SOC.

The topological insulator (TI) case is easier to visualize due to the presence of a single Fermi contour, therefore the topological insulator case is discussed first [41, 42]. It is a material that behaves as an insulator in its interior but whose surface contains conducting states [43], meaning that electrons can only move along the surface of the material [see Fig.1.5(a)]. Topological insulators have non-trivial symmetry-protected topological order; however, having a conducting surface is not unique to topological insulators, since ordinary band insulators can also support conductive surface states [44–46]. What is special about topological insulators is that their surface states are symmetry-protected Dirac fermions by particle number conservation and time-reversal symmetry. In the bulk of a non-interacting topological insulator, the electronic band structure resembles an ordinary band insulator, with the Fermi level falling between the conduction and valence bands [see Fig.1.5(b)]. On the surface of a topological insulator there are special states that fall within the bulk energy gap and allow surface metallic conduction. To explain better, topological insulators display spin-split surface states where spin-momentum locking is present (as Rashba interaction in the 2DEG). Indeed, when a charge current flows in the surface states of the topological insulator this can also be seen as a well-defined momentum shift $\Delta\mathbf{k}$ in the reciprocal space, resulting in a different occupation of the spin-polarized branches of the Dirac cone. This unbalance, accordingly to the structure of the topological insulator band dispersion relation, produces a spin accumulation in the investigated material, i.e. a CSC conversion occurs.

The spin accumulation is orthogonal to the injected charge current, accordingly to the spin-momentum locking. Due to the fact that these materials display a conductive behaviour on their surface while being insulating on their bulk, the charge current is only allowed to flow on the topological insulator surfaces, this is the origin of the bidimensionality of this CSC mechanism.

1.1.3.4 Other spin-orbit effects

The interplay of SOC and magnetic exchange interactions is yet another research line attracting growing interest [47]. Ferromagnetic systems with broken inversion symmetry display a Dzyaloshinskii–Moriya interaction, i.e.

$$H_{DM} = \sum_{ij} \boldsymbol{D}_{ij} \cdot (\boldsymbol{S}_i \times \boldsymbol{S}_j), \tag{1.26}$$

where $\boldsymbol{D}_{ij}$ is the Dzyaloshinskii–Moriya coupling for spins in lattice sites i, j. According to the Eq.(1.26), the energy of two neighbouring spins $\boldsymbol{S}_1, \boldsymbol{S}_2$ decreases (increases) if the respective orientation are connected by a clockwise (anti-clockwise) rotation around the Dzyaloshinskii– Moriya vector [47, 48]. Such a term enables the formation of chiral spin structures, e.g. domain walls and magnetic skyrmions [48]. The latter are defined as spin textures displaying inverted out-of-plane magnetisation along the rotating pattern [see Fig.1.6]. Skyrmions are characterised by a topological number $S_{sk} = \pm 1$, indicating the protection of the spin texture against smooth deformation and rendering them suitable for device applications [49]. Albeit originally proposed to exist in condensed matter systems as quasiparticles in real-space, skyrmionic band structures in reciprocal space can be established due to the interplay of SOC and magnetic exchange coupling (MEC) [50, 51].

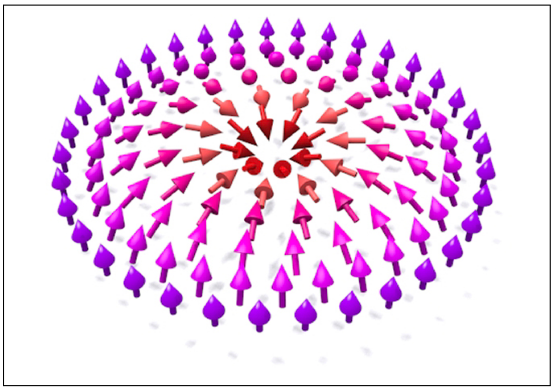

Figure 1.6: *A spin skyrmion. The spin texture is such that inversion of the out-of-plane component is realised by varying some parameter, e.g. the position (real-space skyrmion) or the momentum (momentum- space skyrmion).*

1.2 2D material-based spintronics

1.2.1 The advent of 2D materials

Atomically-thin material sheets have been for a long time only abstract objects, as they were thought not to exist as a stable state of matter. According to the so called Mermin-Wagner theorem in fact, long wavelength fluctuations inevitably destroy the long-range order of 2D crystals [52]. Nevertheless, such 2D systems played an important role as theoretical platforms. For instance, most of the properties of carbon allotropes with complicated geometry, such as carbon nanotubes, were found to be captured by a simplified 2D graphite layer model. Witness to the successful employment of those 2D models is the broad range of applications of carbon allotropes reached nowadays, ranging from antibiotics and flexible screens to solar cells [53–55]. The physical isolation of a carbon monolayer however has not been a reality until the discovery of graphene in 2004 [56], which truly initiated the field of 2D materials. The low dimensionality is the key for unprecedentedly-known electrical, optical, structural and thermal properties [57]. Research on the 2D materials is currently one of the most active areas in condensed matter physics; it is tempting to assume that the 2D materials will soon be materials of choice across a range of applications. The family of 2D materials encompasses numerous and diverse compounds, including insulators (e.g. hexagonal boron-nitride), semiconductors (group-VI transition metals dichalcogenides (TMDs)), semi- metals (graphene) and metals (NbS_2). The progress in exfoliation techniques has allowed for the reduction of essentially any given layered bulk material into the monolayer limit [58–60]. Parallel to that, bottom-up approaches—such as chemical vapour deposition, where gaseous reactants are deposited onto a substrate to grow high quality 2D monolayers, also guarantee production of atomically thin compounds on a large scale [61]. In the following, we discuss the advent of the 2D materials for spintronics purposes and one of the most promising system for technological advances based on Lego-structure. In fact, in the work of this thesis we are interested in graphene-based heterostructures.

1.2.2 Suitability of 2D materials for spintronics and van der Waals heterostructures

Since their advent, the 2D materials have been very attractive for spintronics purposes. Due to the unusual physical characteristics, the 2D materials have provided new platforms to probe the spin interaction with other DOF for electrons, as well as to be used for novel spintronics applications. The ultra-low spin-orbit coupling in graphene already made it one of the most promising candidates for spin channel [62–65]. The unusual spin-momentum locking properties of the surface states in TIs provide a method to control the spin polarization via the charge current direction [66]. The unique spin-valley coupling in 2D TMDs provides a platform to use valley for manipulating the spins [41, 67]. The introduction of magnetism into graphene or the surface states of TIs is particularly interesting towards the quantum anomalous Hall effect (QAHE) [68]. The enhanced SOC in hydrogen doped graphene, silicene, germanane, tin, and 2D TMDs are potential candidates for quantum spin Hall effect [66]. The spin-orbit torque at the TIs/ferromagnet interface has been demonstrated to be significantly larger than conventional heavy metals. The idea of combining different systems of reduced dimensionality into a new compound, which would ideally integrate the best properties of the single host materials, is very interesting. Such a route, concerning the vertical stacking of the 2D layers, is in fact already established experimentally. This Lego-approach gives rise to the so-called van der Waals (vdW) heterostructures, provided that vdW forces are responsible to keep the stack together [see Fig.1.7] [69]. Due to the reduced dimensionality, charge redistribution, structural changes and proximity effects (transfer of properties from one material to another via quantum tunnelling or Coulomb interaction) may occur in a very different way from usual 3D semiconducting heterostructures [70], opening a completely new venue for band structure engineering. Despite the recent origin of the research line, many successes have been reported by implementing vdW stacking. The emergence of superlattice Dirac points, surface reconstruction and gap opening are some examples of what have been observed in graphene on hexagonal boron nitride ($h-BN$) [71–73]. The rapid surge of the vdW heterostructures has also offered unprecedented opportunities for exploration of non-equilibrium effects [74]. For instance, efficient phototransistors can be obtained by combining graphene high carrier mobility and TMDs sensitivity to light absorption [75–77]. Long-living excitons could be created by using layered materials with different work functions, such as MoS_2/WSe_2 [78]. Encapsulation of graphene with $h-BN$ has been shown to give rise to stable gate-controllable plasmonic modes, with low optical losses [79]. In this respect, vdW heterostructures represent a landmark for future technological advances.

1.3 Graphene-based spintronics

1.3.1 Spintronics with Dirac quasiparticles

Historically, graphene has been recognised as an attractive platform to be used in spintronics applications amongst the members of the ever-increasing family of 2D materials, as mentioned above. Low-energy excitations of its many-body ground state have a massless 2D Dirac character described by the continuum-limit Hamiltonian (see Appendix B for details)

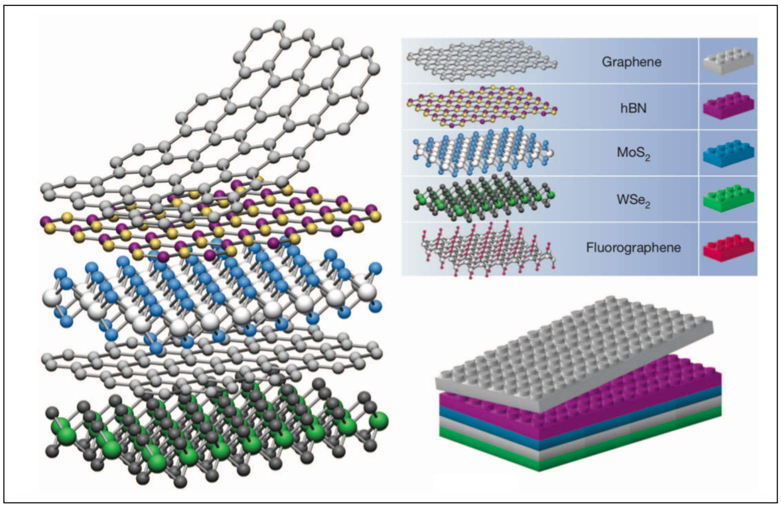

Figure 1.7: *By vertically stacking 2D materials with different properties, one can potentially obtain new platforms with enhanced properties. This Lego-like approach goes under the name of vdW epitaxy. The figure is taken from Ref.[69]*

$$H_G = v(\tau_z\sigma_x k_x - \tau_0\sigma_y k_y), \tag{1.27}$$

where the Fermi velocity $v \simeq 10^6$ m/s is an effective velocity of light. Above σ_i, τ_i, with $i = x, y, z$ are Pauli matrices describing emergent effective $spin-like$ DOFs of Dirac carriers associated with sublattice and valley space. In the following, the set of Pauli matrices s acts in the spin space. The energy dispersion of the Eq.(1.27) has a linear (massless) relativistic behaviour, with six zero-energy band crossing points (Dirac points) at the Brillouin zone corners [see Fig.1.8]. Physically, all the Dirac points are equivalent and connected by the vector of reciprocal lattice. This means that all six points can not be distinguished. However, the six bands can be grouped into two distinct categories due to rotational symmetry of the hexagonal honeycomb lattice (in the Appendix C we discuss briefly the honeycomb lattice properties useful to the system under study), reducing the description to K or K' bands, obtainable from Eq.(1.27) by replacing τ_z with $k = \pm 1$ respectively. The double energy-degenerate extremal band points are referred to as $valleys$. It is well known that in the massless limit, the Dirac equation is decoupled into two separate equations, describing left- and right-handed $chiral$ particles [88]. Mathematically, the chirality of Dirac carriers is encoded in the presence in the Eq.(1.27) of Pauli matrices associated to a spin-like DOF, commonly referred to as $pseudospin$ [89]. To see that, one can rewrite the Eq.(1.27) by introducing the chiral operator $\chi_\sigma = \sigma \cdot \mathbf{k}/|\mathbf{k}|$, whose eigenstates are associated with eigenvalues ± 1. For instance, in the Chapter 4 we will introduce a two combinations of Pauli matrices σ_k and σ_θ that will help us to rewrite and, then, diagonalize the 2D Dirac-Rashba

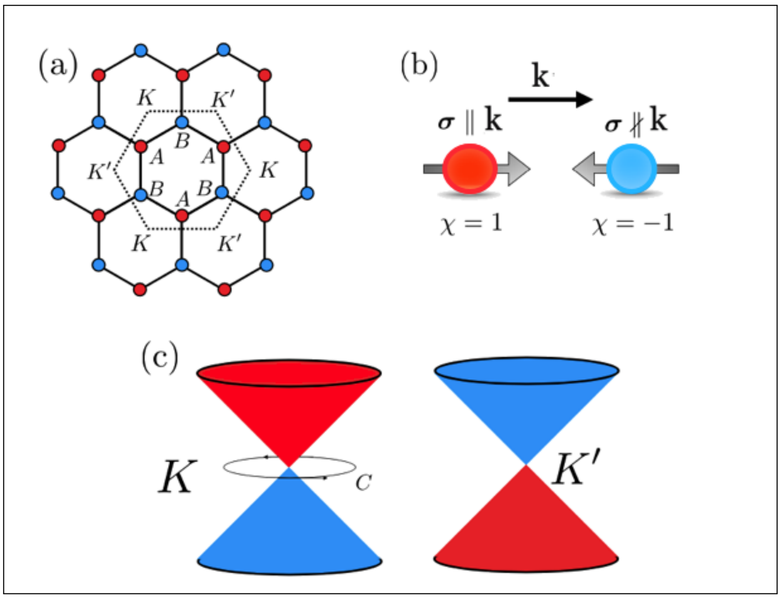

Figure 1.8: *(a) The honeycomb lattice of graphene, with interpenetrating Bravais triangular sublattices A, B, respectively in red and blue. The first Brillouin zone is shown in dashed, with inequivalent corners* K, K$'$. *To describe electron dynamics in this particular crystal environment one adopts a massless Dirac 2D Hamiltonian. Carriers have here a spin-like DOF (pseudospin), stemming from the presence of two sublattices, which can be either parallel or antiparallel to the momentum vector, giving then a chiral characters to Dirac fermions (b). (c) The associated low-energy dispersion is linear, with two zero-energy points at the corners of the Brillouin zone* K, K$'$. *Carriers with positive energy at* K (K$'$) *have positive (negative) chirality, conversely for negative. The chirality of Dirac particles is also responsible for the acquisition of a nonzero Berry phase upon adiabatic loops around the Dirac points, which might result in nontrivial topological phases when a bandgap is opened in the spectrum.*

Hamiltonian. Thus, in analogy to the real spin of massless relativistic particles in the vacuum, the pseudospin of graphene's quasiparticles points in the parallel/antiparallel directions with respect to their momentum [see Fig.1.8(b)]. Note that the chiral symmetry in crystal structures coincides with the sublattice symmetry. Indeed the chiral symmetry inherent to the Dirac Hamiltonian is due to the fact that the electron density is equally shared between A and B sublattice sites of the honeycomb structure. A further signature of the chirality of graphene's quasiparticles manifests upon adiabatic evolution of the electron wavefunction along a closed loop C in $\mathbf{k}$ space [see Fig.1.8(c)]. The eigenstate of the spinor associated to the Hamiltonian changes along this circuit C and at the end returns at its initial state but with a phase factor, which is named *Berry phase* and has a geometrical character [43, 80].

Let us investigate the symmetry properties of the Hamiltonian Eq.(1.27). Space inversion or parity transformation is indicated with $\mathcal{P}$. Parity interchanges the two original sub-lattice and sends $\mathbf{k} \longrightarrow -\mathbf{k}$. Under parity also the two valleys interchange. As a result, we have the parity transformation

$$\sigma_x \tau_x H_G(-\mathbf{k}) \sigma_x \tau_x = H_G(\mathbf{k}), \tag{1.28}$$

hence the graphene Hamiltonian is invariant under $\mathcal{P}$ symmetry operation. Let us indicate with $\mathcal{T}$ the time reversal symmetry operation. In quantum mechanics the time reversal transformation in spin space is $is_y\mathcal{K}$, where $\mathcal{K}$ is the charge conjugation. Under time reversal, $\mathbf{k} \longrightarrow -\mathbf{k}$ and the valleys interchange. The time reversal transformation on the Hamiltonian reads

$$-is_y \tau_x H_G(-\mathbf{k}) is_y \tau_x = H_G(\mathbf{k}), \tag{1.29}$$

so that it is invariant. SOC preserves the time reversal symmetry. By requiring that it does not break the space inversion symmetry as well, we allow for a term in the Hamiltonian of the form

$$H_I = \lambda_{zz} \sigma_z \tau_z s_z, \tag{1.30}$$

that is the so-called *intrinsic* spin-orbit coupling. The eigenvalues of the Hamiltonian Eq.(1.27) with the term Eq.(1.30) are

$$\epsilon = \pm\sqrt{v^2k^2 + \lambda_{zz}^2}, \tag{1.31}$$

for all values of s_z and τ_z with λ_{zz} the strength of coupling. Hence at both Dirac points (identified by $\tau_z = \pm 1$), a gap in the spectrum opens so that the graphene becomes an insulator with the Fermi level falling between the conduction and valence bands. One can verify that the graphene Hamiltonian with SOC exhibits the quantum spin Hall effect. The key ingredient for this to occur is the presence of a gap in the bulk spectrum and the existence of gapless edge states. Such a phenomenology is an example of a TI, as mentioned in the Section 1.1.3. The reason why H_I is usually neglected in the Eq.(1.27), is the smallness of the intrinsic SOC strength λ_{zz}. Early estimations by heuristic arguments in Ref.[43] yielded $\lambda_{zz} \sim 200\mu eV$, whereas later and more accurate tight-binding studies and first-principles results predicted values ranging from $(1-50)\mu eV$, meaning $\lambda_{zz} \ll \hbar v/a \simeq 4.6\mu eV$, where $a = 0.142nm$ is the carbon-carbon bond length, justifying the negligence of the SOC in the minimal Dirac model of graphene Eq.(1.27). In this picture, if $\lambda_{zz} \longrightarrow 0$ the Fermi level approaches to the Dirac point and, only in this case, the graphene exhibits an insulator behaviour.

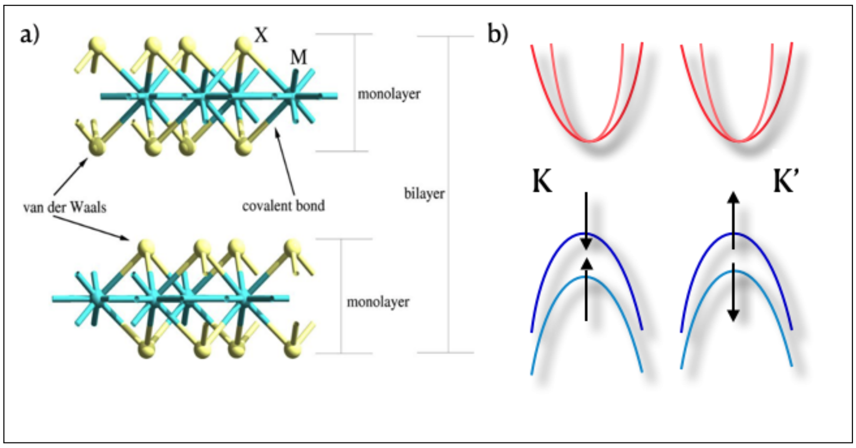

Figure 1.9: *Transition metal dichalcogenides. a) A 3D visualisation of typical* MX_2 *layered compounds. b) Due to the structural inversion asymmetry, TMDs display spin-split bands at* $\mathrm{K}\ \mathrm{K}'$ *points, with a large* $(0.1-0.5)eV$ *band gap. Time reversal symmetry guarantees that the spin polarisation is reversed at opposite valley, allowing selective spin excitation to the conduction bands by circularly polarised light (circular dichroism.)*

1.3.2 Enhancing spin-orbit coupling in carbon layers

One of the first proposals to enhance SOC in graphene [81] concerned adatom decoration. It can produce a very large local SOC thanks to the sp^3 bonding. However the experiments are facing difficulties to show the insulating phase [82–86]. Graphene-based vdW systems with proximity-induced SOC offer good prospects in the circumvention of this situation. In particular, TMD monolayers have been recognised as an ideal matching to graphene. TMDs are compounds of the type MX_2, where M, X are respectively a transition metal and a chalcogen element. Their crystal structure is such that an M layer is "sandwiched" between two X atomic layers in a trigonal prismatic or an octahedral phase [see Fig.1.9(a)] [87–91]. For TMDs, the atoms are heavy and the outer layers electronic states are from d-orbitals that have a strong SOC. This spin-orbit coupling removes the spins degeneracy in both the conduction and valence band i.e. introduces a strong energy splitting between spin up and down states [92, 93]. In the case of MoS_2, the spin-splitting in conduction band is in the meV range, while it is expected to be more pronounced in other materials like WS_2. The spin-orbit splitting in the valence band is several hundred meV. If there are different conduction/valence band extrema in the electronic band structure in k-space, the carriers can be confined in one of these valleys. This degree of freedom opens up a new field of physics: the controlling of carriers k-valley index, also called valleytronics. We briefly underline that more general graphene-on-a-substrate heterostructures, which strictly speaking do not fall into the vdW family—the substrate being a bulk, rather than a layer—are also attracting much attention. Proximity effects can be equally efficient, allowing the transfer of additional interactions to Dirac fermions beyond the SOC. For instance, the anomalous Hall effect (AHE) has been observed in graphene on YIG [85, 94], indicating the successful transfer of MEC to the carbon layer. Another very interesting research line concerns induced superconductivity in graphene. The penetration of Cooper pairs from Nb contacts to graphene sheet has been recently obtained [95]. All these recent developments have paved the way to a new material-science era, having as protagonists atomically well-defined interfaces of materials with tailored on-demand properties.

1.4 Summary and outline

The scope of this thesis is to study theoretically the transport in a system with the charge-spin coupling in 2D Dirac materials with proximity-induced SOC. In particular, we focus on the graphene-on-TMD bilayers that represent today one of the most promising device for spintronic development of next-generation optoelectronic nanodevices and nanoelectronics. As discussed, the advantage of this kind of Lego-structure is the combination of the sizeble SOC proximized by the adjacent layer of transition-metal dichalcogenides and the good electricity carriers in graphene. To derive the kinetic equation for our system, we use the quasiclassical approximation. In general it is of interest since it allows one to obtain simple transport equations even in cases where the quasiparticle approximation fails. The use of quantum field-theoretical methods in transport theory provides a microscopic justification of the semiclassical Boltzmann equation and allows one to generalize this approach to take renormalization and lifetime effects into account in a systematic manner. In particular it is possible to derive systematically the correction terms. The Keldysh formulation provides a convenient and general framework for deriving kinetic equations. In particular, the Keldysh component of the quasiclassical Green's function describes the distribution function. The power of this technique consists in the fact that, even though does not have the elegance of the functional integral methods, provides very often a much clearer physical picture. Even at equilibrium, when the diagrammatic methods are sufficient, the quasiclassical approximation has the advantage of a more compact derivation. For these reasons, we decide to adopt this technique to derive the kinetic equation and, then, the physical observables for our system stressing the original treatment of the work of this thesis.

First of all we prove the consistency of the quasiclassical approach making a link to the phenomenological Boltzmann equation for quasiparticles. We start from a simple system like the massive Dirac fermions. This means to consider only the orbital sublattice-staggered potential, i.e. the massive term, without intrinsic- or extrinsic-like SOC. This represents the minimal model to see the AHE. For such system in the clean and stationary case we use both approaches. The Eilenberger equation, i.e. the equation for the Keldysh component of the quasiclassical Green's function g, gives the same Hall conductivity as that obtained from the linearized Boltzmann equation for the distribution function f. This result confirms the equivalence of both approaches and tells us how to manipulate the different components of g. In fact, in order to obtain the correct result, we have to select only one component, i.e. the $perpendicular$ one, of the equilibrium distribution function. In other words, it means to neglect the component that commutes with the Hamiltonian of the system. We use the terminology $perpendicular$ considering that, using a suitable matrix basis, we may map the space of matrices to a vector space. Within such a mapping, the commutator of two matrices correspond to the cross product of the corresponding vectors. Following this procedure, we perform the same physical observable calculation but with the quasiclassical Green's function and, now, only the perpendicular component of g is selected. These preliminary calculations are useful to study a more interesting system such as the 2D Dirac-Rashba model. The Rashba effect is a momentum-dependent splitting of spin bands similar to the splitting of particles and anti-particles in the Dirac Hamiltonian. In such a model one has two regimes to investigate, i.e. when the Fermi energy intersects a single subband (regime I) or two subbands (regime II). The presence of two bands crossing the Fermi energy makes the mathematical description quite complex. For this reason, we focus first on the one-band regime. Again, in the clean and stationary case, for this model we have to solve a kinetic equation that is formally identical to the massive Dirac fermions one. Now, thanks to the previous results, we know that only selecting the perpendicular component of the equilibrium distribution function one can recover the well-know spin Hall conductivity reported in the recent literature. This finite result- in the stationary model- is not a contradiction, but can be explained by recalling that, without disorder, there is no true stationary state. The vanishing of the spin Hall conductivity occurs in the presence of an arbitrary small concentration of scalar impurities that produces a relaxation mechanism. We underline that the finite spin Hall conductivity shows two-contributions: one describes the processes far from the Fermi surface, whereas the other the processes at the Fermi surface. In particular, the first term is proportional to the Fermi energy. It is important to point out that the quasiclassical approximation captures only the processes at the Fermi surface by definition.

At this stage, we are ready to add the disorder in the 2D Dirac-Rashba Hamiltonian and study it with the help of the Eilenberger kinetic equation. To do that, we introduce the $\mathrm{T}-$matrix approximation in order to write the retarded/advanced self-energy ($\Sigma^{R(A)}$). The latter contains in principle the sum of all possible irreducible diagrams. In practice, one usually adopts some approximation to reduce the complexity of $\Sigma^{R(A)}$ to a subset of diagrams (the Born approximation, the skew-scattering mechanism, etc). Anyway, before any approximation, we are able to write the Keldysh component of the collision integral of the kinetic equation in terms of the disordered-average $\prec \mathrm{T} \succ -$matrix. After a non-trivial manipulation, we write a completely generic expression for the Keldysh component of the collision integral for which the detailed balance is obeyed. This represents one of the main result of the work of this thesis. To start the calculation of the disordered system, we focus on the simplest approximation for the one-band regime in the 2D Dirac-Rashba model. For such a system, we first derive the kinetic equation in the stationary case for the Keldysh component of g. To proceed further, we make an $ansatz$ for the Keldysh quasiclassical Green's function according to which it is proportional to the projector of the band via a scalar function (g_0). This can be justified by the argument that the physical observables we are interested in are of order of the momentum relaxation time. Now we can solve the kinetic equation at the Born level which means to consider the lowest order in the $\mathrm{T}-$matrix expansion. In the end, we obtain the solution for g_0 from which we derive the spin density along the $y-$direction and the charge current along $x-$direction. They coincide exactly with the results obtained via Kubo linear response theory. Furthermore now the spin Hall effect vanishes as expected due to the presence of a relaxation mechanism which yields a stationary solution. These results confirm the equivalence of the present approach with the linear response theory.

To go further in the disorder effects, we consider a more interesting system as the 2D Dirac-Rashba model with spin-valley coupling. This represents the heart of the work of this thesis. To see the (extrinsic) spin Hall effect, the skew-scattering mechanism has to be included. The motivation for including extrinsic skew-scattering effects comes from recent experimental results in graphene on WS_2 systems, where strong room-temperature spin-to-charge conversion efficiency has been measured [96]. The order of magnitude of the measured efficiency cannot be totally explained by SHE and ISGE driven by intrinsic mechanisms. This happens by considering higher-order terms in the $\mathrm{T}-$matrix expansion so as to modify the scattering kernel in the kinetic equation by an additional term. The solution for g_0 can be found using some periodicity properties of the scattering kernel. Introducing two different scattering rates (the parallel and the perpendicular component), we are able to find the analytical expression of the physical observables like the spin Hall and the Edelstein effect. To manipulate these equations, we define the skew-scattering coupling (g_{ss}) and, subsequently, a skew-scattering variable useful for the numerical analysis. As expected from the analytical expression, the Edelstein response is not affected by the skew-scattering mechanism unlike the spin Hall one. In particular, while the skew-scattering is growing, the system response becomes significant also for small values of Rashba coupling.

In the end, we turn our attention to the two-bands regime (regime II). In this case we are not able to define the quasiclassical Green's function due to the presence of the two Fermi surfaces. In the clean and stationary case, we take the advantage of the expansion in the Clifford's basis to bypass the problem and the spin Hall conductivity found agrees with what we recovered by directly selecting the perpendicular component of the equilibrium distribution function. This preliminary calculation helps us to understand how to deal with the presence of disorder. In this case we perform an original manipulation with an alternative trick, i.e. the integration of the Green's function over the momentum instead of the quasiclassical approximation. Thanks to this, we are able to rewrite the kinetic equation as a simple linear system. The complexity lies in the matrix structure of the linear operators but, at the same time, they show a sub-block structure in agreement with the symmetries of system. This means that if one chooses an electric field along a different direction, another sub-block has to be considered to solve the problem. We emphasize that, thanks to the linear operator definitions, all bubble diagrams can be taken into account automatically and this is a very interesting feature. In fact, solving the linear system in the sub-block of our interest, we found the suppression of the SHE due to the vertex corrections, as expected. In the end, at the Born level and in the limit of a good metal, we recover the well-know result for the spin Hall conductivity reported in the recent literature.

1.4.1 Structure of this thesis

Here we present briefly the structure of this thesis chapter by chapter.

In the Chapter 2 we introduce the theoretical tools useful for our purpose. In particular, we discuss briefly the semiclassical treatments commonly adopted to study the transport phenomena and we write the Boltzmann transport equation (BTE). Then we give the guideline to perform the linear response with the well-known Kubo formula. After, we turn to a more interesting technique for systems out of the equilibrium such as the Keldysh formalism. The latter is usually based on the two-point function so that the main mathematical object in the Keldysh technique is the non-equilibrium Green's function (NEGF). This helps us to introduce the quasiclassical approximation which will be the primary tool for this work. Thanks to this, we are able to write the kinetic equation for the Keldysh component of the quasiclassical Green's function.

In the Chapter 3 we present the minimal Dirac-Rashba (DR) model with a insightful diagonalization thanks to the Clifford's algebra. From this, we go further in the discussion and present the generalised model for the Dirac-Rashba system (from $C_{6v} \longrightarrow C_{3v}$ symmetry). We discuss in detail the presence of spin-valley coupling in the system and adopt a suitable parameterization to write the relative eigenstates.

In the Chapter 4 we present our first calculations for the simple model of the massive Dirac fermions without SOC. For such a system we use both methods, the density matrix and the quasiclassical Green's function approximation in order to evaluate the spin Hall (SH) conductivity. Thanks to this manipulation we are able to deal with a more complicated system such as the presence of the Rahsba interaction. For this system we use the Eilenberger equation to derive the spin Hall observable using what we have learned about the massive Dirac fermions. Up to here we studied all of these systems with no disorder effects.

Hence, in Chapter 5 we discuss how to tackle the model in the presence of disorder. The $\mathrm{T}-$matrix approximation is a powerful technique to take into account all scattering due to the impurities, phonons etc. Here we find the generic expression of the collision integral in the kinetic equation that represents one of the main result of this work. Furthermore, we analyze the Born approximation first and the skew-scattering mechanism after. For the single-band regime (regime I) we write the Eilenberger equation in the stationary case and find the observables at the Born level. We discuss the results.

While in Chapter 6 we go beyond the Born approximation and discuss the skew-scattering mechanism for the more interesting system of the 2D Dirac-Rashba with spin-valley coupling. This represents the heart of the original work of this thesis. For such a system we evaluate the physical observables (spin Hall and Edelstein effect). From their analytical expression, we are able to perform some numerical analysis that helps us to understand the behaviour of these physical quantities. Finally we discuss the results.

In the end, the last Chapter 7 contains the study of the transport equation in the two-band regime (regime II). First we analyze the clean system and then we add the disorder effect. In this case we are not able to define the quasiclassical Green's function due to the presence of two bands crossing the Fermi level, so that no Elilenberger equation can be written. In fact we show another way to solve the problem that is more interesting and powerful at the same time. Finally, a final discussion and the conclusion of the work are provided.

2

Theoretical tools

Overview

This is one of the most technical chapters, as its title suggests. We present the various formalisms used in this thesis to develop a novel theory of charge-spin transport phenomena in the 2D Dirac materials. The well known formalisms can be divided into two families: SC (semiclassical) and FQM (full quantum mechanical). The first one encompasses the SC Boltzmann transport theory and its quantum extensions based on the kinetic equation for the density matrix - we will briefly review both below. Their common SC trait is due to the average over some quantum DOF and the partial negligence of quantum coherence. This technical simplification allows for a more transparent physical interpretation of the results. However, lacking a rigorous treatment of the quantum nature of the electrons' wavefunction, its regime of validity is restricted to the situation where $k_F l \gg 1$, with k_F being the Fermi wavevector and l the mean-free path between collisions with impurity (or phonons). A more refined physical description can be obtained within the second class of FQM formalisms, based on a diagrammatic treatment of the Kubo linear response function. However, the main subjects of this work are the formulation of non equilibrium problems within the Keldysh approach and the quasiclassical approximation due to Eilenberger. We present here the Eilenberger semiclassical approach used for graphene systems in the presence of the spin-orbit couplings. This dissertation should be self-contained, but for details we refer the interested reader to the fairly rich literature [97],[98],[99], [100], [101], [33],[102],[103].

2.1 Semiclassical formalism

2.1.1 The 2D Boltzmann equation

The Boltzmann transport equation (BTE) provides a statistical description of a system in terms of the function $f(\mathbf{r},\mathbf{k},t)$, i.e. the density function of quasiparticles that can be found at time t in a very small region $d^d\mathbf{r}d^d\mathbf{k}$ of configuration space centred at $(\mathbf{r},\mathbf{k})$, with d being the dimension of the system. The distribution function f is linked to the total number of particles N via

$$d\Pi(\mathbf{r},\mathbf{k},t) = d^d\mathbf{r}d^d\mathbf{k}f(\mathbf{r},\mathbf{k},t) = dN, \tag{2.1}$$

where dN is the number of particles in the small volume $d\Pi$. Knowing f, the macroscopic observables describing the system can be obtained, as we shall see below. We will consider from now on the case $d = 2$, which is relevant to the work in this thesis. By introducing a momentum distribution function with a precise value at each point in space, the Boltzmann approach clearly violates Heisenberg uncertainty principles, which poses limits to its validity. However the usage of the BTE is justified in terms of wavepackets with well-defined average momentum or centre of mass coordinates, spin, etc. [104],[105]. In a solid, f is also labeled by a band index n that here we omit. The BTE is derived on the assumption of Hamiltonian dynamics for the centre of mass and the average momentum of the wavepacket [106]. Under the SC equations of motion, the assumption of incompressible fluid holds, which means that an external electromagnetic force $\mathbf{F} = -e(\mathbf{E}+\mathbf{v}\times\mathbf{B})$, where $\mathbf{E}$, $\mathbf{B}$ are the electric and magnetic field respectively, only produces a shift in position and momentum of the wavepacket, respectively $\mathbf{r}' = \mathbf{r}+\mathbf{v}dt$, $\mathbf{k}' = \mathbf{k}+\mathbf{F}dt/\hbar$, where $\mathbf{v}$ is the velocity. Instead, the number of particles in $d\Pi$ can only be altered by collisions. For later convenience we use the notation $f_{\mathbf{k}}(\mathbf{r},t) = f(\mathbf{r},\mathbf{k},t)$. Taking the total time derivative of the distribution function, we get

$$d_t f_{\mathbf{k}}(\mathbf{r},t) = \partial_t f_{\mathbf{k}}(\mathbf{r},t) + \mathbf{v}\cdot\boldsymbol{\nabla}_{\mathbf{r}} f_{\mathbf{k}}(\mathbf{r},t) + \frac{1}{\hbar}\mathbf{F}\cdot f_{\mathbf{k}}(\mathbf{r},t) = I[f], \tag{2.2}$$

where on the right-hand side (RHS) of Eq.(2.2) we have the collision integral $I[f]$. To find an analytic form for $I[f]$ we consider transition between states with different momenta $\mathbf{k} \longrightarrow \mathbf{k}'$ induced by a static potential V. The well-known point-like random potentials generated by N_i impurities located at position $\mathbf{r}_i$ is

$$V(\mathbf{r}) = u_0 \sum_i^{N_i} \delta(\mathbf{r} - \mathbf{r}_i), \tag{2.3}$$

where u_0-dimension of energy × area-measures the scattering strength. We have taken here for simplicity a scalar impurity potential, i.e. a potential diagonal in all internal DOFs. Standardly, the random potential is treated by means of a disorder-average procedure over all the possible impurity configuration [100]. After having performed the disorder average and having taken the thermodynamic limit $N, \Omega \longrightarrow \infty$, with Ω the spatial volume, it can be shown that, rather than involving a sum of scattering terms from different centres, the collision integral is reduced to a *single-impurity* term, scaling with the impurity concentration $n_i = N/\Omega$ [100],[107]. The probability of an elastic collision event can be obtained by invoking the Fermi's golden rule [108]

$$W_{\mathbf{k},\mathbf{k}'} = \frac{2\pi n_i}{\hbar} \left| \langle \mathbf{k}' | \mathrm{T} | \mathbf{k} \rangle \right|^2 \delta(\epsilon_{\mathbf{k}} - \epsilon_{\mathbf{k}'}), \tag{2.4}$$

where the Dirac delta function ensures conservation of energy in the scattering event. In the Eq.(2.4) T is the single-impurity T-matrix defined in terms of V as

$$\mathrm{T}_{\mathbf{k},\mathbf{k}'} = \langle \mathbf{k}' | V | \mathbf{\Psi}_{\mathbf{k}} \rangle , \tag{2.5}$$

where $\mathbf{\Psi}_{\mathbf{k}}$ is an eigenstate of the full Hamiltonian of the system $H = H_0 + V$ that satisfies the Lippman-Schwinger equation [100] and $\mathbf{k}'$ represents a plane wave. The collision integral will then be written as ($f_{\mathbf{k}} \equiv f_{\mathbf{k}}(\mathbf{r}, t)$)

$$I[f] = -\frac{1}{\Omega} \sum_{\mathbf{k}'} (W_{\mathbf{k}\mathbf{k}'} f_{\mathbf{k}} - W_{\mathbf{k}'\mathbf{k}} f_{\mathbf{k}'}). \tag{2.6}$$

In addition to a sum over all scattered waves with different momenta $\mathbf{k}'$, collision events also produce a coordinate shift of the centre of mass of the wavepacket, known as $side-jump$ [109–111], which is not included in Eq.(2.6). However it is of secondary importance in this thesis, as we are interested in dominant contributions to transport coefficient in the dilute limit, as we explain in more detail in the following. Note that number conservation imposes [112–114]

$$\int d^2\mathbf{r}\frac{1}{\Omega}\sum_{\mathbf{k}} I[f(\mathbf{r},\mathbf{k},t)] = 0. \tag{2.7}$$

The Fermi-Dirac distribution function

$$f^0_{\mathbf{k}} = \frac{1}{1+e^{(\epsilon_{\mathbf{k}}-\varepsilon)/k_BT}}, \tag{2.8}$$

where ε, k_B, T are the chemical potential, Boltzmann constant and temperature respectively, is a space- and time-independent solution to the BTE, i.e. an equilibrium solution. However, in the presence of weak external forces $\mathbf{F}$ the system is driven out of equilibrium and the electron density is redistributed. A solution to the BTE can be found on the assumption that the system only slightly departs from the local equilibrium, i.e.

$$f_{\mathbf{k}} = f^0_{\mathbf{k}} + \delta f_{\mathbf{k}}, \tag{2.9}$$

where $\delta f_{\mathbf{k}}$ is a correction linear in the external field. The corresponding linearised BTE is written as [107]

$$\frac{\partial \delta f_{\mathbf{k}}}{\partial t} + \mathbf{v}\cdot\boldsymbol{\nabla}\delta f_{\mathbf{k}} + \frac{1}{\hbar}\mathbf{v}\cdot\mathbf{F}\Big(-\frac{\partial f^0_{\mathbf{k}}}{\partial\varepsilon}\Big) = I[\delta f_{\mathbf{k}}]. \tag{2.10}$$

To study the dynamics of electrons in solid-state systems, a label for the electronic bands needs to be added to the distribution function, beyond additional quantum indices including the spin and other quantum DOFs, i.e. $f_{\mathbf{k}} \longrightarrow f_{\alpha,\mathbf{k}}$ with $\alpha = n, s, \ldots$. In the Eq.(2.10) we need to replace $\mathbf{v}$ by the band velocity $v_{\alpha,\mathbf{k}}$. The displacement of the physical observables $\mathcal{O}$ with respect to their equilibrium value are obtainable from the solution of the BTE as

$$\delta\mathcal{O}(\mathbf{r},t) = \sum_{\alpha}\sum_{\mathbf{k}}\langle\mathcal{O}\rangle_{\alpha\mathbf{k}}\delta f_{\alpha\mathbf{k}}(\mathbf{r},t), \tag{2.11}$$

where $\langle\mathcal{O}\rangle_{\alpha\mathbf{k}} = \langle\alpha\mathbf{k}|\mathcal{O}|\mathbf{k}\alpha\rangle$ is the average value of $\mathcal{O}$ on the eigenstate of the system $|\mathbf{k}\alpha\rangle$. For example, the non equilibrium part of the charge current is given by

$$\delta\mathbf{j}(\mathbf{r},t) = \sum_{\alpha}\sum_{\mathbf{k}}\langle\mathbf{j}_{\alpha,\mathbf{k}}\rangle\delta f_{\alpha\mathbf{k}}(\mathbf{r},t) = -e\sum_{\alpha}\sum_{\mathbf{k}} v_{\alpha\mathbf{k}}\delta f_{\alpha\mathbf{k}}(\mathbf{r},t). \tag{2.12}$$

In its simplest form, the BTE presented in this section for electrons in solids completely neglects quantum coherence effects. In the following we discuss shortly about the Kubo linear response theory within the full quantum mechanical formalism.

2.2 Full quantum mechanical formalism

2.2.1 Kubo linear response theory

The SC formalism presented in the previous section describes how the electron distribution, and thus the observables, responds to the application of weak external forces. An analogous FQM approach is given by the Kubo formula [115]. We present here a short discussion. Let us consider an external spatially homogeneous perturbation[1]

$$H_\mu^{ext}(t) = \mathcal{O}_\mu(t)\phi_\mu(t) \tag{2.13}$$

which drives a system out of equilibrium. Above, ϕ_μ is a source field coupled to some operator $\mathcal{O}_\mu$ with index μ related to the spatial orientation of the fields and/or associated matrix structure. Furthermore we suppose that $\phi_\mu(t)$ is sufficiently weak to ensure that the response is linear and that the system is in thermal equilibrium before the external force is applied. As a consequence of this perturbation, the density operator $\rho(t)$ becomes time-dependent, and so also does the ensemble average of the operator, i.e.

$$\langle \mathcal{O}_\mu(t)\rangle = \mathrm{Tr}\Big(\rho(t)\mathcal{O}_\mu(t)\Big). \tag{2.14}$$

We underline that $\langle \mathcal{O}_\mu(t)\rangle$ denotes the quantum average over a basis set of many-body quantum states in the presence of the external field $\{n^{int}\}$. Explicitly

$$\langle \mathcal{O}_\mu(t)\rangle = \frac{1}{Z}\sum_{\{n^{int}\}} e^{-\beta\epsilon_n^{int}}\langle n^{int}(t)|\mathcal{O}_\mu|n^{int}(t)\rangle = \frac{\sum_{\{n^{int}\}} e^{-\beta\epsilon_n^{int}}\langle n^{int}(t)|\mathcal{O}_\mu|n^{int}(t)\rangle}{\sum_{\{n^{int}\}} e^{-\epsilon_n^{int}/k_BT}}, \tag{2.15}$$

where ϵ_n^{int} is the energy of interacting state $|n^{int}(t)\rangle$ and Z the grand partition function. The linear relation between this quantity and the external force has the form

$$\langle \mathcal{O}_\nu(t)\rangle = \langle \mathcal{O}_\nu\rangle + \int dt' \chi_{\nu\mu}(t,t')\phi_\mu(t'), \tag{2.16}$$

where $\langle \mathcal{O}_\nu\rangle = \langle \mathcal{O}_\nu(t=-\infty)\rangle = \mathrm{Tr}(\rho_0\mathcal{O}_\nu)$ and ρ_0 is the density in thermal equilibrium[2]. Here $\phi_\mu(t)$ is assumed to vanish when $t \longrightarrow -\infty$. While $\chi_{\nu\mu}$ is the so-called *response*

---

[1] We work here in the Heisenberg picture, so that operators are time dependent.

[2] Here $\rho_0 = \frac{1}{Z}e^{-\beta H_0}$ with $Z = \mathrm{Tr}(e^{-\beta H_0})$ the grand partition function, H_0 the effective hamiltonian and $\beta = 1/k_BT$.

function, whose explicit form can be derived by means of the Kubo formula [115, 116]. Suppose the external perturbation is switched on at some time $t = t_1$, i.e.

$$H^{tot} = H + H^{ext}_{\mu}(t)\Theta(t-t_1) = H + \phi_{\mu}(t)\mathcal{O}_{\mu}(t)\theta(t-t_1), \tag{2.17}$$

where $\Theta(.)$ is the Heaviside step function. The time evolution of the perturbed states is described by

$$H^{tot}(t)|n^{int}(t)\rangle = i\hbar\partial_t|n^{int}(t)\rangle. \tag{2.18}$$

It is convenient to switch from the Heisenberg to the interaction picture considering

$$|n^{int}(t)\rangle = e^{-\frac{i}{\hbar}Ht}|\hat{n}^{int}(t)\rangle = e^{-\frac{i}{\hbar}Ht}\hat{U}_{\mu}(t,t_1)|\hat{n}^{int}(t_1)\rangle, \tag{2.19}$$

where the hat denotes a quantity taken in the interaction picture. We have introduces above the evolution operator

$$\hat{U}_{\mu}(t,t_1) = Texp\Big(-\frac{i}{\hbar}\int_{t_1}^{t}\hat{H}^{ext}_{\mu}(t')dt'\Big), \tag{2.20}$$

with T the time-ordering operator. The Eq.(2.16) expresses the condition that the differential change of $\mathcal{O}_{\mu}(t)$ is proportional to the external disturbance $\phi_{\mu}(t')$ and the duration of the perturbation $\delta t'$, and further that disturbances at different times act independently of each other. The latter condition implies that the *response function* $\chi_{\nu\mu}$ may only depend on the time difference $t-t'$. Substituting the Eqs.(2.15), (2.19) and (2.20) into the Eq.(2.16) and expanding to linear order in $\phi_{\mu}(t)$, one arrives at the well-known *Kubo formula*, i.e.

$$\chi_{\nu\mu}(t,t') = \chi_{\nu\mu}(t-t') = -\frac{i}{\hbar}\theta(t-t')\langle[\mathcal{O}_{\nu}(t),\mathcal{O}_{\mu}(t')]\rangle. \tag{2.21}$$

In the quantum field theory, the two-points function in the Eq.(2.21) defines the so-called *propagator*, or *correlation* function. In particular the response function $\chi_{\nu\mu}$ is the retarded Green's function of the observable. If the system exhibits translational invariance in time, it is useful to work in frequency space. So that the Eq.(2.16) becomes

$$\delta\langle\mathcal{O}_{\nu}(\omega)\rangle = \chi_{\nu\mu}(\omega)\phi_{\mu}(\omega), \tag{2.22}$$

where $\delta\langle\mathcal{O}_{\nu}(\omega)\rangle$ indicates the time observable variation. For pedagogical purposes here, we consider the 2D conductivity tensor σ_{ij} of disordered electron systems, neglecting many-body effects. σ_{ij} describes how a charge current (precisely the paramagnetic part) builds up in the system in a parallel or transverse direction to an applied electric field $E_j(t)$ homogeneous in space, it means

$$\langle j_i(t)\rangle = \int dt' \sigma_{ij}(t-t')E_j(t'). \tag{2.23}$$

In the static (low frequency) case, a more transparent form of σ_{ij} is commonly referred to as Kubo-Streda formula [117] for which, at zero temperature, the conductivity can be split into two terms [118]: a first one σ^I_{ij}, carrying information about the contribution of electrons at the Fermi level ε, and a second one, σ^{II}_{ij}, taking into account off-Fermi surface processes (see Appendix D for details). They reads

$$\sigma^I_{ij} = \frac{e^2\hbar}{4\pi\Omega}\mathrm{Tr}[v_i(G^R(\epsilon)-G^A(\epsilon))v_jG^A(\epsilon) - v_iG^R(\epsilon)v_j(G^R(\epsilon)-G^A(\epsilon))], \tag{2.24}$$

$$\sigma^{II}_{ij} = \frac{e^2\hbar}{4\pi\Omega}\int d\epsilon' f_0(\epsilon')\mathrm{Tr}[v_iG^R(\epsilon')v_j(\partial_{\epsilon'}G^R(\epsilon')) - v_i(\partial_{\epsilon'}G^R(\epsilon'))v_jG^R(\epsilon') + h.c.], \tag{2.25}$$

where the Tr is meant on motional (position or momentum) and quantum indices, v the velocity and Ω the volume of the sample. It is worth anticipating here that the type-I contribution of generic response functions includes in principle the SC-like part of the response. It is the dominant term in the diffusive limit $k_F l \sim \epsilon\tau \gg 1$, where τ is the effective relaxation time of bare eigenstates at the Fermi level introduced by disorder (see Chapter 5). To deal with the out of equilibrium problems, in the next section we present the Keldysh technique that will be the main tool of our work.

2.3 Out of equilibrium formalism

2.3.1 The Keldysh technique

In this section we present shortly the Keldysh formalism for the treatment of out of equilibrium interacting many–body systems [119]. It provides a systematic way to study non equilibrium systems, usually based on the two-point functions corresponding to excitations in the system. The main mathematical object in the Keldysh formalism is the non-equilibrium Green's function (NEGF), which is a two-point function of particle fields. In this way, it resembles the Matsubara formalism [120], which is based on the equilibrium Green's functions in imaginary-time and treats only equilibrium systems. Let us consider a system with a time-dependent perturbation $H_i(t)$, the full Hamiltonian reads

$$H(t) = H_0 + H_i(t), \tag{2.26}$$

where H_0 represents the free diagonalizable part of H while H_i contains the interactions between particles. We are interested to treat the transport problem beyond semiclassical approximation considering the so-called quantum corrections. In general, at quantum level, one obtains a set of equations which are very complicated. In some important cases, they can be approximated in such a way that they may solved. Now, we consider an Hermitian operator $\mathcal{O}$ in the Heisenberg picture. It is time-dependent but not the state ψ. The expectation value of the operator $\mathcal{O}(t)$ is given by

$$\langle \mathcal{O}(t) \rangle = \langle \psi | U^\dagger(t,0) \mathcal{O}(0) U(t,0) | \psi \rangle, \tag{2.27}$$

where $\mathcal{O}(t) = U^\dagger(t,0)\mathcal{O}(0)U(t,0)$ represents the time evolution operator in the Heisenberg picture while $U(t_1,t_2)$ is the time-evolution unitary operator. It is written as the time-ordered exponential of Hamiltonian integral as follows

$$U(t_2,t_1) = T\left(e^{-i\int_{t_1}^{t_2} H(t')dt'}\right). \tag{2.28}$$

If the Hamiltonian at a certain time commutes with the Hamiltonian at different times, the time-ordered product disappears in the formula Eq.(2.28). In the quantum field theory, the interaction picture is often more convenient to describe the perturbative quantum mechanics. From this point of view, the operator reads

$$\mathcal{O}_{\mathcal{I}} = U_0^\dagger(t,0)\mathcal{O}(0)U_0(t,0), \tag{2.29}$$

where $U_0(t_1,t_2) = e^{-iH_0(t_1-t_2)}$. Then, one can define the naturally time-ordered $S-$matrix as follows

$$S(t_1,t_2) = U_0^\dagger(t_1,t_2)U(t_1,t_2) = T\left(e^{-i\int_{t_2}^{t_1} H_i(t')dt'}\right). \tag{2.30}$$

Using the $S-$matrix, the Eq.(2.27) can be rewritten as[3]

$$\langle \mathcal{O}(t) \rangle = \langle \psi | S^\dagger(t,0)\mathcal{O}_{\mathcal{I}}S(t,0) | \psi \rangle = \langle \psi | S^\dagger(t_3,0)S(t_3,t)\mathcal{O}_{\mathcal{I}}S(t,0) | \psi \rangle, \tag{2.31}$$

---

[3] Here we use the following relation for the time-evolution unitary operators $U(t_3,t_2)U(t_2,t_1) = U(t_3,t_1)$.

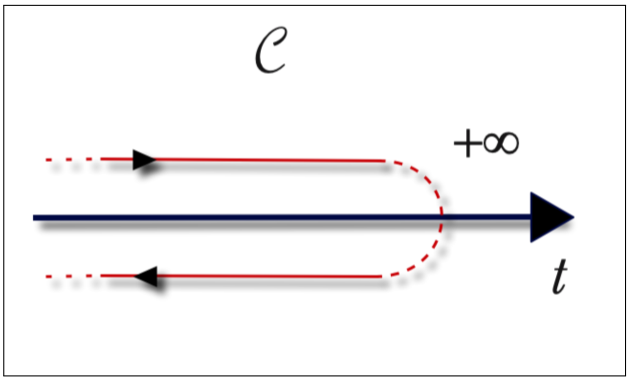

Figure 2.1: *The Keldysh contour in the complex t-plane. It starts at* $t = 0$*, proceeds to* $t = \infty$*, and then returns to* $t = 0$*.*

where t_3 is a time value greater than t. The problem is how to connect the time evolution of the $S-$matrix in the interaction picture with the relation between the free and interacting states of the Heisenberg picture. An important step in this procedure is the so-called adiabatic switching on in the "far" past and off in the "far" future of interactions (i.e. in the far past and future there is no interaction). This assumption assures that at $t \longrightarrow \pm\infty$ the system lies in the same eigenstate as the non-interacting part H_0. In terms of state vectors, this means

$$\psi_{\mathcal{I}}(\pm\infty) = \psi_{H_0}, \qquad \psi_{\mathcal{I}}(0) = \psi \tag{2.32}$$

or, at all time,

$$\psi = S(0,-\infty)\psi_{H_0}, \qquad \psi_{\mathcal{I}}(t) = S(t,0)\psi. \tag{2.33}$$

Using these relations and by introducing $S^{(\dagger)} \equiv S^{(\dagger)}(-\infty,\infty)$, the Eq.(2.31) becomes

$$\langle \mathcal{O}_{\mathcal{I}} \rangle = \langle \psi_{H_0} | S^{\dagger} \mathcal{O}_{\mathcal{I}}(t) S | \psi_{H_0} \rangle, \tag{2.34}$$

where now the average is not over the interacting state but the free one. At this stage, the problem is that $S^{\dagger}$ is anti-time ordered while S is time-ordered. A solution is to replace the operator $\mathcal{O}_{\mathcal{I}}(t)$ with a contour-ordered operator. The contour $\mathcal{C}$ parametrizes the contour path on the time axis starting at $t = 0$, proceeding to $t = \infty$, and then returning to $t = 0$. This path is known as the Keldysh contour and is shown in Fig.[2.1]. In this way one can consider both time and anti-time ordered operator via the ordering operators $T_{\mathcal{C}}$ defined as

$$T_{\mathcal{C}}\{\psi(t_1)\psi(t_2)\} = \begin{cases} \psi(t_1)\psi^{\dagger}(t_2), & t_1 >_{\mathcal{C}} t_2 \\ \pm\psi^{\dagger}(t_2)\psi(t_1), & t_1 <_{\mathcal{C}} t_2 \end{cases} \tag{2.35}$$

where the ± sign corresponds to bosons ad fermions. With this notation, the Eq.(2.34) becomes

$$\langle \mathcal{O}_{\mathcal{I}}(t)\rangle = \langle \psi_{H_0}|T_{\mathcal{C}}(\mathcal{O}_{\mathcal{I}}(t)S_{\mathcal{C}})|\psi_{H_0}\rangle, \tag{2.36}$$

where $S_{\mathcal{C}} \equiv T_{\mathcal{C}}(e^{-i\int_{\mathcal{C}} H_i(t')dt'})$. One of the important consequence of the Keldysh time path is that the definition of the Green's function is like the equilibrium case, i.e.

$$G(x_1,x_2) = -i\langle T_{\mathcal{C}}\psi(x_1)\psi^\dagger(x_2)\rangle, \tag{2.37}$$

with $x_i = (\mathbf{x}_i,t_i)$ the space-time coordinates. The price to pay is that there are actually several Green functions to calculate. For this reason it is convenient to introduce a matrix structure in the so-called Keldysh space as

$$G_{\mathcal{C}}(x_1,x_2) \mapsto \underline{G} \equiv \begin{pmatrix} \hat{G}_{11} & \hat{G}_{12} \\ \hat{G}_{21} & \hat{G}_{22} \end{pmatrix}. \tag{2.38}$$

A matrix element $\hat{G}_{ij}$ corresponds to $x_1 \in \mathcal{C}_i, x_2 \in \mathcal{C}_j$. Explicitly one has

$$\begin{aligned}
\hat{G}_{11}(x_1,x_2) &= -i\langle T\left(\psi(x_1)\psi^\dagger(x_2)\right)\rangle, \\
\hat{G}_{12}(x_1,x_2) &= G^{<}(x_1.x_2) = +i\langle\psi^\dagger(x_2)\psi(x_1)\rangle, \\
\hat{G}_{21}(x_1,x_2) &= G^{>}(x_1,x_2) = -i\langle\psi(x_1)\psi^\dagger(x_2)\rangle, \\
\hat{G}_{22}(x_1,x_2) &= -i\langle\tilde{T}\left(\psi(x_1)\psi^\dagger(x_2)\right)\rangle,
\end{aligned}$$

where $\tilde{T}(...)$ is the anti-time-ordering operator. Furthermore, the Green's functions are not all independent and obey the causality condition [121] that reads

$$\hat{G}_{11} + \hat{G}_{22} = \hat{G}_{12} + \hat{G}_{21}. \tag{2.39}$$

A convenient representation was introduced by Larkin and Ovchinnikov [98, 122], i.e.

$$\check{G} \equiv L\sigma_3\underline{G}L^\dagger, \tag{2.40}$$

with $L = 1/\sqrt{2}(\sigma_0 - i\sigma_2)$ and σ_i the Pauli matrices where $i = 0,1,2,3$. In this way the Green's function reads

$$G^R(x_1,x_2) = -i\theta(t_1 - t_2)\langle\Big\{\psi(x_1),\psi^\dagger(x_2)\Big\}\rangle, \tag{2.41}$$

$$G^A(x_1,x_2) = i\theta(t_2 - t_1)\langle\Big\{\psi(x_1),\psi^\dagger(x_2)\Big\}\rangle, \tag{2.42}$$

with $\Big\{\psi(x_1),\psi^\dagger(x_2)\Big\} = \psi(x_1)\psi^\dagger(x_2) + \psi^\dagger(x_2)\psi(x_1)$. Otherwise G^K, the Keldysh component of $\check{G}$ that carries information about system distribution, is

$$G^K(x_1,x_2) = -i\langle\Big\{\psi(x_1),\psi^\dagger(x_2)\Big\}\rangle. \tag{2.43}$$

In the end, with this representation the Keldysh Green's function Eq.(2.38) can be rewritten as

$$\check{G} \equiv \begin{pmatrix} G^R & G^K \\ 0 & G^A \end{pmatrix}. \tag{2.44}$$

To appreciate the physical meaning of the retarded/advanced and Keldysh Green's function, it is useful to consider the simple case of Fermi gas [123]. In this case the field operator has the form of the wave function and the $G^{R(A)}$ Fourier transform reads

$$G^{R(A)}(\mathbf{k},\omega) = \mp\frac{i}{\hbar}\int dt' e^{i(\omega - \epsilon(\mathbf{k})/\hbar)t'} = \frac{1}{\hbar\omega - \epsilon(\mathbf{k}) \pm i0^+}, \tag{2.45}$$

where $\epsilon(\mathbf{k})$ is the system energy dispersion and ω the energy. While the Keldysh component can be written as

$$G^K(\mathbf{k},\omega) = [G^R(\mathbf{k},\omega) - G^A(\mathbf{k},\omega)]F(\omega), \tag{2.46}$$

with $F(\omega)$ the distribution function. The Eqs.(2.45)-(2.46) tell us that $G^{R(A)}$ have the information about the spectrum of the excitations, while G^K about their statistical occupation. At equilibrium, $F(\omega)$ is fixed and reads

$$F(\omega) = \tanh\left(\frac{\omega}{2T}\right). \tag{2.47}$$

The equation of motion for G^K, the quantum kinetic equation, can be thought of as a generalization of the Boltzmann equation. In fact, in the semiclassical limit it reduces to the Boltzmann result. The representation given by the Eq.(2.44) is particularly convenient since its triangular structure is preserved whenever one deals with a string of (triangular) operators $\mathcal{O}_1, \mathcal{O}_2, ...\mathcal{O}_n$ (standard matrix multiplication is assumed)

$$\mathcal{O}_1\mathcal{O}_2...\mathcal{O}_n = \mathcal{O}' = \begin{pmatrix} (\mathcal{O}')^R & (\mathcal{O}')^K \\ 0 & (\mathcal{O}')^A \end{pmatrix}. \tag{2.48}$$

Such a string is the kind of object Wick's theorem produces. In other words, in this representation the structure of the Feynman diagrams is the simplest possible. We will not go deeper in this discussion (for details see [98]), but we will rather move on to study the equation of motion of $\check{G}$ in the quasiclassical approximation. In the following we go further in the quasiclassical approximation and, from now, on spin-$1/2$ fermions we will considered.

2.3.2 Quasiclassical approximation

In this section we want to show how to compute the quantum corrections to electrical transport. As mentioned in the previous section, the equation for G^K is equivalent to the Boltzmann one. The first step in this direction is to consider the Dyson equation and its complex conjugate [97, 98], i.e.

$$\begin{aligned} [\check{G}_0^{-1}(x_1,x_2) - \check{\Sigma}(x_1,x_2)] \otimes \check{G}(x_2,x_1') &= \delta(x_1 - x_1'), \qquad (2.49) \\ \check{G}(x_1,x_2) \otimes [\check{G}_0^{-1}(x_2,x_1') - \check{\Sigma}(x_2,x_1')] &= \delta(x_1 - x_1'), \qquad (2.50) \end{aligned}$$

where the symbol "$\otimes$" indicates convolution in space-time. The matrix multiplication in the Keldysh space is

$$\check{A}(x_1,x_2) \otimes \check{B}(x_2,x_1') \equiv \int dx_2 \begin{pmatrix} A^R & A^K \\ 0 & A^A \end{pmatrix} (x_1,x_2) \begin{pmatrix} B^R & B^K \\ 0 & B^A \end{pmatrix} (x_2,x_1') \tag{2.51}$$

and the $\delta-$function has to be interpreted as

$$\delta(x_1 - x_1') = \begin{pmatrix} \delta(x_1 - x_1') & 0 \\ 0 & \delta(x_1 - x_1') \end{pmatrix}. \tag{2.52}$$

Furthermore, the inverse of the free Green's function $\check{G}_0^{-1}$ reads[4]

$$\check{G}_0^{-1}(x_1,x_2) \equiv [i\partial_{t_1} - H_0(x_1)]\delta(x_1 - x_1') \tag{2.53}$$

and the self-energy $\check{\Sigma}$ that contains the effects due to interactions (electron-phonon, electron-electron and so on, but also disorder) has the same triangular matrix structure of the Eq.(2.44), i.e.

$$\check{\Sigma}(x_1,x_2) \equiv \begin{pmatrix} \Sigma^R & \Sigma^K \\ 0 & \Sigma^A \end{pmatrix}. \tag{2.54}$$

The Dyson equation contains too much information for our purposes. What we are looking for is a kinetic equation with as clear and simple structure as possible - that means a good compromise between physical transparency and amount of information retained. The trick is to subtract the two Dyson equations Eqs.(2.49)-(2.50) so that the delta functions cancel. With this in mind, we introduce the Wigner coordinates defined as follow

$$\begin{aligned} &\mathbf{x} = \tfrac{\mathbf{x}_1+\mathbf{x}_2}{2}, \qquad t = \tfrac{t_1+t_2}{2} \\ &\mathbf{r} = \mathbf{x}_1 - \mathbf{x}_2, \quad \eta = t_1 - t_2. \end{aligned} \tag{2.55}$$

From this point of view, by taking the Fourier transform with respect to $\mathbf{r}$ and η, the Green's function and the self-energy will depend on $\mathbf{x}, t$ and $\mathbf{k}, \omega$. The key assumption in the derivation of the transport equation is that the center-of-mass space-time variable $\mathbf{x}, t$ is a slow variable compared to the fast one $\mathbf{k}, \omega$. One can start from the left-right (LR) subtracted Dyson equation

$$\left[\left(\check{G}_0(x_1,x_2)\right)^{-1}, \check{G}(x_2,x_{1'})\right] = \left[\check{\Sigma}(x_2,x_{1'}), \check{G}(x_2,x_{1'})\right], \tag{2.56}$$

and perform the gradient expansion [124] obtaining for $\check{G}(\mathbf{x},t,\mathbf{k},\omega) \equiv \check{G}$ the following equation (here we set $e = 1$ for simplicity)

$$\partial_t \check{G} + \frac{1}{2}\left\{\boldsymbol{\sigma}\cdot, (\nabla - \mathbf{E}\partial_\omega)\check{G}\right\} + i\left[h(\mathbf{k}), \check{G}\right] - \frac{1}{2}\left\{\mathbf{E}\cdot, \nabla_{\mathbf{k}}\check{G}\right\} = -i\left[\check{\Sigma}, \check{G}\right]. \tag{2.57}$$

---

[4] External fields, like electromagnetic one, can also be included.

Here, $h(\mathbf{k})$ is the disorder-free Hamiltonian density evaluated on the eigenstates of the momentum and the square and curly brackets define the commutating and anticommutating operation. The inclusion of an external electromagnetic field is achieved by means of the standard minimal replacement $-i\nabla+\mathbf{A}$, with $\mathbf{A}$ the vector potential. In the Eq.(2.57), a uniform and static electric field via the gauge choice $\mathbf{k}=\mathbf{A}(t)=-\mathbf{E}t$ with no electric potential is chosen. In a compact form, the Eq.(2.57) is an equation for all the components of the Green's function Eq.(2.44). For the reasons discussed in the previous section, we are looking for the Keldysh component to derive the kinetic equation. In particular, the RHS term of the Keldysh component of the Eq.(2.57) is usually named $collision\ integral$ and in the language of the Boltzmann equation can be divided in a in- and out-term. Using the triangular structure given by the Eqs.(2.44) and (2.54), one can perform the matrix multiplication and select only the Keldysh component, i.e. the collision integral, that reads

$$I \equiv -i\left[\check{\Sigma},\check{G}\right]^K = -i\left(\Sigma^R G^K - G^K\Sigma^A\right) + i\left(G^R\Sigma^K - \Sigma^K G^A\right) \equiv I_{out} + I_{in}. \tag{2.58}$$

At this stage one can integrate the Eq.(2.57) over the energy ω, corresponding to the equal-time limit, in order to obtain a semiclassical kinetic equation. Introducing the more familiar distribution function as [97, 98]

$$f(\mathbf{k},\mathbf{x},t) = \frac{1}{2}\left(1+\int\frac{d\omega}{2\pi i}G^K(\mathbf{x},t,\mathbf{k},\omega)\right), \tag{2.59}$$

which reduces to the Fermi function in equilibrium, we obtain the Boltzmann equation for impurity scattering ($f(\mathbf{k},\mathbf{x},t)\equiv f$)

$$\partial_t f + \frac{1}{2}\left\{\boldsymbol{\sigma}\cdot,(\nabla-\mathbf{E}\partial_\omega)f\right\} + i\left[h(\mathbf{k}),f\right] - \frac{1}{2}\left\{\mathbf{E}\cdot,\nabla_{\mathbf{k}}f\right\} = \mathscr{I}, \tag{2.60}$$

where

$$\mathscr{I} = \int\frac{d\omega}{2\pi i}I. \tag{2.61}$$

Another way is to introduce the *quasiclassical Green's function* that is usually defined as follow [125]

$$\check{g}(\mathbf{x},t,\mathbf{n},\omega) \doteq \frac{i}{\pi}\int_{C} d\xi\,\check{G}(\mathbf{x},t,\mathbf{k},\omega), \tag{2.62}$$

where we have introduced the variable measuring the distance from the Fermi energy ε as $\xi = \epsilon(\mathbf{k}) - \varepsilon$. The integration contour $\mathcal{C}$ captures the contribution of the pole of the Green's function. The ξ-integration leaves unaffected the dependence on the orientation of the momentum $\mathbf{n} = \mathbf{k}/|\mathbf{k}|$. The so-called Eilenberger equation is then obtained by applying the ξ-integration to the Eq.(2.57) by *reasonably* assuming that the self-energy does not have a further singular behavior, which may add to the pole of the Green's function. The Eilenberger equation then reads

$$\partial_t \check{g} + \frac{1}{2}\{\boldsymbol{\sigma}\cdot, (\nabla - \mathbf{E}\partial_\omega)\check{g}\} + i\left[h(\mathbf{k_F}), \check{g}\right] = -i\left[\check{\Sigma}, \check{g}\right]. \tag{2.63}$$

Notice that $h(\mathbf{k}_F)$ is the Hamiltonian density at the Fermi energy. The quasiclassical Green's function has the same triangular matrix structure of the original Green's function, i.e.

$$\check{g} = \begin{pmatrix} g^R & g^K \\ 0 & g^A \end{pmatrix}. \tag{2.64}$$

and in the clean system, the retarded (advanced) quasiclassical Green's function at certain band is

$$g^{R(A)} = \pm P(\mathbf{k}_F), \tag{2.65}$$

with $P(\mathbf{k}_F)$ the projector at the Fermi level for that band. For instance, in the single-band effective mass Hamiltonian with free-particle dispersion $g^{R(A)}$ is the unity. At this stage, one selects only the Keldysh component of the Eq.(2.63) and obtains ($g^K \equiv g$)

$$\partial_t g + \frac{1}{2}\{\boldsymbol{\sigma}\cdot, (\nabla - \mathbf{E}\partial_\omega)g\} + i\left[h(\mathbf{k_F}), g\right] = \mathcal{I}, \tag{2.66}$$

where

$$\mathcal{I} = \frac{i}{\pi}\int_{\mathcal{C}} d\xi I. \tag{2.67}$$

In the end, once the solution for quasiclassical Green's function g is known one may obtain the observables as the electrical current, the spin polarization and the spin current. According with the general recipe in the Abelian case [126], we can write the density matrix as the integral over the momentum of the Green's function. Using the notation [98]

$$\int \frac{d\mathbf{k}}{(2\pi)^2} \int \frac{d\omega}{2\pi i} \approx N_F \int \frac{d\hat{\mathbf{k}}}{2\pi} \int \frac{d\omega}{2\pi i} \int d\xi, \tag{2.68}$$

with N_F the density of state (DOS) at the Fermi level, if $\mathcal{O}$ indicates a generic observable, one has[5]

$$\langle \mathcal{O} \rangle \;=\; i \int \frac{d\omega}{2\pi} \int \frac{d\mathbf{k}}{(2\pi)^2} \mathrm{Tr}\left(\mathcal{O} G^{<}(\mathbf{k},\omega)\right) = -\frac{N_F}{4} \left\langle \int d\omega \mathrm{Tr}\left(\mathcal{O} g\right) \right\rangle, \tag{2.69}$$

where $\langle \ldots \rangle$ indicates the average over the angles.

In the next Chapter we discuss in details the minimal Dirac-Rashba model first and then the generalised one. In the first case, we provide a parameterization never used before and we are able to write the eigenstates in a simple way that will be used for the transport equation in the Chapter 5. In the second case, we focus on specific SOC which is named $spin - valley$ coupling. In particular, for such a system we present a very compact notation to write the eigenstates that will be useful to derive the kinetic equations (see Chapter 6)

---

[5] Here we use the relation $G^{<} = \frac{1}{2} G^{K} + \frac{i}{2} A$, with A a contribution does not depend on the state of system and shall henceforth be dropped when non equilibrium is considered [98].

3

The 2D material Hamiltonian

Overview

To set the basis of our study of the spin-orbit phenomena in honeycomb layers, we discuss the fundamental electronic properties of the 2D Dirac materials with broken mirror symmetry $z \longrightarrow -z$, starting from low-energy continuum models (see Appendix B for details). In this respect, the starting point is the minimal 2D Dirac-Rashba model, where the bare graphene Hamiltonian is supplemented with a Rashba interaction resulting from the interfacial breaking about the 2D plane (e.g. in the presence of a substrate). From a symmetry standpoint, this is described by the C_{6v} group of the hexagonal lattice (see Appendix C for more details). Honeycomb layer with C_{6v} symmetry are invariant under six-fold rotations about the $\hat{z}$ axis, such that the A, B sublattice sites remain equivalent; however asymmetric spin-flip hopping among nearest-neighbours is allowed [see Fig.3.1(b)]. Another important class is represented by honeycomb layers which are invariant under the C_{3v} point symmetry group [see Fig.3.1(c)]. This is the case of graphene/TMD heterostructures, where the small lattice mismatch produces different effective fields on the A, B carbon atoms sitting closer to either the chalcogen or the metal element. In the continuum limit, this is reflected in the appearance of additional orbital and SOC terms in the Hamiltonian. In the following, we discuss the properties of the minimal 2D Dirac-Rashba without disorder. In particular we show how diagonalize the Hamiltonian and evaluate the projectors of the system. In the end, the $spin-valley$ interaction interaction is included. We present a compact parameterization to write the eigenstates of the system that will be useful for the analysis of the kinetic equation.

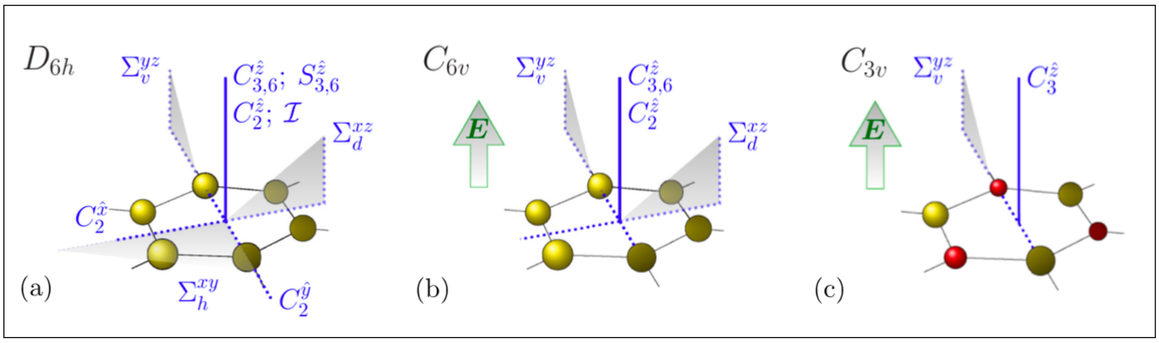

Figure 3.1: *Point-group symmetries of the honeycomb lattice. a) The bare hexagonal plaquette is characterised by the* D_{6h} *point symmetry group. b) Breaking of inversion symmetry about the 2D plane (e.g. by application of perpendicular electric field, or a substrate) reduces the point symmetry group* $D_{6h} \longrightarrow C_{6v}$*. c) If the sublattice symmetry is also broken, the symmetry group is further reduced* $C_{6v} \longrightarrow C_{3v}$*. The latter model is representative of graphene/TMD system we are interested in. Figure adapted from Ref.[5]*

3.1 The minimal clean Dirac-Rashba model

The effective low-energy Hamiltonian describing the electronic properties of 2D Dirac fermions in a clean system subject to a uniform Rashba interaction is (Appendix B)

$$H = \tau_z(\hbar v \boldsymbol{\sigma} \cdot \mathbf{k} + \lambda(\boldsymbol{\sigma} \times \boldsymbol{s}) \cdot \hat{z}), \tag{3.1}$$

where v is the bare velocity of massless Dirac fermions, $\mathbf{k} = -i\boldsymbol{\nabla}$ is the 2D momentum operator, λ is the SOC strength and τ_i, σ_i, s_i $(i = x, y, z)$ are Pauli matrices associated respectively with valley, sublattice (pseudospin) and spin DOFs. To simplify the notation, we use in the following discussion the natural units ($\hbar \equiv 1 \equiv e$). It is convenient to define the Hamiltonian density on a given valley K, K' associated with index $\tau_z = +1(-1)$. At this stage, to simplify the discussion, we also neglect intervalley scattering processes. Fixing the valley index $\tau_z = 1$, the Hamiltonian Eq.(3.1) can be rewritten as

$$H = (k_x \sigma_x + k_y \sigma_y) + \lambda \left(\sigma_x s_y - \sigma_y s_x\right), \tag{3.2}$$

where $v = 1$ for simplicity. For entire work we use the Clifford algebra [127, 128] to describe the system under study. It is generated by the product

$$\gamma_{\mu,\nu} = \sigma_\mu \otimes s_\nu, \tag{3.3}$$

where σ is the pseudospin and s the spin DOF. The momentum components are $k_x = k\cos(\theta)$ and $k_y = k\sin(\theta)$. We define the unit versor along the direction of the momentum $\hat{k} = (\cos(\theta), \sin(\theta))$ and the unit versor $\hat{\theta} = (-\sin(\theta), \cos\theta))$, which is perpendicular to

$\hat{k}$. Given the structure of the Hamiltonian Eq.(3.2), it is useful to define the following combinations of Pauli matrices

$$\sigma_k = \hat{k}\cdot\boldsymbol{\sigma}, \quad \sigma_\theta = \hat{\theta}\cdot\boldsymbol{\sigma}, \qquad s_k = \hat{k}\cdot\mathrm{s}, \quad s_\theta = \hat{\theta}\cdot\mathrm{s}. \tag{3.4}$$

Using the above relations, the Eq.(3.2) becomes

$$H = k\sigma_k + \lambda\left(\sigma_k s_\theta - \sigma_\theta s_k\right). \tag{3.5}$$

The eigenstates of σ_k that diagonalize the Hamiltonian in the absence of Rashba SOC are

$$|\pm 1\rangle_{\sigma_k} = \frac{1}{\sqrt{2}}\left(\begin{array}{c} 1 \\ \pm e^{i\theta} \end{array}\right), \tag{3.6}$$

while we define the eigenvalues of s_θ as

$$|\pm 1\rangle_{s_\theta} = \frac{1}{\sqrt{2}}\left(\begin{array}{c} 1 \\ \pm ie^{i\theta} \end{array}\right). \tag{3.7}$$

For sake of simplicity we call α and a the states of σ_k and s_θ respectively $(\alpha = \pm 1, a = \pm 1)$. By defining the direct product of states as

$$|\alpha, a\rangle \equiv |\pm 1, \pm 1\rangle = |\pm 1\rangle \otimes |\pm 1\rangle, \tag{3.8}$$

it is easy to see that

$$(k\sigma_k + \lambda\sigma_k s_\theta)\,|\alpha, a\rangle = (\alpha k + \alpha a\lambda)\,|\alpha, a\rangle. \tag{3.9}$$

We also note that the action of the other two matrices on these eigenstates is

$$\sigma_\theta|\alpha\rangle = -i\alpha|-\alpha\rangle, \qquad s_k|a\rangle = ia|-a\rangle. \tag{3.10}$$

From the above, it is clear that the last term of the Hamiltonian Eq.(3.5) couples the states defined in Eq.(3.8) in pairs: i) $|1,1\rangle, \quad |-1,-1\rangle$; ii) $|1,-1\rangle, \quad |-1,1\rangle$. In the first case the Hamiltonian reads

$$H_{4,2} = \left(\begin{array}{cc} \lambda + k & -\lambda \\ -\lambda & \lambda - k \end{array}\right)$$

and has eigenvalues $\epsilon_4 = \lambda + \sqrt{k^2+\lambda^2}$ and $\epsilon_2 = \lambda - \sqrt{k^2+\lambda^2}$. In the second case the Hamiltonian reads

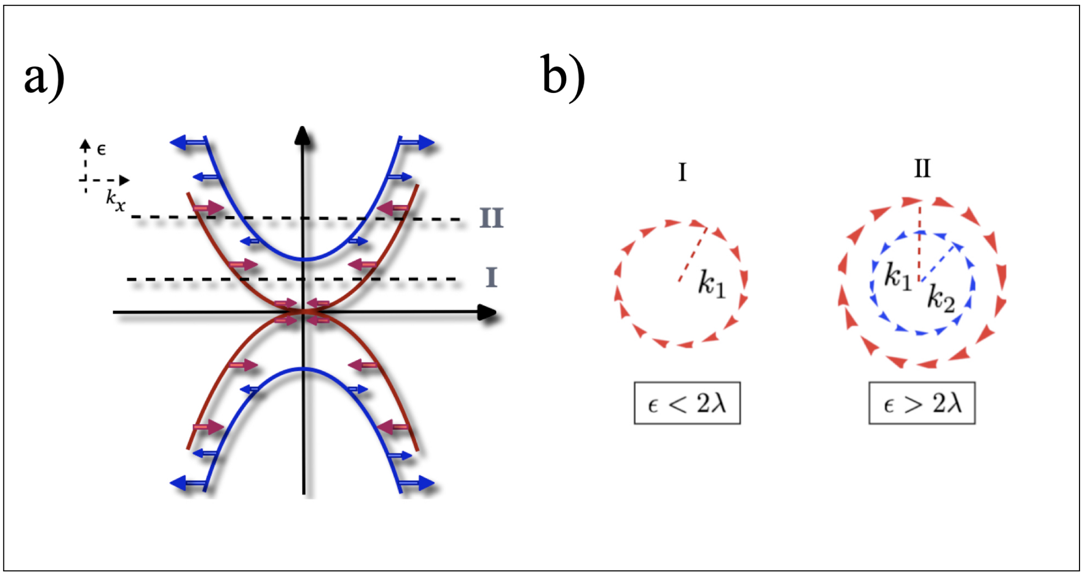

Figure 3.2: *a) Energy dispersion of the Dirac-Rashba model around the* $\mathcal{K}$ *point. The splitting of the Dirac bands leads to a spin gap or pseudogap of width* 2λ*. b) Tangential winding of the spin texture in regimes I and II.*

$$H_{3,1} = \begin{pmatrix} -\lambda + k & \lambda \\ \lambda & -\lambda - k \end{pmatrix}$$

and has eigenvalues $\epsilon_3 = -\lambda + \sqrt{k^2+\lambda^2}$ and $\epsilon_1 = -\lambda - \sqrt{k^2+\lambda^2}$. The subscripts of energy dispersion ($i = 1,2,3,4$) indicate the 4 bands of system under study as showed in the Fig.[3.2(a)]. It is now useful to define the coherence factors[1] as

$$u = \sqrt{\frac{1}{2}\left(1 + \frac{k}{\sqrt{k^2+\lambda^2}}\right)}, \qquad v = \sqrt{\frac{1}{2}\left(1 - \frac{k}{\sqrt{k^2+\lambda^2}}\right)}, \tag{3.11}$$

for which we have the following relations

$$u^2 - v^2 = \frac{k}{\sqrt{k^2+\lambda^2}}, \qquad 2uv = \frac{\lambda}{\sqrt{k^2+\lambda^2}}. \tag{3.12}$$

As a result we obtain the explicit relations of eigenvalues and eigenvectors as (they are numbered such that 1 is the lowest and 4 the highest in the energy scale)

$$\epsilon_4 = \lambda + \sqrt{k^2+\lambda^2}, \qquad |4\rangle = u|1,1\rangle - v|-1,-1\rangle,$$

---

[1] Note that $u^2 + v^2 = 1$.

$$\begin{aligned}
\epsilon_3 &= -\lambda+\sqrt{p^2+\lambda^2}, \quad |3\rangle = u|1,-1\rangle + v|-1,1\rangle, \\
\epsilon_2 &= \lambda-\sqrt{k^2+\lambda^2}, \quad\quad |2\rangle = v|1,1\rangle + u|-1,-1\rangle, \\
\epsilon_1 &= -\lambda-\sqrt{k^2+\lambda^2}, \quad |1\rangle = -v|1,-1\rangle + u|-1,1\rangle.
\end{aligned}$$

In the end the energy dispersion relation associated with the Hamiltonian Eq.(3.2) can be written

$$\epsilon_{ln}(\mathbf{k}) = l\lambda + n\sqrt{\lambda^2+|\mathbf{k}|^2}, \tag{3.13}$$

where $l,n=\pm 1$ represents the various subbands [see Fig.3.2(a)]. While the quantum index n is associated to the carrier polarity, $n=1$ ($n=-1$) for electrons (holes), l is related to the spin chirality of energy states. It is known that the Rashba interaction aligns the electron spin at right angles to the wavevector [51], the so-called spin-momentum locking configuration [see Fig.3.2(b)]. For Fermi energy $|\epsilon| > 2|\lambda|$ (region II), the split Fermi surface displays counter-rotating spin textures reminiscent of (non chiral) 2DEGs with Rashba interaction [123]. A regime (region I) where the Fermi energy intersects a single subband, with electronic states having well-defined spin helicity, extends for energy $|\epsilon| < 2|\lambda|$, which is strictly similar to the situation for surface states of TIs [129, 130]. In the conventional 2DEG this circumstance only happens at a single point, i.e. the intersection between the parabolic bands. For brevity of notation, we assume $\epsilon, \lambda > 0$ in the remainder of this work.

For the following discussion and explicit calculation of Green's function, we need to construct the projectors of the system to derive the self-energy and then the kinetic equation (see the Chapter 4). The projectors in terms of fermionic field are defined as

$$P_{ln}(\mathbf{k}) = |\psi(\mathbf{k})_{ln}\rangle\langle\psi(\mathbf{k})_{ln}| \tag{3.14}$$

with l,n the band indices an ψ the state. After some manipulation, they become (also shown schematically in the Table 3.1)

$$P_4 \equiv P_{11} = \tfrac{1}{4}\left(\sigma_0\otimes s_0+\sigma_k\otimes s_\theta\right)+\tfrac{u^2-v^2}{4}\left(\sigma_0\otimes s_\theta+\sigma_k\otimes s_0\right)-\tfrac{uv}{2}\left(\sigma_z\otimes s_z+\sigma_\theta\otimes s_k\right),$$

$$P_3 \equiv P_{1-1} = \tfrac{1}{4}\left(\sigma_0\otimes s_0-\sigma_k\otimes s_\theta\right)-\tfrac{u^2-v^2}{4}\left(\sigma_0\otimes s_\theta-\sigma_k\otimes s_0\right)+\tfrac{uv}{2}\left(\sigma_z\otimes s_z-\sigma_\theta\otimes s_k\right),$$

$$P_2 \equiv P_{-11} = \tfrac{1}{4}\left(\sigma_0 \otimes s_0 + \sigma_k \otimes s_\theta\right) - \tfrac{u^2-v^2}{4}\left(\sigma_0 \otimes s_\theta + \sigma_k \otimes s_0\right) + \tfrac{uv}{2}\left(\sigma_z \otimes s_z + \sigma_\theta \otimes s_k\right),$$

$$P_1 \equiv P_{-1-1} = \tfrac{1}{4}\left(\sigma_0 \otimes s_0 - \sigma_k \otimes s_\theta\right) + \tfrac{u^2-v^2}{4}\left(\sigma_0 \otimes s_\theta - \sigma_k \otimes s_0\right) - \tfrac{uv}{2}\left(\sigma_z \otimes s_z - \sigma_\theta \otimes s_k\right).$$

	$\sigma_0 \otimes s_0$	$\sigma_p \otimes s_\theta$	$\sigma_0 \otimes s_\theta$	$\sigma_p \otimes s_0$	$\sigma_z \otimes s_z$	$\sigma_\theta \otimes s_p$
P_{11}	1	1	u^2-v^2	u^2-v^2	$-2uv$	$-2uv$
P_{1-1}	1	-1	$-(u^2-v^2)$	(u^2-v^2)	$2uv$	$-2uv$
P_{-11}	1	1	$-(u^2-v^2)$	$-(u^2-v^2)$	$2uv$	$2uv$
P_{-1-1}	1	-1	$+(u^2-v^2)$	(u^2-v^2)	$-2uv$	$2uv$

Table 3.1: Clifford's algebra decomposition of projectors with $\hat{k}$ and $\hat{\theta}$ versor. A factor $1/4$ in front is omitted for the sake of simplicity. The columns represent the operators that appear in the Clifford's algebra decomposition. It is evident that all the columns sum up to zero except the one for the identity $\sigma_0 \otimes s_0$.

In certain circumstances, as the derivation of the kinetic equation reported in the Chapter 4, we need to take the average over the angle θ, i.e.

$$\langle \dots \rangle = \frac{1}{2\pi}\int_0^{2\pi} d\theta \dots \quad . \tag{3.15}$$

So, one obtains $\langle \sigma_k \rangle = 0, \langle \sigma_\theta \rangle = 0,\ \langle s_k \rangle = 0, \langle s_\theta \rangle = 0.$ In particular one has the following relations (in Table 3.2 we list the result of the averaged projectors)

$$\langle \sigma_k \otimes s_\theta \rangle = \langle \hat{k}_i \hat{\theta}_j \rangle \sigma_i \otimes s_j = \frac{1}{2}(\sigma_1 \otimes s_2 - \sigma_2 \otimes s_1) \equiv \frac{1}{2}\gamma_R \tag{3.16}$$

and

$$\langle \sigma_\theta \otimes s_k \rangle = \langle \hat{\theta}_i \hat{k}_j \rangle \sigma_i \otimes s_j = -\frac{1}{2}(\sigma_1 \otimes s_2 - \sigma_2 \otimes s_1) \equiv -\frac{1}{2}\gamma_R, \tag{3.17}$$

where γ_R is the Clifford's matrix defined as $\gamma_R = \sigma_1 \otimes s_2 - \sigma_2 \otimes s_1$.
In terms of the projectors, the momentum propagators are[2]

---

[2] Here we refer to the spectral theorem for which a linear operator or a matrix can be written in terms of system projectors.

	$\sigma_0 \otimes s_0$	$\gamma_R/2$	$\sigma_z \otimes s_z$	$-\gamma_R/2$
$\langle P_4 \rangle$	1	1	$-2uv$	$-2uv$
$\langle P_3 \rangle$	1	-1	$2uv$	$-2uv$
$\langle P_2 \rangle$	1	1	$2uv$	$2uv$
$\langle P_1 \rangle$	1	-1	$-2uv$	$2uv$

Table 3.2: Clifford's algebra decomposition of averaged projectors. Of course, also in this case, all the columns sum up to zero except the one for the identity $\sigma_0 \otimes s_0$.

$$G^{R(A)}(\mathbf{k},\omega) = \sum_{ln} \frac{P_{ln}(\mathbf{k})}{\omega - \epsilon_{ln}(\mathbf{k}) \pm i0^+}, \tag{3.18}$$

where $\epsilon_{ln}(\mathbf{k})$ is the energy dispersion given by the Eq.(3.13). In the next section we discuss the generalised Dirac-Rashba model. In this case other SOC and massive terms can be add to the minimal DR-Hamiltonian.

3.2 The generalised clean Dirac-Rashba model

We now focus on the C_{3v} model. In the broken sublattice-symmetry conditions, the bare Hamiltonian in Eq.(3.1) has to be supplemented by sublattice-resolved intrinsic SOC terms $\lambda_{zz}^{A,B}$, plus an orbital mass Δ. Re-introducing here for convenience the valley index, the associated Hamiltonian density reads

$$H = \tau_z(\boldsymbol{\sigma}\cdot\mathbf{k} + \lambda(\boldsymbol{\sigma}\times\boldsymbol{s})\cdot\hat{z} + \Delta\sigma_z) + \frac{(\sigma_z + \tau_z\sigma_0)s_z}{2}\lambda_{zz}^A + \frac{(\sigma_z - \tau_z\sigma_0)s_z}{2}\lambda_{zz}^B. \tag{3.19}$$

It is convenient to define the following parameters

$$\frac{\lambda_{zz}^A \pm \lambda_{zz}^B}{2} = \{\lambda_{zz}, \lambda_{sv}\}. \tag{3.20}$$

Whereas the average of $\lambda_{zz}^A, \lambda_{zz}^B$ yields the intrinsic SOC- compatible already with C_{6v} symmetry. A non vanishing difference between them encodes the broken sublattice symmetry, with the associated term commonly referred to as $spin-valley$ interaction. Making use of these newly-defined parameters, the Eq.(3.1) takes the form

$$H = \tau_z(\boldsymbol{\sigma}\cdot\mathbf{k} + \lambda(\boldsymbol{\sigma}\times\boldsymbol{s})\cdot\hat{z} + \Delta\sigma_z + \lambda_{sv}s_z) + \lambda_{zz}\sigma_z s_z. \tag{3.21}$$

The intrinsic-like SOC λ_{zz}, also known as Kane-Mele term [43], however is typically very small in graphene-based heterostructures of interest for this thesis and can therefore be ignored here [131]. The orbital sublattice-staggered potential ($\propto \Delta$) due to the proximity effect is believes to play a minor role in graphene/TMD bilayers and is neglected in the following discussion [132]. While λ_{sv} is the strength of spin-valley coupling which acts as a Zeeman interaction [133]. We focus only on this latter interaction. So that the Hamiltonian density for massive Dirac fermions with Rashba and spin-valley coupling under study reads (for a single valley)

$$H = \boldsymbol{\sigma} \cdot \mathbf{k} + \lambda(\boldsymbol{\sigma} \times \boldsymbol{s}) \cdot \hat{z} + \lambda_{sv}\sigma_0 s_z \tag{3.22}$$

and the corresponding eigenvalues can be written in a compact way as

$$\epsilon_{ln}(\mathbf{k}) = l\sqrt{k^2 + M_n^2}, \tag{3.23}$$

where $M_n = \sqrt{2\lambda^2 + \lambda_{sv}^2 + 2n\sqrt{\lambda^4 + k^2(\lambda^2 + \lambda_{sv}^2)}}$ and $l, n = \pm 1$ label polarity and spin as before. It is easy to see that one recover the energy dispersion Eq.(3.13) if $\lambda_{sv} \longrightarrow 0$. Inverting the Eq.(3.23) and evaluating the energy dispersion at the chemical potential $\epsilon_{ln} = \varepsilon$, one obtains the generic expression of the Fermi momentum $k_{ln} = k(\epsilon_{ln} = \varepsilon)$ in terms of SOC constants, i.e.

$$k = \sqrt{\lambda_{sv}^2 + \varepsilon^2 \pm 2\sqrt{-\lambda^2\lambda_{sv}^2 + \lambda^2\varepsilon^2 + \lambda_{sv}^2\varepsilon^2}}. \tag{3.24}$$

Writing the momentum as a plane wave $\mathbf{k}_{ln} = k_{ln}(\cos(\theta), \sin(\theta))$, the eigenvector has the following dependence on it

$$\Phi(k_{ln}, \theta) = \begin{pmatrix} e^{-i\theta} \\ i\alpha \\ \beta \\ i\gamma e^{i\theta} \end{pmatrix} \tag{3.25}$$

with

$$\alpha = \frac{(\epsilon_{ln} - \lambda_{sv})^2 - k_{ln}^2}{2\lambda k_{ln}}, \qquad \beta = \frac{\epsilon_{ln} - \lambda}{k_{ln}}, \qquad \gamma = \frac{(\epsilon_{ln} - \lambda_{sv})^2 - k_{ln}^2}{2\lambda(\epsilon_{ln} + \lambda_{sv})}. \tag{3.26}$$

Due to the particle-hole symmetry of the energy dispersion Eq.(3.23), in the pure Dirac-Rashba model there are only two bands crossing the Fermi energy ε [see Fig.3.2]. Otherwise the presence of a non-zero spin-valley coupling generates a Mexican hat dispersion as shown

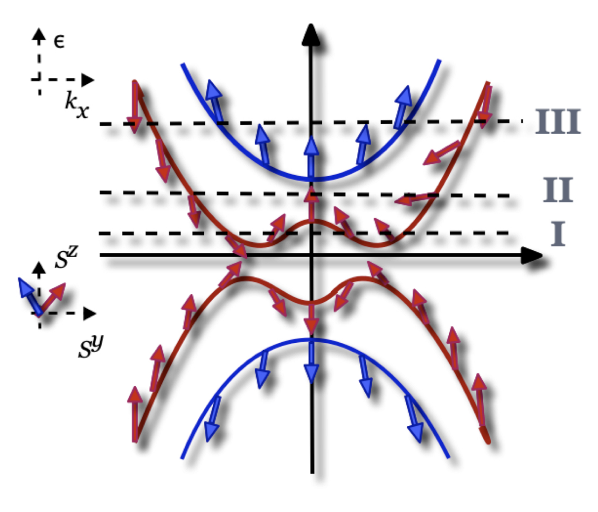

Figure 3.3: Energy bands and spin texture in systems with spin-valley coupling. As result a gap is opened and the Dirac spectrum at the Fermi energy, is splitted into 3 branches: regions I, II and III. For visualisation purposes, the bands are plotted along k_x (spins lie only in the yz plane).

in Fig.[3.3]. The spin-valley coupling opens a gap and splits the Dirac spectrum, at the Fermi energy, into 3 branches. In the Chapter 6, we focus only in one of the regime when the Fermi energy ε is in the range

$$\lambda_{sv} < \varepsilon < \sqrt{4\lambda^2 + \lambda_{sv}^2}, \tag{3.27}$$

i.e. the so called regime II in the Fig [3.3]. In this case only one band, ($l = 1$, $n = -1$) crosses the Fermi energy with one Fermi momentum (k_{1-1} as given in the Eq.(3.24)). In the Chapter 6 we use the formalism here presented to derive the kinetic equation for the quasiclassical Green's function. This system parameterization will be useful to write all physical quantities in a very compact way.

Conclusions

In this chapter we have presented a convenient way to diagonalize the Dirac-Rashba Hamiltonian not previously reported in the recent literature. We made use of the Clifford's algebra to do that and recover the well-known energy dispersion relation associated to the Dirac-Rashba Hamiltonian. Thanks to this, we have been able to write the projectors of such a system. Then, using the Clifford's algebra decomposition of projectors, the momentum propagators are defined. After, we discussed briefly the generalised Dirac-Rahsba model with all intrinsic SOC and massive terms. In particular we went deeper in the Dirac-Rashba Hamiltonian with spin-valley coupling that reduces the symmetries of the system $C_{6v} \longrightarrow C_{3v}$. The parameterization here presented for such a system is very compact and easy to manipulate. In fact, we were able to write eigenvector and eigenstates with a simple algebra that will be useful to derive the kinetic equation in the following.

4

The first steps: from Dirac fermions to graphene

Overview

In this Chapter we want to prove the consistency of the quasiclassical approximation. We start from a simple system like the massive Dirac fermions. This means to consider only the orbital sublattice-staggered potential, i.e. the massive term, without intrinsic- or extrinsic-like SOC. This represents the minimal model to see the anomalous Hall effect (AHE). The idea is to derive the physical observable from both the kinetic equations and verify that the results coincide. As shown in the Chapter 2, starting from the Hamiltonian operator, we are able to write both the BTE and Eilenberger equations. For the system under study, we evaluate the physical current, i.e. the Hall current, in the clean and stationary system using both approach. Furthermore, we show the preparatory calculation with the density matrix because it helps to understand some physical features useful for the more complex case with SOC. In particular, we learn how manipulate all the component of the density matrix function and which of these gives the proper result. In fact, thanks to it, we are able to derive the well-known result for the spin Hall conductivity in the 2D Dirac-Rashba model only selecting the perpendicular component of the density matrix function. The spin Hall result differs from zero despite the stationary model we are studying. As we shall discuss below, this is not in contradiction with the conservation law for the spin current and it can be physically explained.

4.1 The kinetic equations for Dirac fermions

We can start from a simple model of the massive Dirac fermions without intrinsic- or extrinsic-like SOC. This means $\Delta \neq 0$ and $\lambda = \lambda_{sv} = 0$ in the Eq.(3.21), i.e. only an orbital sublattice-staggered potential due to the proximity effect is taken into account. This minimal model has both ingredient to see the AHE, i.e. the magnetization ($\propto \Delta$) and the spin-orbit interaction. The former breaks time-reversal symmetry and exerts a force acting on electron spins while the latter couples the spins to orbital DOF thus giving rise to the transport effect. Many ferromagnetic materials exhibit this finite Hall effect, i.e. transverse voltage in response to a current, without applying external magnetic field [134]. So that quite generally the Hamiltonian operator takes the form (for a single valley)

$$H = \boldsymbol{\sigma} \cdot (-i\boldsymbol{\nabla}) + \Delta\sigma^z + e\boldsymbol{\sigma} \cdot \mathbf{A}(\mathbf{r},t) - e\Phi(\mathbf{r},t), \tag{4.1}$$

where as known $\mathbf{k} = -i\boldsymbol{\nabla}$. The fermions velocity is v and Δ is their mass. Φ and $\mathbf{A}$ are the electromagnetic scalar and vector potential respectively. As a first simple example that shows how the formalism works, we study a stationary system with a uniform and constant external field along the x-direction, i.e

$$\mathbf{E} = (E_x, 0, 0), \qquad \mathbf{B} = (0,0,0) \tag{4.2}$$

for which the Hamiltonian Eq.(4.1) becomes

$$H = v(-i\boldsymbol{\nabla} \cdot \boldsymbol{\sigma}) + \Delta\sigma^z + e\mathbf{E} \cdot \mathbf{r}. \tag{4.3}$$

Now, it is easy to write the Hamiltonian density vector of the Eq.(4.3) as

$$h(\mathbf{k}) \equiv \mathbf{h}_{\mathbf{k}} = (vk_x, vk_y, \Delta). \tag{4.4}$$

Inserting the Hamiltonian density vector Eq.(4.4) in the Eqs.(2.60) and (2.66), one obtains the BTE and the Eilenberger equation respectively for the Dirac fermions system. In the following, we study first the clean case and than we add the Rashba SOC in the Boltzmann kinetic equation. For the clean case, we also discuss the quasiclassical approximation in order to prove the equivalence between the two approaches.

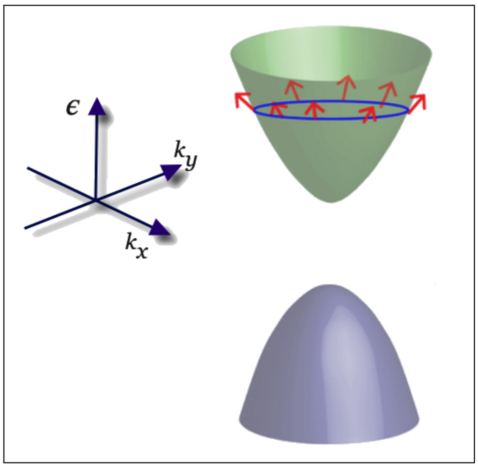

Figure 4.1: Schematic diagram of the band structure and spin orientation for massive Dirac fermions. The presence of a massive term opens a gap between the valence and the conduction band.

4.1.1 The linearized BTE

In this section, we find the Hall conductivity with the kinetic equation for the density distribution function in the simple clean model (no disorder and SOC). As mentioned in the Chapter 2 on the linearized BTE Eq.(2.10), the matrix distribution function for systems slightly out of equilibrium will be of the form $f = f_{eq} + \delta f$, where f_{eq} describes a state of local equilibrium [135]. Assuming that f vanishes at $\pm\infty$, the Boltzmann kinetic equation for such a system reads

$$-e\mathbf{E}\cdot\boldsymbol{\nabla}_{\mathbf{k}} f_{eq} + i[\mathbf{h}_{\mathbf{k}}\cdot\boldsymbol{\sigma}, \delta f] = 0, \tag{4.5}$$

where $\mathbf{h}_{\mathbf{k}}$ is the Hamiltonian density vector Eq.(4.3). Using the spectral theorem for the equilibrium density matrix f_{eq}, we have

$$f_{eq}(\mathbf{k}) = \sum_l P_l(\mathbf{k}) f_{FD}(\epsilon_l(k) - \varepsilon), \tag{4.6}$$

where $P_l(\mathbf{k})$ are the projectors of the two bands [see Fig.4.1] of the system with index $l = \pm 1$ and ε is the Fermi energy. ϵ_l are the corresponding eigenvalues. For the Hamiltonian Eq.(4.3) one has two eigenvalues which we call $\epsilon_{+1,-1} \equiv \pm h$, so that at $T = 0$ one obtains

$$f_{eq}(\mathbf{k}) = \frac{\sigma^0 + \hat{\mathbf{h}}_{\mathbf{k}}\cdot\boldsymbol{\sigma}}{2}\Theta(h - \varepsilon) + \frac{\sigma^0 - \hat{\mathbf{h}}_{\mathbf{k}}\cdot\boldsymbol{\sigma}}{2}\Theta(-h - \varepsilon), \tag{4.7}$$

where $\Theta(\pm h - \varepsilon)$ is the well-known Heaviside function and $\hat{\mathbf{h}}_{\mathbf{k}} = \mathbf{h}_{\mathbf{k}}/\mathrm{h}_{\mathrm{k}}$ the versor. If $\varepsilon > 0$, the function $\Theta(-h - \varepsilon) = 1$, then

$$\nabla_{\mathbf{k}} f_{eq}(\mathbf{k}) = \nabla_{\mathbf{k}}(\hat{\mathbf{h}_{\mathbf{k}}}\cdot\boldsymbol{\sigma})\frac{\Theta(\varepsilon-h)-1}{2} + \frac{\sigma^0+\hat{\mathbf{h}_{\mathbf{k}}}\cdot\boldsymbol{\sigma}}{2}\delta(\varepsilon-h)(-\nabla_{\boldsymbol{k}}h) \tag{4.8}$$

and

$$\nabla_{\mathbf{k}}(\hat{\mathbf{h}_{\mathbf{k}}}\cdot\boldsymbol{\sigma}) = \nabla_{\mathbf{k}}\left(\frac{{\mathrm{h}_{\mathrm{k}}}^{i}\sigma^{i}}{\mathrm{h}_{\mathrm{k}}}\right) = -\frac{\mathbf{h}_{\mathbf{k}}}{{\mathrm{h}_{\mathrm{k}}}^{3}}\mathrm{h}^{\mathrm{i}}_{\mathrm{k}}\sigma^{i} + \frac{1}{\mathrm{h}_{\mathrm{k}}}\nabla_{\mathbf{k}}({\mathrm{h}_{\mathrm{k}}}^{i}\sigma^{i}). \tag{4.9}$$

Now, we can project the kinetic equation Eq.(4.5) in the basis of Pauli matrices, i.e. $\delta f = \delta f^0\sigma^0 + \boldsymbol{\delta f}\cdot\boldsymbol{\sigma}$ and choose only the vectorial component (we are interested in the current physical response). Using the commutation property $[\boldsymbol{a}\cdot\boldsymbol{\sigma},\boldsymbol{b}\cdot\boldsymbol{\sigma}] = 2i(\boldsymbol{a}\times\boldsymbol{b})\cdot\boldsymbol{\sigma}$, we find the following simple equation of motion

$$\boldsymbol{c} = 2\mathbf{h}_{\mathbf{k}}\times\boldsymbol{\delta f}, \tag{4.10}$$

where $\boldsymbol{c} = -e\mathbf{E}\cdot\nabla_{\mathbf{k}} f_{eq}$ represents the vector of known terms. Multiplying both side of equation by the vector $\mathbf{h}_{\mathbf{k}}$ we can write[1]

$$\mathbf{h}_{\mathbf{k}}\times\boldsymbol{c} = \mathbf{h}_{\mathbf{k}}\times\mathbf{h}_{\mathbf{k}}\times\boldsymbol{\delta f} = -{\mathrm{h}_{\mathrm{k}}}^{2}(\boldsymbol{\delta f} - \hat{h}(\hat{h}\cdot\boldsymbol{\delta f})). \tag{4.11}$$

The right hand side term of Eq.(4.11) selects only the "perpendicular" component of $\boldsymbol{\delta f}$. The product $\hat{h}(\hat{h}\cdot\boldsymbol{\delta f})$ defines the "parallel" one. In particular, this means we have to subtract the parallel part from the total equilibrium density matrix. From this point of view, the δ-term of the Eq.(4.8) disappears and the kinetic equation becomes ($\boldsymbol{\delta f}\equiv\boldsymbol{\delta f}_{\perp}$)

$$e\frac{(1-\Theta(\varepsilon-h))}{2}\mathbf{E}\cdot\left(\nabla_{\mathbf{k}}\frac{\mathbf{h}_{\mathbf{k}}}{\mathrm{h}_{\mathrm{k}}}\right) = 2\mathbf{h}_{\mathbf{k}}\times\boldsymbol{\delta f}. \tag{4.12}$$

Following the strategy discussed before with the field choice Eq.(4.2), i.e $\mathbf{E} = E\hat{x}$ one has

$$\boldsymbol{\delta f} = -\frac{e}{4}\frac{\mathbf{h}_{\mathbf{k}}}{{\mathrm{h}_{\mathrm{k}}}^{3}}(1-\Theta(\varepsilon-h))(\mathbf{E}\cdot\nabla_{\mathbf{k}}\mathbf{h}_{\mathbf{k}}) = -\frac{e}{4}(1-\Theta(\varepsilon-h))E\frac{\mathbf{h}_{\mathbf{k}}\times\hat{x}}{{\mathrm{h}_{\mathrm{k}}}^{3}}v, \tag{4.13}$$

where $\boldsymbol{v} = \nabla_{\mathbf{k}}\mathbf{h}_{\mathbf{k}} = v\boldsymbol{\sigma}$. To derive the (anomalous) Hall response, we select the y-component of density matrix function

---

[1] Here we use the property $\boldsymbol{a}\times\boldsymbol{b}\times\boldsymbol{c} = \boldsymbol{b}(\boldsymbol{a}\cdot\boldsymbol{c}) - \boldsymbol{c}(\boldsymbol{a}\cdot\boldsymbol{b})$

$$\boldsymbol{\delta f}_y = -\frac{evE}{4}(1-\Theta(\varepsilon-h))\frac{\mathrm{h_z}}{\mathrm{h_k}} = \frac{evE}{4}(1-\Theta(\varepsilon-h))\frac{\Delta}{(v^2\mathbf{k}^2+\Delta^2)^{3/2}} \tag{4.14}$$

and using the Eq.(2.12), the physical current density reads

$$j_y = (-e)v\int\frac{d\mathbf{k}}{(2\pi)^2}2\boldsymbol{\delta f}_y, \tag{4.15}$$

where the factor 2 takes into account the sum over spin DOF. If one call $t=\sqrt{v^2\mathbf{k}^2+\Delta^2}$, after some manipulation one obtains

$$j_y = \frac{e^2E}{2}\frac{\Delta}{2\pi}\int_\Delta^\infty\frac{dt}{t^2}(1-\Theta(\varepsilon-t)) = \frac{e^2}{4\pi}\frac{\Delta}{\varepsilon}E \equiv \sigma_y E. \tag{4.16}$$

In the Eq.(4.16), j_y defines the Hall current according to the chosen geometry. It is written in response to the electric field where σ_y is the intrinsic component of the anomalous Hall conductivity [134]. In the end we demonstrate only selecting the perpendicular component of density matrix $\boldsymbol{\delta f}$, one can recover the proper result. This gives us information about the possibility to neglect some term of the density matrix in order to have the right description of our system of interest. In the next section we perform the calculation of Hall current for the same system but with the help of the quasiclassical approximation.

4.1.2 The Eilenberger equation

In the following we show the kinetic equation for the quasiclassical Green's function $\check{g}(\varepsilon,\mathbf{k}) \equiv g$ in the same clean and stationary system. This calculation aims to verify the equivalence between the Boltzmann and the Eilenberger equation. As done in the previous section for the density matrix, we write the linearized Eilenberger equation for $g = g_{eq}+\delta g$ as

$$i[\mathbf{h}_F\cdot\boldsymbol{\sigma},\delta g] - \frac{1}{2}\{ev\boldsymbol{\sigma}\cdot\mathbf{E},\partial_\omega g_{eq}\} = 0, \tag{4.17}$$

where $\mathbf{h}_F$ is the density Hamiltonian at the Fermi level and ω is the energy. Note that the integration over the variable ξ automatically sets the physical quantities at the Fermi energy, by definition. In equilibrium, the quasiclassical Green's function in terms of the upper band projector[2] reads (we assume positive Fermi energy as usual)

$$g_{eq}(\omega) = 2\tanh\left(\frac{\omega}{2T}\right)\frac{\sigma^0+\hat{\mathrm{h}}_\mathrm{F}\cdot\boldsymbol{\sigma}}{2}. \tag{4.18}$$

---

[2] For the massive Dirac fermions system under study the projectors of the two bands are $P_\pm = \frac{\sigma^0\pm\hat{\mathrm{h}}_\mathrm{F}\cdot\boldsymbol{\sigma}}{2}$, where ± indicates the upper and the lower band respectively [119, 136].

Following the procedure shown in the previous section, we project the quasiclassical Green's function in the basis of Pauli matrices and choose only the vectorial component $\boldsymbol{\delta}\mathbf{g}$. Setting $\mathbf{E} = E\hat{x}$, one has

$$-2\mathbf{h}_F \times \boldsymbol{\delta}\mathbf{g} - \frac{evE}{2}\partial_\omega \tanh\Big(\frac{\omega}{2T}\Big)\hat{x} = 0. \tag{4.19}$$

Using the commutation property already mentioned and multiplying both side by vector $\mathbf{h}_F$, we obtain the following equation

$$-2\mathbf{h}_F \times \mathbf{h}_F \times \boldsymbol{\delta}\mathbf{g} = \frac{evE}{2}\partial_\omega \tanh\Big(\frac{\omega}{2T}\Big)\mathbf{h}_F \times \hat{x}. \tag{4.20}$$

Performing the vectorial product, we automatically select the perpendicular component. So the relation for the quasiclassical Green's function $\boldsymbol{\delta}\mathbf{g}_\perp$ becomes

$$\boldsymbol{\delta}\mathbf{g}_\perp = \frac{evE}{4}\partial_\omega \tanh\Big(\frac{\omega}{2T}\Big)\frac{\mathbf{h}_F \times \hat{x}}{\mathrm{h}_F^2}. \tag{4.21}$$

At this stage, take into account the density Hamiltonian vector Eq.(4.4) and setting the Fermi energy $\mathrm{h}_F \equiv \varepsilon$, we can write the y-component of the quasiclassical Green's function in the form

$$\delta g_y = \frac{evE}{4}\partial_\omega \tanh\Big(\frac{\omega}{2T}\Big)\frac{\Delta}{\varepsilon^2}. \tag{4.22}$$

According to the Eq.(2.69), the current density along the y-direction becomes

$$j_y = (-e)\Big(-\frac{N_F}{2}\Big)\int d\omega v \delta g_y = \frac{e\varepsilon v}{4v^2\pi}\Big(evE\frac{\Delta}{\varepsilon^2}\Big) = \frac{e^2}{4\pi}\frac{\Delta}{\varepsilon}E, \tag{4.23}$$

where $N_F = \varepsilon/2\pi v^2$ is the density of the states (DOS) at the Fermi level. This result coincides with the Eq.(4.16) and confirms the consistence of the quasiclassical approximation.

In the next section we go further in the calculation and move on the Dirac-Rashba model without disorder. For such a system we find the spin Hall conductivity reported in the literature using the components manipulation here discussed.

4.2 Dirac-Rashba model with the density matrix

In this section, we show the density matrix evaluation of the spin Hall conductivity for graphene with Rashba spin-orbit interaction in the same stationary and clean system. The method is similar to one explained in the Section 4.1.1 for f. From the Eq.(3.21), the density

Hamiltonian in the presence of Rashba interaction $\lambda \neq 0$ is (we consider as usual single valley $\tau_z = 1$ and $v = 1$ for simplicity)

$$H^{RSC} = (\sigma_x k_x + \sigma_y k_y) + \lambda(\sigma_x s_y - \sigma_y s_x). \tag{4.24}$$

Of course, the kinetic equation for the density matrix function is in the form of the Eq.(4.5), i.e.

$$-e\mathbf{E} \cdot \boldsymbol{\nabla}_{\mathbf{k}} f_{eq} + i[H^{RSC}, \delta f] = 0, \tag{4.25}$$

where now the equilibrium distribution function can be written as

$$f_{eq}(\mathbf{k}) = \sum_{ln} P_{ln}(\mathbf{k}) f_{FD}(\epsilon_{ln}(\mathbf{k}) - \varepsilon), \tag{4.26}$$

with $P_{ln}(\mathbf{k}) = |\Phi(\mathbf{k},\theta)_{ln}\rangle\langle\Phi(\mathbf{k},\theta)_{ln}|$ the projector corresponding to the eigenvalue with indices ln. Here the eigenstates are given by the Eq.(3.23) with $\lambda_{sv} = 0$. The index $l,n = \pm 1$ label the eigenstates ϵ_{ln} reported in the Eq.(3.25). As done before we set the chemical potential as positive, i.e. $\varepsilon > 0$. From the kinetic equation Eq.(4.25), it is evident that the parallel component of δf commutes with the Hamiltonian. This means that only the perpendicular part of the derivative of the equilibrium function Eq.(4.26) has to be selected, i.e.[3]

$$\partial_{\mathbf{k}} f_{eq}^{(y)}(\mathbf{k}) = \sum_{ln} (\partial_{\mathbf{k}} P_{ln}) f_{FD}. \tag{4.27}$$

Both $f = f_{eq} + \delta f$ and $H^{RSC} \equiv H$ live in the matrix space. Let $\{t^a\}$ be a basis in the space of $N \times N$ matrices, we project the Eq.(4.25) on this basis[4]

$$-e\mathbf{E} \cdot \boldsymbol{\nabla}_{\mathbf{k}} t^a f_{eq}^a + \frac{i}{N} \mathrm{Tr}\Big([t^a, H] t^b\Big) \delta f^b = 0, \tag{4.28}$$

where

$$f_{eq} = \sum_a t^a f_{eq}^a, \qquad \delta f = \sum_b t^b \delta f^b. \tag{4.29}$$

---

[3] The total derivative of equilibrium distribution function reads $\partial_{\mathbf{k}} f_{eq}^{(y)}(\mathbf{k}) = \sum_{ln} (\partial_{\mathbf{k}} P_{ln}) f_{FD} + \sum_{ln} P_{ln} (\partial_{\mathbf{k}} f_{FD})$. Of course, the second term commutes with H^{RSC} because the projectors and the Hamiltonian are in the same basis and this automatically defines the parallel component of f_{eq}.

[4] In this passage we consider the identity $\mathrm{Tr}(A[B,C]) = \mathrm{Tr}(ABC - ACB) = \mathrm{Tr}([A,B],C)$.

In the space of 4×4 matrices, t^a is referred to the Clifford's algebra previously defined in the Eq.(3.3). If one consider $t^y \equiv \sigma_0 \otimes s_y$, i.e. the spin operator along y-direction, the commutator term of the Eq.(4.28) becomes

$$[\sigma_0 \otimes s_y, H] = -\lambda[s_y, \sigma_y s_x] = i2\lambda\sigma_y \otimes s_z. \tag{4.30}$$

Then the kinetic equation reads

$$-e\mathbf{E} \cdot \boldsymbol{\nabla}_{\mathbf{k}} f^{(y)}_{eq} - 2\lambda\delta f^{(yz)} = 0 \tag{4.31}$$

or

$$\delta f^{(yz)} = -\frac{e\mathbf{E} \cdot \boldsymbol{\nabla}_{\mathbf{k}}}{2\lambda} f^{(y)}_{eq}. \tag{4.32}$$

According to the Eq.(2.12), the physical spin current along y-direction and with z-polarization reads (here we renintroduce the velocity v)

$$j^z_y = v \int \frac{d\mathbf{k}}{(2\pi)^2} 2\delta f^{(yz)} = -\frac{ev}{\lambda} \int \frac{d^2\mathbf{k}}{(2\pi)^2} \mathbf{E} \cdot \boldsymbol{\nabla}_{\mathbf{k}} f^{(y)}_{eq}, \tag{4.33}$$

where the factor 2 takes into account the sum over the spin DOF. As done in the Section 4.1.1, using the field choice Eq.(4.2), the spin Hall conductivity is

$$\sigma^z_{yx} = -\frac{ev}{\lambda} \int \frac{d\mathbf{k}}{(2\pi)^2} \partial_{k_x} f^{(y)}_{eq} \tag{4.34}$$

and by looking at the Eq.(4.27), we need the explicit form of projector $P^{(y)}_{ln}$ (or in the Clifford's sense $P^{(02)}_{ln}$). According to what reported in the Section 3.1, the y-component of projector reads[5]

$$P^{(y)}_{ln}(k) = \frac{1}{4} \sum_{ln} ln(u^2 - v^2)\sigma_0 \otimes (\hat{\theta} s_y) = \frac{1}{4} \sum_{ln} ln \frac{vk}{\sqrt{v^2 k^+ \lambda^2}} cos(\theta), \tag{4.35}$$

where we use the definition of coherence factor Eq.(3.12) and $\tan(\theta) = k_y/k_x$. As a consequence, the Eq.(4.34) becomes

$$\sigma^z_{yx}(\mathbf{k}) = -\frac{ev}{\lambda} \int \frac{d\mathbf{k}}{(2\pi)^2} \frac{1}{4} \sum_{ln} \partial_{k_x} \left(ln \frac{v}{\sqrt{v^2 k^2 + \lambda^2}} k_x \right) f_{FD}(\epsilon_{ln}(\mathbf{k}) - \varepsilon). \tag{4.36}$$

---

[5] Note that our Hamiltonian parameterization gives the same results reported in literature [127, 128], i.e. the $\sigma_0 \otimes s_2$-projector reads $P^{(02)}_{ln} = \sum_{ln} ln \frac{1}{cosh(\theta_l)} cos(\theta)$, where $\theta_l = arcsinh(-l\lambda/vk)$.

In the $T \longrightarrow 0$ limit, the Fermi-Dirac function reduces to the Heaviside-theta function. For $\varepsilon > 0$, the contribution from the fully occupied bands vanishes so that $\Theta(\varepsilon - l\lambda + \sqrt{v^2k^2 + \lambda^2}) = 1$ for both $l = \pm 1$ where $n = 1$. After the angle average and the integration, one finds the spin Hall conductivity in agreement with the Ref.[127, 137], i.e.

$$\sigma^z_{yx} = -\frac{e}{16\pi\lambda}\Big[\frac{\varepsilon(\varepsilon+2\lambda)}{\varepsilon+\lambda} - \Theta(\varepsilon-2\lambda)\frac{\varepsilon(\varepsilon-2\lambda)}{\varepsilon-\lambda}\Big], \tag{4.37}$$

where the Heaviside step function takes into account the regime outside the pseudogap, while is zero when $0 < \epsilon < 2\lambda$. This result needs a comment. We recall here the covariant conservation law of the spin current for the 2DEGs subject to a uniform Rashba interactions [138]. The spin-y component satisfies the following relation

$$\partial_t \boldsymbol{j}^y_0(\mathbf{x},t) + \partial^i \boldsymbol{j}^y_i(\mathbf{x},t) = -2\lambda m \boldsymbol{j}^z_y(\mathbf{x},t), \tag{4.38}$$

where j^a_0 $(a = x, y, z)$ is the spin density, j^a_i is the pure spin current flowing in the $i = x, y$ direction and m is the effective electron mass. The main difference with respect to the charge continuity equation originates from the non-Abelian nature of spin. The Eq.(4.38) suggests that, in the steady state of a homogeneous system, j^z_y is zero. The apparent contradiction of the finite result Eq.(4.37) for the spin Hall conductivity[6] is resolved by recalling that, without disorder, there is no true stationary state. The electric field $\mathbf{E}$ transfers energy to the electrons which are accelerated. In order to obtain a zero conductivity, some relaxation mechanism needs. In fact, the suppression of the SHE occurs in the presence of an arbitrary small concentration of scalar impurities. Formally, the disorder corrections resulting from the resummation of ladder diagrams exactly cancel the "clean" spin Hall conductivity [139–141]. In the Chapter 5 we discuss the presence of disorder in the 2D Dirac-Rashba model for which the spin Hall response vanishes. In the end, the evaluation reported in the Section 4.1 on the massive Dirac-fermions tells us how manipulate all the components of the density matrix. In the following we add some comments on the finite result given by the Eq.(4.37) showing some interesting feature.

4.2.1 About the spin Hall conductivity

The spin Hall conductivity in the absence of disorder found in the previous section and reported in the Eq.(4.37) has two contributions. The first term in the square bracket is due to the $3rd-$band, i.e. ϵ_{1-1} as given in the Eq.(3.23). While the second term is due to the $4th$-band, i.e. ϵ_{11}. For both bands one can divide the contribution in two terms, or rather (we omit the electrical charge e for simplicity)

---

[6] The finite result for σ^z_{yx} is also found using the linear response theory [127, 128, 137].

$$\sigma_{sH}^{(3)} = -\frac{\varepsilon}{16\pi\lambda}\frac{\varepsilon+2\lambda}{\varepsilon+\lambda} = -\frac{1}{16\pi}\frac{\varepsilon}{\lambda} - \frac{1}{16\pi}\frac{\varepsilon}{\varepsilon+\lambda} \tag{4.39}$$

and

$$\sigma_{sH}^{(4)} = -\frac{\varepsilon}{16\pi\lambda}\frac{\varepsilon-2\lambda}{\epsilon-\lambda} = \frac{1}{16\pi}\frac{\varepsilon}{\lambda} - \frac{1}{16\pi}\frac{\varepsilon}{\varepsilon-\lambda}. \tag{4.40}$$

According to the Streda equation [142] as discussed in the Chapter 2, we have two contributions to the spin Hall conductivity. The contribution proportional to the Fermi energy ($\propto \varepsilon$) describes the processes "far" from the Fermi surface (σ^{II}), whereas the second term ($\propto \varepsilon/(\varepsilon \pm \lambda)$) is due to processes "at" the Fermi surface (σ^{I}). It is easy to note that $\sigma^{II} = 0$ while

$$\sigma^{I} = -\frac{1}{8\pi}\frac{\epsilon^2}{\epsilon^2-\lambda^2}. \tag{4.41}$$

This discussion is consistent with what reported in Ref.[127]. The ω-integration first, which leads to the equation for the density matrix, reproduces the Eq.(4.37). On the other hand the ξ-integration, which leads to the equation for the quasiclassical Green's function, captures the processes "at" the Fermi surface. The reason why the ξ-integration only gets the contribution σ^{I} is evident from the expression of σ^{II} Eq.(2.25), that for spin Hall observable reads [127]

$$\sigma_{sH}^{II} \propto Re(Tr[G^R(\epsilon) j_y^z \partial_k G^R(\epsilon) v_x]), \tag{4.42}$$

where $v_x = v\sigma_1 s_0$ is the bare charge current vertex. The Eq.(4.42) contains only retarded Green's functions and would give zero upon residue integration. On the contrary, the type I contribution to the conductivity Eq.(2.24) results to be

$$\sigma_{sH}^{I} \propto Tr[j_y^z G^R(\epsilon) v_x \partial_k G^A(\epsilon)], \tag{4.43}$$

for which the residue integration of the retarded/advanced combination of Green's function doesn't give zero. This explains why only the σ^{I} contribution does not vanish after integration over ξ. This observation is very important to understand the results obtained with the quasiclassical approximation which we will discuss in the next Chapters.

Conclusions

In this chapter we have briefly exposed how to derive the kinetic equations for the massive Dirac fermions. In particular, the Hall conductivity in the clean and stationary system is obtained using the linearized BTE. According with the chosen geometry, we found the well-known linear relation between the current and the external field. In order to obtain the proper result, we showed that one has to select only one component of the density matrix. Using the same procedure, we derive the spin density current with the Eilenberger equation selecting only the "perpendicular" component of the quasiclassical Green's function. The agreement between the two obtained results confirms the consistence of the quasiclassical approximation. What we have learned so far help us to study a quite complicated system, i.e. the massive Dirac fermions with Rashba SOC. In the same clean and stationary condition, we performed the calculation for the physical spin current with the linearized BTE. As done for the massive Dirac fermions, we neglected the "parallel" component of the equilibrium density matrix. By doing this, we obtained the spin Hall conductivity result reported in the recent literature. In particular the type II contribution to the conductivity is zero according to the Ref.[127], while the total σ^I (outside the pseudogap $\epsilon > 2\lambda$) without disorder does not vanish, as expected. This can be explained by recalling that there is not a true stationary state in such a system without disorder and this is not in contradiction with the covariant conservation law for the spin current.

5

The disorder effects

Overview

In the following we describe the disorder effects in the transport equation. The presence of disorder breaks the translation invariance that is restored only after the average over all possible impurity configurations. In order to consider all the possible diagrams, the well-known $\mathrm{T}-$matrix approximation is presented thanks to which we are able to write all the components of the self-energy in the Keldysh technique. To do that, one needs the disordered-average Green's function. We choose the so-called white noise potential, i.e. a scalar impurities point-like random potential, for which the average is simple to perform. Here we derive one of the main result of the work of this thesis, i.e. the expression for the collision integral that appears in the kinetic equation. This expression is of course in terms of disordered-average $\mathrm{T}-$matrix and is completely generic. We also prove that the detailed balance is obeyed, as expected. Then, we go further in the self-consistent Born approximation, i.e. the lowest order in the $\mathrm{T}-$matrix expansion. In particular we find the expression of the retarded (advanced) self-energy with the help of the Clifford's algebra for both regimes (I and II). In the end, we focus on the single-band regime. To derive the Eilenberger kinetic equation, an $ansatz$ for the Keldysh quasiclassical Green's function needs. It can be motivated by physical reasons and it is sufficient for our scopes. Thanks to it, we derive a generic expression for the scattering kernel of the kinetic equation. The latter is an equally important result. From it, we see in details the Born approximation and derive the physical observable such as the spin density and the charge current. In this chapter, the reader can find part of the original work of this thesis.

5.1 The T-matrix approach

In this section we want to illustrate the $\mathrm{T}-$matrix approach that takes into account the effects of disorder. To do that, we have to consider a scattering potential different from zero, i.e. $V(\mathbf{x}) \neq 0$ in the form of the Eq.(2.3). From this point of view the retarded/advanced Green's function is rewritten as

$$G^a(\mathbf{x}_1,\mathbf{x}_2;\omega) = \langle \mathbf{x}_1 | \frac{1}{(G_0^a(\omega))^{-1} - V} | \mathbf{x}_2 \rangle, \tag{5.1}$$

where $G_0^a(\omega)$ is the Green's function of free 2D Dirac-Rashba fermions introduced with the relation Eq.(3.18) and $a = R(A)$. In the presence of disorder randomly distributed across the material, translation invariance is broken and the Green's function depends on both the spatial coordinates $\mathbf{x}_1, \mathbf{x}_2$. The standard procedure requires a Feynman expansion of the two-point Green's function in terms of interaction lines with the scattering potential. This produces a series of diagrams with an arbitrary number of interaction vertices. These diagrams are then averaged over all possible impurity configurations, which yields contractions of scattering potential legs u_0 with impurity density n_i crosses (to all orders in n_i and u_0) as shown in Fig.[5.1]. After the disordered-average procedure, translational invariance is restored and the averaged Green's function only depends on the difference $\mathbf{x}_1 - \mathbf{x}_2$: $\mathcal{G}^a(\mathbf{x}_1 - \mathbf{x}_2, \omega) = \overline{G^a(\mathbf{x}_1,\mathbf{x}_2;\omega)}$. The latter — whose diagrammatic representation is reported in Fig.[5.1] — is in fact the central quantity in our approach. Its momentum representation is

$$\mathcal{G}^a(\mathbf{k}) = \frac{1}{[G_0^a(\mathbf{k})]^{-1} - \Sigma^a(\mathbf{k},\omega)}, \tag{5.2}$$

where

$$\Sigma^a(\mathbf{k},\omega) = \int d(\mathbf{x}-\mathbf{x}')e^{-i\mathbf{k}(\mathbf{x}-\mathbf{x}')}\overline{\langle \mathbf{x}' | V \frac{1}{1 - G_0^a(\omega)V} | \mathbf{x} \rangle}, \tag{5.3}$$

is the disordered-average self-energy within the non-crossing approximation. The latter neglects coherent multiple impurity scattering corrections, which justified in the diffusive regime with $\omega\tau \gg 1$ [143]. In fact, generally Σ^a contains two physically different class of diagrams that are higher order in the impurity density n_i: those with crossing impurity lines and those without. The former describe correlated scattering processes off multiple impurities, while the latter describe uncorrelated processes taking place at higher impurity density. For this reason, terms without crossing impurity lines can be easily included in the $\mathrm{T}-$matrix in a self consistent way. On the other hand, crossing diagrams are not in general easy to re-sum; however, these diagrams are associated with an extra factor of smallness

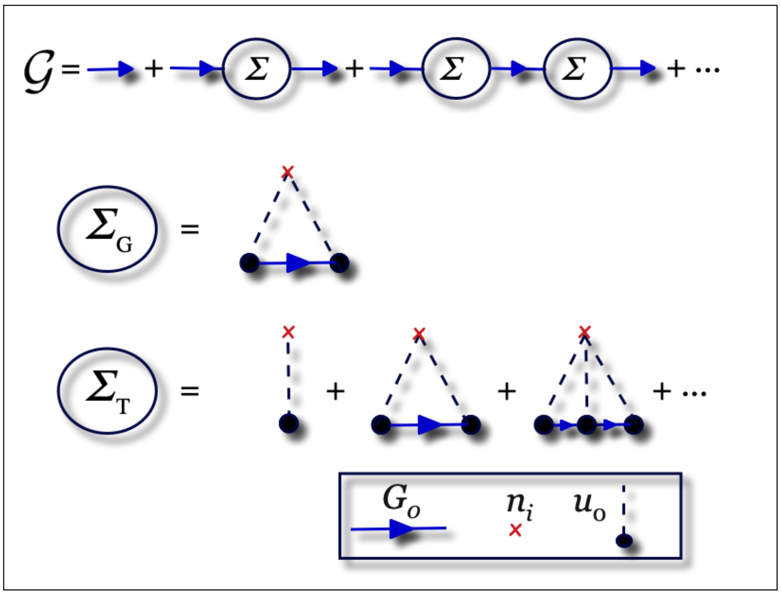

Figure 5.1: Diagrammatic representation of the disordered Green's function and of self energy. In the first line, the disorder-average Green's function (blue arrow), which can be represented as a function of the self-energy Σ. The other lines contains the Gaussian and the T-matrix approximation respectively. In the first case one only consider the "triangle diagram" Σ_G with an impurity density cross n_i (red cross). While in the second one all diagrams to all powers in the scattering potential u_0 (dashed legs with dots) but with one impurity density insertion are taken into account.

of the order $(k_F l)^{-1}$, where k_F is the Fermi momentum and l is the mean free path. In our case, the self-energy associated with the short-range spin-transparent (scalar) impurities is $\mathbf{k}-$independent, $\Sigma^a(\mathbf{k}) \equiv \Sigma^a(\omega)$ and hence we drop this index in what follows. The retarded (advanced) local (i.e. evaluated at coinciding space arguments) Green's function obeys the Dyson equation of the type (we omit the energy dependence for simplicity of notation[1])

$$G^a = G_0^a + G_0^a \Sigma^a G^a. \tag{5.4}$$

In the presence of random diluted nonmagnetic impurities, the retarded and advanced disorder-averaged Green's functions are obtained once are known the corresponding self-energies. According to the Eq.(5.3), the retarded (advanced) self-energy is given by the average over disorder ($\prec ... \succ$) of the T$-$matrix expansion as shown in the Fig.[5.1], i.e.

$$\Sigma^a = \mathcal{T}^a \equiv \prec T^a \succ = u_0 G_0^a + u_0 G_0^a u_0 G_0^a + ... = \frac{u_0^2 G_0^a}{1 - u_0 G_0^a}, \tag{5.5}$$

where T^a is the single-impurity T-matrix in the R/A sector and the disorder average is defined by

---

[1] We underline that the energy dependence is not relevant for static impurities.

$$\begin{aligned}\prec V(\mathbf{x}) \succ &= u_0 \\ \prec V(\mathbf{x})\, V\left(\mathbf{x}'\right) \succ &= u_0^2 \delta\left(\mathbf{x}-\mathbf{x}'\right) \\ \prec V(\mathbf{x})\, V\left(\mathbf{x}'\right) V\left(\mathbf{x}''\right) \succ &= u_0^3 \delta\left(\mathbf{x}-\mathbf{x}'\right) \delta\left(\mathbf{x}'-\mathbf{x}''\right),\end{aligned}$$

and so on and so forth. The self-consistent approach gives a way to write the Green's function in terms of non-interacting one [144] in the form

$$G^a = G_0^a + G_0^a T^a G_0^a. \tag{5.6}$$

We underline that keeping the full T$-$matrix structure one effectively re-sum all topologically equivalent two-particle non-crossing diagrams at all orders in V. The additional terms generated by the T$-$matrix insertions encompass not only the skew-scattering from arbitrarily strong potentials (see Chapter 6), but also important corrections we discuss in the following. In the kinetic equation one determines the Green's function self-consistently by replacing G_0^a with the disordered-average one $\mathcal{G}^a$. If one stops at the lowest order in u_0 in the Eq.(5.5), only the first term of the series is kept. This define the so-called Born approximation. Considering high-order terms in the T$-$matrix expansion, also the skew-scattering mechanism is included that is well discussed in the Chapter 6. In the following, we present and discuss one of the main result of this work that is the general expression of the collision integral Eq.(2.58) of the kinetic equation in terms of T-matrices.

5.1.1 The detailed balance

Here we discuss how to rewrite the collision integral Eq.(2.58) with the T$-$matrix approximation. This is one of the main result of the work of this thesis. We start from the definition of T$-$matrix and the self-energy Eq.(5.5), the $out-$contribution of the collision integral Eq.(2.58) becomes

$$I_{out} = -i\left(\mathcal{T}^R G^K - G^K \mathcal{T}^A\right). \tag{5.7}$$

Let us now turn our attention to the Keldysh self-energy, which determines the in-contribution of the collision integral in Eq.(2.58). The reason why we call it $in-$ will be clear in a while. The perturbation expansion of the Keldysh Green function reads quite different from Eq.(5.6).

At each order in u_0 there are many terms as positions in which the Keldysh component can be placed with the additional requirement that on the left of the Keldysh component there can be only retarded Green functions, whereas the advanced one must be always on the right. This feature is a consequence of the triangular matrix structure of the Green's function (see Chapter 2). In the end, the Keldysh self-energy then reads

$$\Sigma^K = \prec u_0 G^K u_0 \succ = \prec T^R \mathcal{G}^K T^A \succ, \tag{5.8}$$

where it is understood that the disordered-average only concerns the T$-$matrices, because $\mathcal{G}^K$ is already meant to be the self-consistent disordered-average Green's function. We then see that in the Keldysh self-energy there appears the disordered-average of the product of the retarded and advanced T-matrices. This corresponds to the T$-$matrix insertion in the vertex correction of the Kubo linear response formalism. The $in-$contribution to the collision integral Eq.(2.58) finally reads

$$I_{in} = i\Big(\mathcal{G}^R \prec T^R \mathcal{G}^K T^A \succ - \prec T^R \mathcal{G}^K T^A \succ \mathcal{G}^A\Big). \tag{5.9}$$

To make more transparent the formulae obtained, one can introduce explicit dependence on momenta (it is possible because we use disordered-average Green's functions). Then it is convenient to define

$$\mathcal{G}_0^a \equiv \int \frac{d\mathbf{k}'}{(2\pi)^2} \mathcal{G}_{\mathbf{k}'}^a \tag{5.10}$$

and to introduce the following notation

$$\mathcal{T}^a = u_0^2 \mathcal{G}_0^a \overline{\mathcal{T}}^a, \tag{5.11}$$

where

$$\overline{\mathcal{T}}^a = \frac{1}{1 - u_0 \mathcal{G}_0^a}. \tag{5.12}$$

Using the relations Eqs.(5.10) and (5.11), the $in-$ and $out-$contributions Eqs.(5.9)-(5.7) become respectively

$$I_{in} = i u_0^2 \Big(\mathcal{G}_{\mathbf{k}}^R \overline{\mathcal{T}}^R \mathcal{G}_0^K \overline{\mathcal{T}}^A - \overline{\mathcal{T}}^R \mathcal{G}_0^K \overline{\mathcal{T}}^A \mathcal{G}_{\mathbf{k}}^A \Big) \tag{5.13}$$

and

$$I_{out} = -iu_0^2\Big(\mathcal{G}_0^R\overline{\mathcal{T}}^R\mathcal{G}_{\mathbf{k}}^K - \mathcal{G}_{\mathbf{k}}^K\mathcal{G}_0^A\overline{\mathcal{T}}^A\Big). \tag{5.14}$$

The above expressions makes obvious the link with the Boltzmann language. Making explicit $\mathcal{G}_0^{R,A,K}$ given by Eq.(5.10) and remembering that the Keldysh Green's function describes the distribution function, it is easy to see that the Eq.(5.13) provides the $in-$ scattering processes, i.e. $\mathbf{k}' \longrightarrow \mathbf{k}$, while the Eq.(5.14) the $out-$ processes $\mathbf{k} \longrightarrow \mathbf{k}'$.
It is evident that the two contributions (I_{in} and I_{out} given by the Eqs.(5.13) and (5.14)) have not the same structure, so some manipulation is required. We focus on I_{out} term and project it in the basis in which $\mathcal{G}_0^{R(A)}$ (and then also $\overline{\mathcal{T}}^{R(A)}$) is diagonal. So, the (ij)-element reads

$$\begin{aligned}(I_{out})_{ij} &= -iu_0^2\Big(\mathcal{G}_{0,i}^R\overline{\mathcal{T}}_i^R\mathcal{G}_{\mathbf{k},(ij)}^K - \mathcal{G}_{\mathbf{k},(ij)}^K\mathcal{G}_{0,j}^A\overline{\mathcal{T}}_j^A\Big) \\ &= -iu_0^2\mathcal{G}_{\mathbf{k},(ij)}^K\Big(\mathcal{G}_{0,i}^R\overline{\mathcal{T}}_i^R - \mathcal{G}_{0,j}^A\overline{\mathcal{T}}_j^A\Big).\end{aligned} \tag{5.15}$$

Using the expression Eq.(5.12), one can rewrite it as

$$\begin{aligned}(I_{out})_{ij} &= -iu_0^2\mathcal{G}_{\mathbf{k},(ij)}^K\Big(\frac{\mathcal{G}_{0,i}^R}{1-u_0\mathcal{G}_{0,i}^R} - \frac{\mathcal{G}_{0,j}^A}{1-u_0\mathcal{G}_{0,j}^A}\Big) = \\ &= -iu_0^2\mathcal{G}_{\mathbf{k},(ij)}^K\Big(\mathcal{G}_{0,i}^R - \mathcal{G}_{0,j}^A\Big)\overline{\mathcal{T}}_i^R\overline{\mathcal{T}}_j^A.\end{aligned} \tag{5.16}$$

From the above result, we can recover the matrix relation for the $out-$term being careful of the position of each element. In particular one obtains

$$I_{out} = -iu_0^2\Big(\mathcal{G}_0^R\overline{\mathcal{T}}^R\mathcal{G}_{\mathbf{k}}^K\overline{\mathcal{T}}^A - \overline{\mathcal{T}}^R\mathcal{G}_{\mathbf{k}}^K\overline{\mathcal{T}}^A\mathcal{G}_0^A\Big). \tag{5.17}$$

The latter expression has the same matrix structure of the $in-$relation Eq.(5.13), as expected. In the end, if we make explicit the $\mathcal{G}_0^{R,A,K}$ using the Eq.(5.10), one obtains a completely generic equation for the collision integral $I = I_{in} + I_{out}$, i.e.

$$I = iu_0^2\int\frac{d^2\mathbf{k}'}{(2\pi)^2}\Big(\mathcal{G}_{\mathbf{k}}^R\overline{\mathcal{T}}^R\mathcal{G}_{\mathbf{k}'}^K\overline{\mathcal{T}}^A - \overline{\mathcal{T}}^R\mathcal{G}_{\mathbf{k}'}^K\overline{\mathcal{T}}^A\mathcal{G}_{\mathbf{k}}^A - \mathcal{G}_{\mathbf{k}'}^R\overline{\mathcal{T}}^R\mathcal{G}_{\mathbf{k}}^K\overline{\mathcal{T}}^A + \overline{\mathcal{T}}^R\mathcal{G}_{\mathbf{k}}^K\overline{\mathcal{T}}^A\mathcal{G}_{\mathbf{k}'}^A\Big). \tag{5.18}$$

From the point of view of the kinetic equation, $\mathbf{k}$ and $\mathbf{k}'$ are the momentum before and after the scattering, depending whether one considers the in- and out-contributions. One can easily check that the detailed balance is obeyed in the Eq.(5.18). If $\mathbf{k} \longrightarrow \mathbf{k}'$ (and vice versa), the $in-$ and $out-$terms are interchanged and then the microscopic reversibility of the scattering probability is preserved [145]. The general expression Eq.(5.18) is an important result and it will be useful in the following discussion. For instance, the specific case of the Fermi gas with Gaussian white-noise correlation can be easily obtained by neglecting the matrix structure. In the next section, we go further in the Born-approximation and study the Eilenberger kinetic equation for the 2D Dirac-Rashba graphene Hamiltonian.

5.2 The Born approximation

In this section we present the so-called Born approximation from which only the first term in the expansion of the Eq.(5.5) is taken into account, i.e. $\overline{\mathcal{T}}^a \longrightarrow 1$. From this point of view, the corresponding self-energies given by the Eq.(5.5) are

$$\Sigma^a = \mathcal{T}^a = u_0^2 \int \frac{d\mathbf{k}'}{(2\pi)^2} G^a_{\mathbf{k}'} = \mp i\pi u_0^2 N_{ln} \left\langle P_{ln}\left(\mathbf{k}_F\right)\right\rangle , \tag{5.19}$$

where $l = 1, n = \pm 1$ for the two bands crossing the positive Fermi energy ($\varepsilon > 0$), i.e. the third and fourth one, and N_{ln} the corresponding DOS at the Fermi level ε. In the Eq.(5.19), $\langle \ldots \rangle$ indicates the angle average over the direction of the versor $\mathbf{n}$ and $a = R(A)$. In the Chapter 3, we derived the projectors for all the bands of the 2D Dirac-Rashba model. Using the results of the Section 3 as the energy dispersion Eq.(3.13) and the Clifford's algebra decomposition of the projectors [see Table 3.1], one can compute the corresponding self-energy. Let us evaluate the DOS of the two bands under study first, i.e. N_{11} and N_{1-1} as

$$d\epsilon_{11} = d(\lambda + \sqrt{k^2+\lambda^2}) = \frac{kdk}{\sqrt{k^2+\lambda^2}} \to N_4 \equiv N_{11} = \frac{1}{2\pi}(\varepsilon - \lambda) \tag{5.20}$$

and

$$d\epsilon_{1-1} = d(-\lambda + \sqrt{k^2+\lambda^2}) = \frac{kdk}{\sqrt{k^2+\lambda^2}} \to N_3 \equiv N_{1-1} = \frac{1}{2\pi}(\varepsilon + \lambda). \tag{5.21}$$

It is then useful to introduce a basic scattering time in terms of the DOS of pure graphene ($N_0 = \varepsilon/(2\pi)$) without the SOC as

$$\frac{1}{\tau} = 2\pi N_0 u_0^2. \tag{5.22}$$

As a result, the total self-energy in the regime II ($\epsilon > 2\lambda$), when both bands are occupied [see Fig.3.2], reads

$$\Sigma_{II}^{a} = \mp i\frac{1}{2\tau}\sigma_0 \otimes s_0. \tag{5.23}$$

When the Fermi energy is in the regime I ($0 < \epsilon < 2\lambda$) with only one band occupied, the self-energy is

$$\Sigma_{I}^{a} = \mp i\frac{1}{4\tau}\Big(\Big(1+\frac{\lambda}{\varepsilon}\Big)\sigma_0 \otimes s_0 - \frac{1}{2}(\sigma_x \otimes s_y - \sigma_y \otimes s_x) + \frac{\lambda}{\varepsilon}\sigma_z \otimes s_z\Big). \tag{5.24}$$

In the Table 5.1 we report the contributions from the various components of the Clifford's algebra for all the bands. It is evident from the Eqs.(5.23) and (5.24) that the disordered-average self-energy in regime II has a simpler matrix structure then the one in regime I, but the presence of the two bands crossing the Fermi energy makes the mathematical description quite complicated. For this reason, we focus on the *one-band* regime first, while the *two-band* regime will be discussed in the Chapter 7. In particular, in the rest of this Chapter we derive the kinetic equation for the quasiclassical Green's function in the Born approximation. Otherwise, in the Chapter 6 we go beyond this approximation and the skew-scattering mechanism will be presented.

	$\sigma_0 \otimes s_0$	$\gamma_R/2$	$\sigma_z \otimes s_z$	$-\gamma_R/2$
Σ_4	$1-\lambda/\varepsilon$	$1-\lambda/\varepsilon$	$-\lambda/\varepsilon$	$-\lambda/\varepsilon$
Σ_3	$1+\lambda/\varepsilon$	$-1-\lambda/\varepsilon$	λ/ε	$-\lambda/\varepsilon$
Σ_2	$1-\lambda/\varepsilon$	$1-\lambda/\varepsilon$	$-\lambda/\varepsilon$	$-\lambda/\varepsilon$
Σ_1	$1+\lambda/\varepsilon$	$-1-\lambda/\varepsilon$	λ/ε	$-\lambda/\varepsilon$

Table 5.1: Clifford's algebra decomposition of the retarded self-energy for all the bands in units of $-i/(4\tau) = -i\varepsilon u_0^2/4$. Σ_3 is the expression of the self-energy in the regime I reported in the Eq.(5.24), while the sum $\Sigma_3 + \Sigma_4$ is the regime II one given by the Eq.(5.23).

5.3 The one-band regime

In order to derive the Eilenberger equation in the presence of disorder, we start from the kinetic equation Eq.(2.63). Again, we focus on the stationary case. Performing the

$\xi-$integration of the collision integral Eq.(5.18) and using the definition of the scattering time Eq.(5.22), one has

$$\mathcal{I} = -\frac{1}{2\tau}\left[\left(\left\langle g^R\right\rangle \overline{\mathcal{T}}^R g \overline{\mathcal{T}}^A - \overline{\mathcal{T}}^R g \overline{\mathcal{T}}^A \left\langle g^A \right\rangle\right) - \left(g^R \overline{\mathcal{T}}^R \left\langle g \right\rangle \overline{\mathcal{T}}^A - \overline{\mathcal{T}}^R \left\langle g \right\rangle \overline{\mathcal{T}}^A g^A\right)\right]. \quad (5.25)$$

Here for brevity $g^{R,A,K} \equiv g^{R,A,K}(\theta)$ and $\left\langle g^{R,A,K}\right\rangle = \left\langle g^{R,A,K}(\theta')\right\rangle$ with θ and θ' the angles of $\mathbf{k}$ and $\mathbf{k}'$, respectively. From the Eq.(5.25) one can confine oneself to the Born approximation if the matrices $\overline{\mathcal{T}}^a$ are evaluated to lowest order in the disorder potential u_0, when it reduces to unity. To proceed further, following the Ref.[129], we make an $ansatz$ for the Keldysh quasiclassical Green's function of a single band ($l = 1, n = -1$) in the form

$$g(\mathbf{k}_F) = P_{1-1}(k_F) g_0(\theta), \quad (5.26)$$

where g_0 is a scalar function and $\mathbf{k}_F = k_F(cos(\theta), sen(\theta))$ is the momentum at the Fermi energy. Notice that, although g is still a matrix, its structure is entirely constrained. The ansatz can be motivated by the following argument. Inspection of the Eq.(2.66) shows that, at leading order in the weak-disorder expansion ($\varepsilon\tau \gg 1$), the solution must commute with the Hamiltonian and be of order $g \sim \tau$. In such a way, the commutator in the left hand side (LHS), although of order $\varepsilon\tau \gg 1$ vanishes and the remaining terms in the equation are of order of the unity. Notice that the ansatz may not be sufficient when one is dealing with sub-leading terms in the weak-disorder expansion. In the work of this thesis, the physical observables which we are interested in (like the extrinsic spin Hall and Edelstein effect which are relevant in recent experiments in graphene WS_2 systems [96]) are of the order of the momentum relaxation time so the ansatz is justified. It is useful to recall here that from the Eq.(2.46) it is easy to see that in equilibrium the scalar function reads

$$g_0(\omega) = f(\omega) = 2\tanh\left(\frac{\omega}{2T}\right). \quad (5.27)$$

Using the Eq.(3.18) one can verify that the retarded/advanced component of the quasiclassical Green's function in the regime I is

$$g^a = \frac{i}{\pi}\int d\xi G^a(\mathbf{k},\omega) = \frac{i}{\pi}\int d\xi \frac{P_{1-1}(\mathbf{k},\omega)}{-\xi \pm i0^+} = \pm P_{1-1}(\mathbf{k}_F). \quad (5.28)$$

i.e. it coincides with the projector of the band crossing the Fermi level. Now we have all the ingredients to rewrite the collision integral after the $\xi-$integration. By taking the trace of the Eq.(5.25) and using the Eqs.(5.26) and Eq.(5.28), one gets a scalar collision integral for g_0, i.e.

$$\mathcal{I}_0 = -\int_0^{2\pi} \frac{\mathrm{d}\theta'}{2\pi} W(\vartheta) \left[g_0(\theta) - g_0\left(\theta'\right) \right], \tag{5.29}$$

where the scattering kernel is a function of angle difference that from now we call $\vartheta \equiv \theta - \theta'$.[2] It reads

$$W(\vartheta) = \frac{N_F}{N_0} \frac{1}{\tau} \mathrm{Tr}\left(P_{1-1}(k_F,\theta) \overline{\mathcal{T}}^R P_{1-1}(k_F,\theta') \overline{\mathcal{T}}^A \right), \tag{5.30}$$

with N_F the DOS of the third band. In the self-consistent Born approximation, which amounts to confine to second order in the disorder potential expansion ($\overline{\mathcal{T}}^{R(A)} \longrightarrow 1$), the effective transport equation Eq.(2.66) for the scalar quasiclassical Green's function becomes[3]

$$\mathbf{E}\partial_\omega f \cdot \mathbf{v}_{eff} = \frac{1}{2\pi} \int_0^{2\pi} d\theta' W(\vartheta) \left(g_0(\theta,\omega) - g_0\left(\theta',\omega\right) \right). \tag{5.31}$$

In the above kinetic equation we introduced the effective velocity vertex as

$$\mathbf{v}_{eff}(k_F,\theta) = \frac{1}{4} \mathrm{Tr}\left(\boldsymbol{\sigma} \mathrm{P}_{1-1}(\mathrm{k_F},\theta) \right). \tag{5.32}$$

In this case, only the first term in the T$-$matrix expansion of the Eq.(5.30) is selected, so that the effective scattering kernel reads

$$W(\vartheta) = \frac{N_F}{N_0} \frac{1}{\tau} \mathrm{Tr}\Big(P_{1-1}(k_F,\theta), P_{1-1}\left(k_F,\theta'\right) \Big). \tag{5.33}$$

Because a common shift $\theta \to \psi$, $\theta' \to \psi$ cannot change the trace due to the periodicity of the projectors, the effective scattering kernel can only depend on the difference of the two angles. Furthermore, due to the cyclic property of the trace, the expression is symmetric under the interchange of the two angles, implying that the effective kernel is an *even periodic function* of the difference $\vartheta \equiv \theta - \theta'$. The transport equation Eq.(5.31) together with the expressions of the effective kernel Eq.(5.33) and the velocity vertex Eq.(5.32), defines a complete theory for charge and spin response in the projected band crossing the Fermi energy. This is one of the main result of the present thesis. In order to show how the formalism can be used let us consider the case when there is no spin-valley SOC first, i.e. $\lambda_{sv} = 0$. In this case N_F is given by the Eq.(5.21) and the Eq.(5.33) becomes

---

[2] We underline that $W(\vartheta)$ is the effective scattering kernel from momentum state $k_F(cos(\theta), sen(\theta))$ to $k_F(cos(\theta'), sen(\theta'))$.

[3] Note that the commutator term of the Eq.(2.66) does not give contribution because $h(\mathbf{k}_F) \equiv \varepsilon P_{1-1}(\mathbf{k}_F)$.

$$W(\vartheta) = \frac{1}{\tau} \frac{((2\lambda+\varepsilon)\cos(\theta-\theta')+\varepsilon)^2}{2\varepsilon(\lambda+\varepsilon)}. \tag{5.34}$$

In this case no spin Hall effect can be expected, as already discussed in the Chapter 4. As mentioned, the presence of impurity scattering gives rise a relaxation mechanism that makes spin Hall conductivity zero. Notice that $W(\vartheta)$ (Eq.(5.34)) contains only the first three even harmonics of the angle difference. The velocity vertex, with the electric field choice Eq.(4.2), reads

$$v_{eff,x} = -\frac{1}{4} \frac{\sqrt{\varepsilon\,(\varepsilon+2\lambda)}}{\varepsilon+\lambda} \cos(\theta), \tag{5.35}$$

so that a possible solution for $g_0(\theta,\omega)$ can be written in the form

$$g_0(\theta,\omega) = A(\omega) cos(\theta), \tag{5.36}$$

with $A(\omega)$ a function of the model parameters. Let us define

$$W_0 = \langle W(\vartheta) \rangle, \qquad \langle W(\vartheta) g_0(\theta') \rangle \equiv W_1 \cos(\theta), \tag{5.37}$$

with $\langle ... \rangle$ the angle average, from the Eq.(5.31) the equation for A becomes (here we reintroduce the electrical charge e)

$$A = -\frac{1}{(W_0 - W_1)} (-eE\tau \partial_\omega f) \frac{1}{4} \sqrt{\frac{\varepsilon(2\lambda+\varepsilon)}{(\lambda+\varepsilon)^2}}. \tag{5.38}$$

In the end, the solution for the transport equation is

$$g_0(\theta,\omega) = (eE\tau\partial_\omega f) \frac{\varepsilon\sqrt{\varepsilon(2\lambda+\varepsilon)}}{4\lambda^2+\varepsilon^2} \cos(\theta). \tag{5.39}$$

By inserting this last relation in the Eq.(2.69) with $\mathcal{O} = (1/2)\sigma_0 \otimes s_2$, which is the spin density along the $y-$direction and after integration over ω, one has[4]

$$s_y = -eE\tau \frac{\varepsilon^2(2\lambda+\varepsilon)}{16\pi(4\lambda^2+\varepsilon^2)}, \tag{5.40}$$

while the charge current along the $x-$direction reads[5]

---

[4] Here the inverse spin-galvanic vertex results $\mathrm{Tr}\,(\sigma_0 \otimes s_2 P_{1-1}(k_F,\theta)) = -\frac{\sqrt{\varepsilon(\varepsilon+2\lambda)}}{\varepsilon+\lambda}\cos(\theta)$.

[5] Here the inverse charge vertex results $\mathrm{Tr}\,(\sigma_1 \otimes s_0 P_{1-1}(k_F,\theta)) = +\frac{\sqrt{\varepsilon(\varepsilon+2\lambda)}}{\varepsilon+\lambda}\cos(\theta)$.

$$j_x = -2S_y. \tag{5.41}$$

The Eqs.(5.40) and (5.41) above coincide exactly with the results for the electric-field-induced spin polarization [37] obtained via the Kubo linear response theory [128] and confirm the equivalence of the present approach. Otherwise the spin Hall response vanishes as expected. To see the spin Hall effect, we consider the $\mathrm{T}-$matrix expansion beyond the second order. In the Chapter 6, we carry out the expansion of $\mathrm{T}-$matrix to third order.

Conclusions

In this chapter we discussed the presence of disorder in the system under study and how it modifies the analytical expression of the Green's function. Here we introduced the $\mathrm{T}-$matrix approximation to derive the self-energy in terms of the disordered-average Green's function. In particular, we derived a completely generic equation for the collision integral for which we proved that the detailed balance is obeyed. This represents one of the most important results of the work of this thesis. Then we selected only the first term in the $\mathrm{T}-$matrix expansion, i.e. the so-called Born approximation, to derive the self-energies in both regime of the 2D Dirac-Rashba model ($\epsilon > 2\lambda$ and $0 < \epsilon < 2\lambda$). They are obtained in the Clifford's algebra matrix decomposition. The achieved results tell us that the disordered-average self-energy in regime II has a simpler matrix structure than one in regime I. However the presence of two bands makes the manipulation of the equations more difficult. For this reason we derived the kinetic equation for the single-band regime first. For such a system, we use an $ansatz$ for the Keldysh quasiclassical Green's function for which g results to be proportional by scalar function to the band projector. This assumption is motivated by physical arguments and is sufficient to derive the physical observables of the order of the momentum relaxation time. Hence we wrote the effective transport equation for the scalar quantity and, from it, the physical observables are found. Another important result is the generic expression of the scattering kernel in terms of the projector of the third band and the $\mathrm{T}-$matrix. In the end we found the spin density and the charge current in the self-consistent Born approximation. These results agree with what has been reported in the literature and confirm the consistency of the quasiclassical approximation.

6

Beyond the Born approximation and the skew-scattering mechanism

Overview

In the following we go beyond the Born approximation and present the so-called skew-scattering mechanism thanks to the $\mathrm{T}-$matrix formalism discussed in the previous Chapter. This means to consider higher order term in the $\mathrm{T}-$matrix expansion so that we expect to see the (extrinsic) spin Hall effect. We now turn our attention to consider a more interesting system with finite spin-valley coupling. Precisely, in the system under study we have to consider two types of SOC variables, i.e. Rashba (λ) and spin-valley (λ_{sv}). We start to provide the solution of the transport equation. In order to do that, in such a system, we rewrite the scattering kernel of the kinetic equation. Using the formalism discussed in the Section 3.2, we are able to write in a very compact way the additional term in the presence of skew-scattering. Thanks to its periodicity properties, we can derive the solution of the kinetic equation similar to what done at the Born level for the 2D Dirac-Rashba model. Of course in this case the manipulation is more complicate. In such a manipulation, we need to define two different scattering rates (parallel and perpendicular component) from which we learn a lot about the system response. In the end, we provide the explicit analytical expressions of physical observables such as the spin Hall and the Edelstain effect. In the end, from the numerical analysis of these expressions, we discuss the behaviour of the physical system response as a function of SOC variables in the presence of the skew-scattering. Here the reader can find the heart of the work of this thesis with all the original results.

6.1 The skew-scattering mechanism

In the following, we discuss how to include the so-called skew-scattering[1] mechanism in the transport equation. The effect of skew-scattering can be included by considering higher-order terms in the $\mathrm{T}-$matrix expansion Eqs.(5.11) and (5.12). In the language of diagrammatic representation, it means to take into account also the graph with three legs and one impurity density insertion [see the third line in the Fig.5.1]. It is clear that one can directly evaluate this diagram with the Feynman rules and then add it to the previous one (see Appendix E for a pedagogical exposition). Otherwise, one can start from the generic scattering kernel Eq.(5.30) and use the formalism presented in the previous Chapter. Explicitly, when the potential is not too strong, one may expand the matrices $\overline{\mathcal{T}}^a$ Eq.(5.12) as[2]

$$\overline{\mathcal{T}}^a \simeq 1 + u_0 Re\mathcal{G}_0^a \mp i u_0 Im\mathcal{G}_0^a. \tag{6.1}$$

It is important to underline that the real part in the expansion Eq.(6.1) does not give contribution to the skew-scattering mechanism, but only renormalizes the lowest-order scattering amplitude. This is apparent from the fact that the sign of this correction in the Eq.(6.1) is the same for both the retarded and advanced $\mathrm{T}-$matrix. The sign of the imaginary part depends, instead, on the retarded/advanced nature of the $\mathrm{T}-$matrix and gives rise to the *skewness* in the effective scattering kernel, as shown below. By inserting the expression Eq.(6.1) into the right hand side of the Eq.(2.66), one obtains an additional term on the right-hand side of the Eq.(5.31), i.e. $W \to W + W_{ss}$ with

$$W_{ss}(\vartheta) = -2\pi i u_0 N_F \frac{N_F}{N_0}\frac{1}{\tau} \times \mathrm{Tr}\left(\left\langle \mathrm{P}_{1-1}\left(\theta''\right)\right\rangle \left[\mathrm{P}_{1-1}(\theta), \mathrm{P}_{1-1}\left(\theta'\right)\right]\right), \tag{6.2}$$

where all the projectors are evaluated at the Fermi momentum k_F and $\langle \ldots \rangle$ indicates the average over the angle θ''. N_F is the DOS of the third band, as usual. The commutator under the trace implies that W_{ss} vanishes when $\theta = \theta'$. Furthermore it is odd upon the interchange of θ and θ' because this amounts to interchange the matrices in the commutator. A common shift $\theta + \psi$, $\theta' + \psi$ clearly leaves W_{ss} unchanged because of the periodicity with respect to both angles, and hence there can be no dependence on the sum $\theta + \theta'$. As a result, W_{ss} must be an *odd periodic function* of ϑ and of the form[3]

---

[1] In the following we use the subscript ss to indicate the skew-scattering contribution.

[2] Here we write $\mathcal{G}_0^a = Re\mathcal{G}_0^a \pm Im\mathcal{G}_0^a$.

[3] The subscript $n+1$ will be useful for the Fourier expansion of the total scattering kernel Eq.(6.10). In particular, the coefficients W_0 and W_1 are linked to the kernel at the Born level.

$$\delta W_{ss}\left(\vartheta\right) = \sum_{n=1}^{\infty} W_{n+1} sin\left[n\left(\theta-\theta'\right)\right] \tag{6.3}$$

where the coefficients W_{n+1} will be functions of the parameters of the Hamiltonian. In the next section we study a model with also spin-valley coupling. For such a system we expect to see the spin Hall effect and we show that it is possible to write the analytical expressions for the physical observables.

6.2 The kinetic equation for spin-valley Hamiltonian

We now turn to consider the more interesting situation with finite spin-valley coupling $\lambda_{sv} \neq 0$ in the Hamiltonian Eq.(3.21). Before considering the results, we provide the formal solution to the transport equation Eq.(5.31). We consider the effective kernel in the form

$$W\left(\vartheta\right) = W(\vartheta) + W_{ss}(\vartheta) \tag{6.4}$$

and we introduce the skew-scattering dimensionless coupling g_{ss} as

$$g_{ss} = 2\pi u_0 N_F. \tag{6.5}$$

Here we use the Hamiltonian parameterization discussed in the Section 3.2 for the generalised Dirac-Rashba model. For such a system the projector $P_{1-1}(k_F,\theta)$ is a complicated matrix. According to what done in the Chapter 5, quite generally, we write a solution of the kinetic equation in the form

$$g_0(\theta) = (-eE\partial_\omega f) v_{eff,x}(\lambda,\lambda_{sv},k_F)\tilde{g}_0(\theta), \tag{6.6}$$

where[4]

$$v_{eff,x}(\lambda,\lambda_{sv},k_F) \equiv \mathcal{V} = \frac{1}{4}\mathrm{Tr}\left\{\sigma_1 \otimes s_0 P_{1-1}(\theta,k_F)\right\} \tag{6.7}$$

generalizes to the case with finite spin-valley coupling the velocity vertex of the Eq.(5.35). In the end, the final equation can be written as

$$cos(\theta) = -\langle W(\vartheta)\rangle \tilde{g}_0(\theta) + \frac{1}{(2\pi)}\int_0^{2\pi} d\theta' W(\vartheta)\tilde{g}_0(\theta'). \tag{6.8}$$

---

[4] Note that $v_{eff,x}(\lambda,\lambda_{sv},k_F) = A(\lambda,\lambda_{sv},k_F)cos(\theta)$, see the Eq.(6.14).

To solve the above equation for $\tilde{g}_0(\theta)$, one may consider the Fourier expansion for all quantities. In particular, according to the Eqs.(5.33) and (6.3), one can write[5]

$$\begin{aligned} y(\theta) &\equiv cos(\theta) = y_1 e^{i\theta} + y_{-1} e^{-i\theta} \\ W(\vartheta) &= W_0 + W_1 cos(\vartheta) + W_2 sen(\vartheta) + W_3 sen(2(\vartheta)). \end{aligned} \tag{6.9}$$

In this picture, the coefficients that we need for the calculation are

$$y_1 = y_{-1} = \frac{1}{2}, \quad W_0 = \langle W(\vartheta)\rangle, \quad W_1 = 2\langle W(\vartheta)cos(\vartheta)\rangle, \quad W_2 = 2\langle W(\vartheta)sen(\vartheta)\rangle.$$

As a result, if we call $Q \equiv -\langle W(\vartheta)\rangle$ in the Eq.(6.8), we find the coefficients for the Fourier expansion of $\tilde{g}_0(\theta)-$ function in the form

$$\tilde{g}_0^{(n)} = \frac{y_n}{Q + W_n}. \tag{6.10}$$

It is evident that, in this picture, we need only the coefficients with $n = \pm 1$. After some manipulation, the solution Eq.(6.6) reads[6]

$$g_0(\theta) = (eE\tau\partial_\omega f)\mathcal{V}\left\{ \frac{\tau_{\parallel}^{-1}}{(\tau_{\parallel}^{-1})^2 + (\tau_{\perp}^{-1})^2} cos(\theta) + \frac{\tau_{\perp}^{-1}}{(\tau_{\parallel}^{-1})^2 + (\tau_{\perp}^{-1})^2} sen(\theta) \right\}, \tag{6.11}$$

where we defined two different scattering rates, i.e. the parallel $\tau_{\parallel}^{-1}$ and the perpendicular component $\tau_{\perp}^{-1}$ as

$$\tau_{\parallel}^{-1} = \frac{1}{2\pi} \int_0^{2\pi} d\theta' W(\vartheta)\Big(1 - cos(\vartheta)\Big), \tag{6.12}$$

$$\tau_{\perp}^{-1} = \frac{1}{2\pi} \int_0^{2\pi} d\theta' W(\vartheta) sen(\vartheta). \tag{6.13}$$

---

[5] Note that the even term of $W(\theta - \theta')$ comes from the effective kernel at Born level, while the rest odd part from the additional contribution due to the skew-scattering.

[6] Note that the Fourier expansion is $g_0(\theta) = g_0^{(1)} e^{i\theta} + g_0^{(-1)} e^{-i\theta}$.

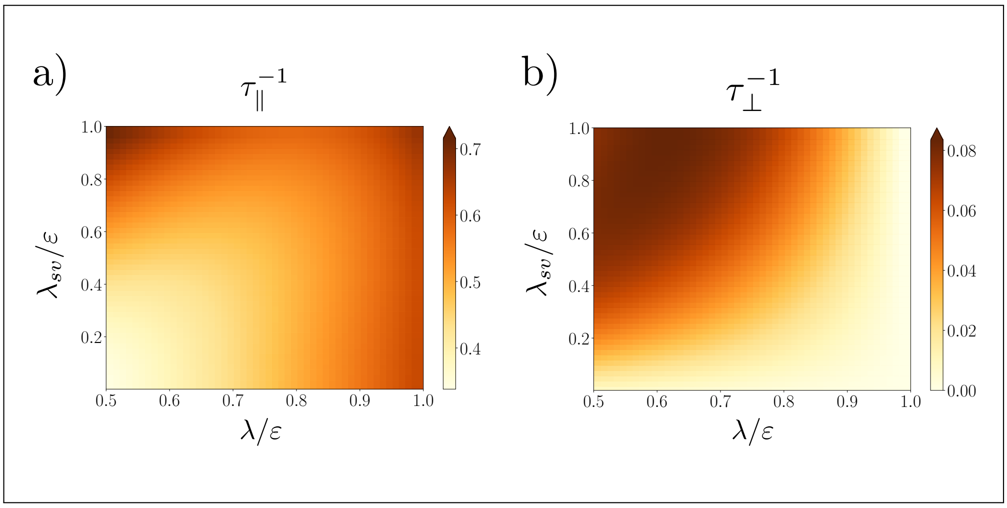

Figure 6.1: Numerical color plots of a) $\tau_{\parallel}^{-1}$ and b) $\tau_{\perp}^{-1}$ as function of SOC variables in units of τ and skew-scattering coupling g_{ss}. The parallel component becomes more relevant for high values of SOC, while the perpendicular one increases with λ_{sv} for small values of the Rahsba one. In particular, the numerical results show an order of magnitude difference between the two rates. For both plots $\varepsilon\tau = 10$ with $\varepsilon = 1$. Furthermore, the Rashba and spin-valley parameters are in units of the Fermi energy.

To understand better these results, in the Fig.[6.1] we report the Eqs.(6.12) and (6.13) in units of τ and g_{ss} (note that only $\tau_{\perp}^{-1}$ depends on the skew-scattering coupling). The SOC variables are chosen in units of the Fermi energy ε and may map a range of values according to the regime II condition given by the Eq.(3.27). At the same time, we choose $\varepsilon\tau = 10$ in agreement with the good metal limit ($\varepsilon\tau \gg 1$). First of all we note that $\tau_{\parallel}^{-1}$ becomes more relevant for high values of SOC, while $\tau_{\perp}^{-1}$ increases with λ_{sv} at small values of Rashba coupling. Then, at the same SOC conditions, there is an order of magnitude difference between the parallel and perpendicular component. This means that one can neglect $(\tau_{\perp}^{-1})^2$ in the Eq.(6.11). In the next section, we discuss better this point and comment the results. The Eq.(6.11) is the general solution for the scalar Green's function in the system under study. It is clear that, using the relation Eq.(2.69) one can evaluate the physical observable. In the next section we derive the analytical expression for the Drude conductivity, the Edelstein and spin Hall effect. Furthermore, we perform the numerical calculation for each observable and discuss the obtained results.

6.3 The physical observables

In this section we evaluate the physical observables for the 2D Dirac-Rashba model with spin-valley coupling. We focus on the charge current, spin Hall and Edelstein effect evaluated at the leading order in the relaxation time due to the chosen ansatz Eq.(5.26). The expressions found in the following represent part of the original results of the work of this thesis. Keeping in mind the expression for the averaged observable Eq.(2.69), we define the effective vertices for the charge ($V_{eff} = 4\mathcal{V}$), the inverse-spin galvanic and the spin Hall response respectively as

$$V_{eff} = \mathrm{Tr}\left(\sigma_{\mathrm{x}} \otimes \mathrm{s}_0 \mathrm{P}_{1-1}\left(\mathrm{k_F}, \theta\right)\right) = \frac{2(\beta+\alpha\gamma)}{1+\alpha^2+\beta^2+\gamma^2}\cos(\theta), \tag{6.14}$$

$$S^y_{eff} = \mathrm{Tr}\left(\sigma_0 \otimes \mathrm{s_y} \mathrm{P}_{1-1}\left(\mathrm{k_F}, \theta\right)\right) = \frac{2(\alpha+\beta\gamma)}{1+\alpha^2+\beta^2+\gamma^2}\cos(\theta), \tag{6.15}$$

$$J^z_{y,eff} = \mathrm{Tr}\left(\sigma_{\mathrm{y}} \otimes \mathrm{s_z} \mathrm{P}_{1-1}\left(\mathrm{k_F}, \theta\right)\right) = \frac{2(\beta-\alpha\gamma)}{1+\alpha^2+\beta^2+\gamma^2}\sin(\theta), \tag{6.16}$$

where α, β and γ depend on the parameters of the Hamiltonian and on the Fermi energy, as defined in the Eq.(3.25). To understand better the effect of SOC, we perform a numerical calculation of these vertices in units of $cos(\theta)$ and $sin(\theta)$, respectively. We call them

$$\overline{V}_{eff} = \frac{V_{eff}}{cos(\theta)}, \qquad \overline{S}^y_{eff} = \frac{S^y_{eff}}{cos(\theta)}, \qquad \overline{J}^z_{y,eff} = \frac{J^z_{y,eff}}{sin(\theta)}$$

and report the results in the Fig.[6.2]. As done before, we chose the same dimensionless SOC-values in units of the Fermi energy and fix $\varepsilon = 1$ with $\varepsilon\tau = 10$. It is interesting to notice that the effective charge vertex decreases slowly and quite linearly with SOC variables. While the Edelstein and spin Hall one show a quite complementary behaviour. In particular, this result tells us that $\overline{J}^z_{y,eff}$ is bigger in absolute value when the spin-valley becomes strong. For the following calculation we need the expression of the DOS at the Fermi level in the regime II Eq.(3.27) for the spin-valley Hamiltonian Eq.(3.21), i.e.

$$N_F^{sv} = \frac{\varepsilon(\lambda^2+\lambda_{sv}^2+\sqrt{\lambda^2\varepsilon^2+\lambda_{sv}^2(\varepsilon^2-\lambda^2)})}{2\pi\sqrt{\varepsilon^2(\lambda^2+\lambda_{sv}^2)-\lambda^2\lambda_{sv}^2}}. \tag{6.17}$$

It is easy to see that we recover the DOS of the pure Dirac-Rashba graphene model Eq.(5.21) if $\lambda_{sv} \to 0$. Finally, by recalling the expression Eq.(2.69) for the physical observables, the Drude conductivity, the Edelstein and the Spin Hall response read respectively

$$J_x = -\frac{N_F}{4}\int_0^{2\pi}\frac{d\theta}{2\pi}g_0(\theta)4v_{eff}(\theta) = -\frac{N_F}{8}\frac{\tau_{\parallel}^{-1}}{(\tau_{\parallel}^{-1})^2+(\tau_{\perp}^{-1})^2}\frac{(\beta+\alpha\gamma)^2}{(1+\alpha^2+\beta^2+\gamma^2)^2}, \tag{6.18}$$

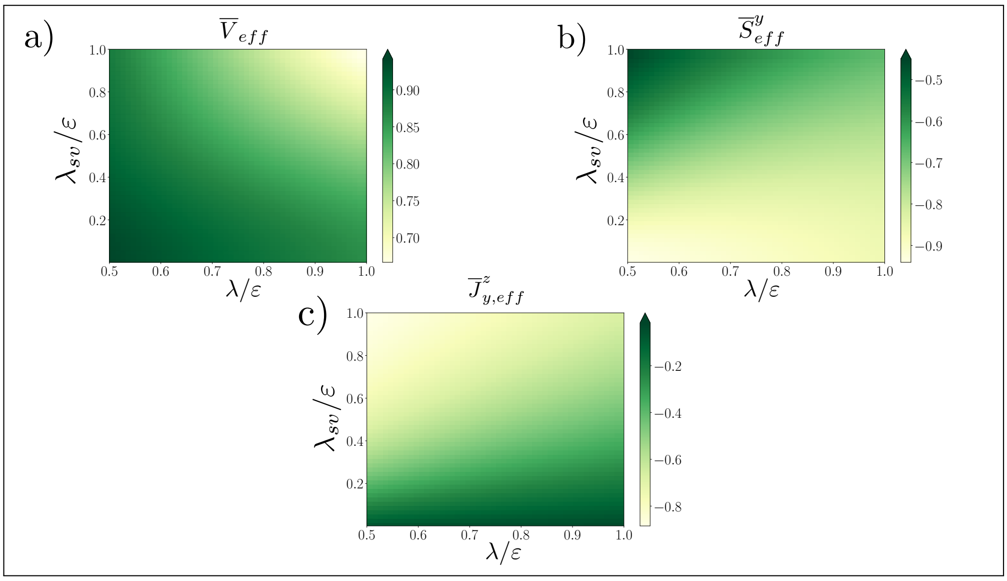

Figure 6.2: Numerical color plots of the effective vertices for a) the charge, b) inverse-spin galvanic and c) spin Hall response. The plots show the coefficients of $\cos(\theta)$ and $\sin(\theta)$ in the Eqs.(6.14)-(6.16). The vertex $\overline{V}_{eff}$ decreases slowly and linearly with the spin-valley and Rashba variables. While $\overline{S}_{y,eff}$ and $\overline{J}^{z}_{y,eff}$ show a quite complementary behaviour in terms of the SOC values. For all the plots we fix $\varepsilon\tau = 10$ with $\varepsilon = 1$. Furthermore, the Rashba and spin-valley parameters are in units of the Fermi energy.

$$S_y = -\frac{N_F}{4}\int_0^{2\pi}\frac{d\theta}{2\pi} g_0(\theta) S^y_{eff}(\theta) = -\frac{N_F}{8}\frac{\tau_{\parallel}^{-1}}{(\tau_{\parallel}^{-1})^2+(\tau_{\perp}^{-1})^2}\frac{(\alpha+\beta\gamma)(\beta+\alpha\gamma)}{(1+\alpha^2+\beta^2+\gamma^2)^2} \tag{6.19}$$

and

$$J^z_y = -\frac{N_F}{4}\int_0^{2\pi}\frac{d\theta}{2\pi} g_0(\theta) J^z_{y,eff}(\theta) = -\frac{N_F}{8}\frac{\tau_{\perp}^{-1}}{(\tau_{\parallel}^{-1})^2+(\tau_{\perp}^{-1})^2}\frac{(\beta-\alpha\gamma)()\beta+\alpha\gamma)}{(1+\alpha^2+\beta^2+\gamma^2)^2}, \tag{6.20}$$

where $g_0(\theta)$ is the final expression Eq.(6.11) and N_F is defined in the Eq.(6.17). The Fig.[6.3] shows the numerical evaluation of the analytical expressions Eqs.(6.19) and (6.20) at the same fixed Fermi energy and in the same metallic regime. Defining $g^0_{ss} = \pi u_0 N_0$, the skew-scattering coupling Eq.(6.5) becomes

$$g_{ss} = \frac{2g^0_{ss}N_F}{N_0} \tag{6.21}$$

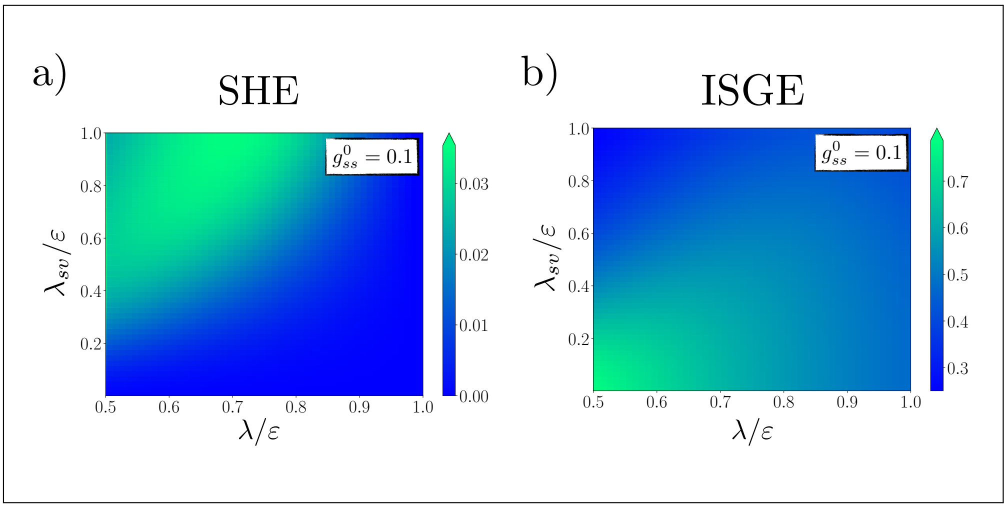

Figure 6.3: Numerical color plots show the behaviour of physical observables for the spin-valley and Dirac Rashba graphene system in regime II: a) the Spin Hall response increases slowly with the spin-valley coupling at small values of the Rahsba one; while b) the Edelstein effect becomes relevant for small values of SOC. For both graphs we fix $g^0_{ss} = 0.1$ and $\varepsilon = 1$ with $\varepsilon\tau = 10$. Furthermore, the Rashba and spin-valley parameters are in units of the Fermi energy.

and, for both plots, we fix $g^0_{ss} = 0.1$. In particular, the SHE increases slowly with the spin-valley coupling at small λ and the ISGE is relevant for small values of SOC. The resulting plots give us also information about the behaviour of the two different physical responses and confirm the presence of the spin Hall effect when the spin-valley coupling starts to be relevant.

From the physical observable expressions Eqs.(6.18)-(6.20), it is evident that the dependence of skew-scattering is only in the scattering-rate combination. As mentioned in the previous section, one can neglect $(\tau_\perp^{-1})^2$ in the Eq.(6.11) and then in the expressions of the physical observables Eq.(6.18)-(6.20). The result is that only J^z_y, i.e the spin Hall response, is affected by the skew-scattering mechanism, unlike J_x and S_y. To investigate in details the effect of skew-scattering, we perform a numerical calculation for J^z_y and S_y using g^0_{ss} as a variable according to the Eq.(6.21). As expected, for small values of g^0_{ss} the behaviour of the Edelstein response does not change significantly, so only the SHE analysis is reported in the Fig.[6.4]. We choose some skew-scattering values that show a modification in the system response. In particular, for small values of skew-scattering coupling the SHE is relevant only in the high range of spin-valley coupling at small values of the Rashba one. When g^0_{ss} grows, the system response becomes significant also for small values of SOC.

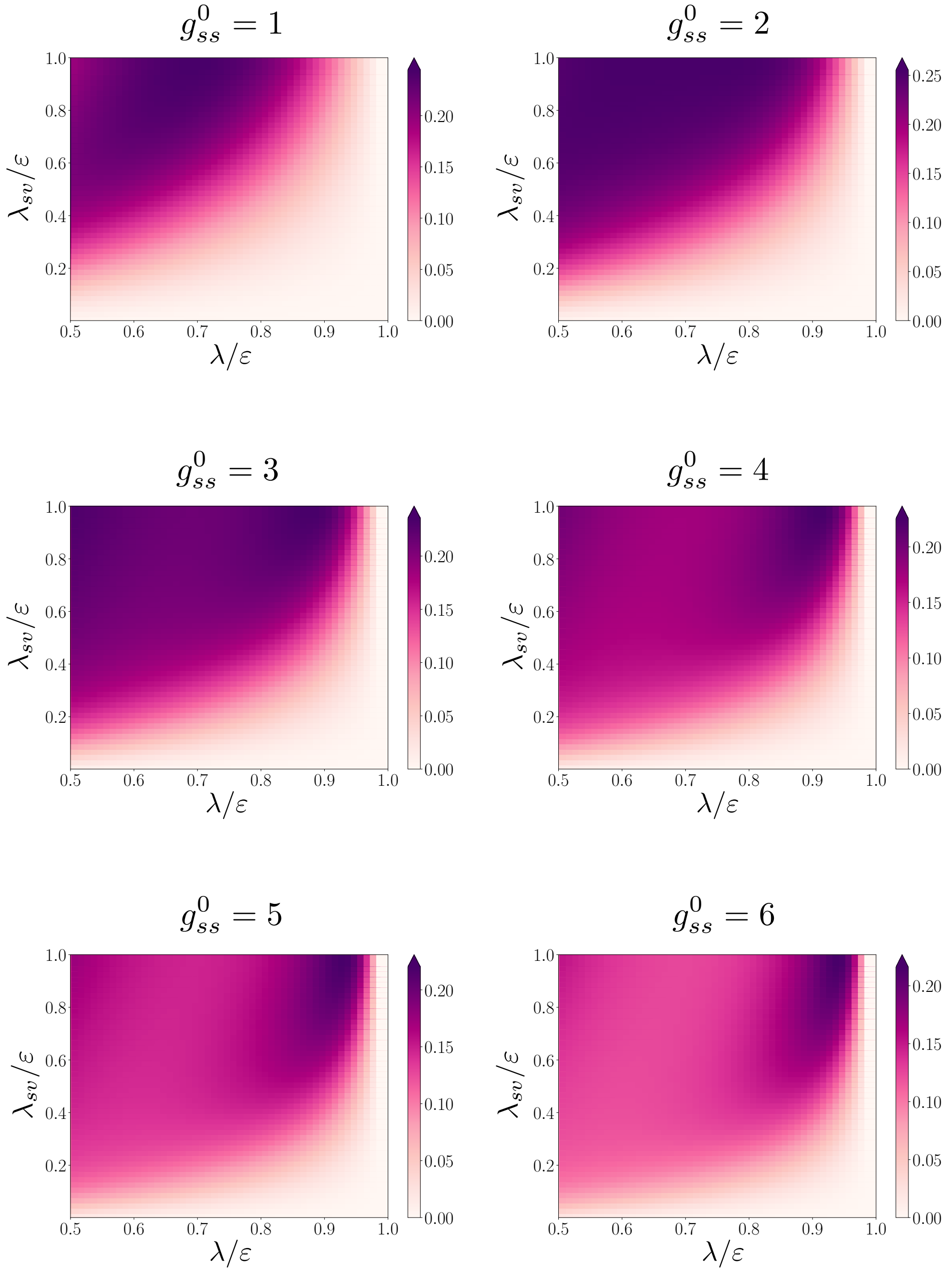

Figure 6.4: SHE color plots for different values of the skew-scattering coupling $g^0_{ss} = n$ with $n = 1, ..6$. The spin Hall response is significant for high values of spin-valley coupling when the skew-scattering is small. On the contrary, when g^0_{ss} becomes high, the effect starts to be relevant also for small values of SOC. For all the graphs $\varepsilon\tau = 10$ with $\varepsilon = 1$. Furthermore, the Rashba and spin valley parameters in units of the Fermi energy.

Conclusions

In this Chapter we presented the original treatment of the transport problem via the Eilenberger equation for the 2D Dirac-Rashba model with spin-valley coupling. For such a system, we analysed the skew-scattering mechanism in the one-band regime. We showed how take it into account from the $\mathrm{T}-$matrix approximation, i.e. considering higher order term in the $\mathrm{T}-$matrix expansion. From this point of view, we derived the new scattering kernel of the kinetic equation that results to be a sum of two terms. The first one coincides with the one found at the Born level, the second is an additional contribution due to the presence of the skew-scattering mechanism. In particular, this new term results to be an odd periodic function of the angle difference so that one can easily write it using the Fourier expansion. Hence, we introduced the skew-scattering coupling g_{ss} to write the Eilenberger equation in a compact way. After some manipulation, we found the solution of the kinetic equation from which we derived the analytical expressions of the physical observables that represent a very important result. To do that, we introduced two scattering rates, i.e. the parallel and the perpendicular component. After a numerical analysis, we found that the parallel scattering rate is one order of magnitude larger than the perpendicular one. This means that the latter can be neglect in the general solution of the kinetic equation, i.e. $g_0(\theta)$. Furthermore, $\tau_{\|}^{-1}$ is also the component that doesn't depend on the skew-scattering mechanism. This explains why the Edelstein effect is not significantly affected by the skew-scattering, while the SHE shows a more interesting modification. In particular, when the skew-scattering parameter g_{ss}^{0} grows, the system response becomes relevant also for small Rashba coupling.

7

The two-band regime

Overview

In this last Chapter, the two-band regime in the simpler Dirac-Rashba Hamiltonian is discussed, i.e. the regime II ($\varepsilon > 2\lambda$) [see Fig.3.2]. In particular, we analyse the clean 2D DR model first for both density matrix and quasiclassical Green's function. We show that in the stationary case, the kinetic equation can be written as a simple linear system in the basis of the Clifford's algebra. In order to take into account only the correct component of the density matrix function, we perform a commutation operation that automatically selects the perpendicular one (as already discussed in the Chapter 4). We find the well-know result for the spin Hall observable, as expected. This kind of matrix manipulation helps us to deal with the problem of disorder. As we emphasize in the following, the presence of two bands crossing the Fermi level in the regime II makes the definition of the quasiclassical Green's function not obvious. It is clear that the problem is how to write the variable ξ, i.e. the variable measuring the distance from the Fermi energy. In the clean case, we take advantage of the Clifford's algebra expansion to bypass the problem. While in the presence of disorder we use a suitable trick that is one of the main result of the work of this thesis. In this latter case, we show how manipulate the kinetic equation before the $\xi-$integration and rewrite the problem in terms of a simple linear system. The latter is quite easy to solve, apart from the complicated matrix structure of the linear operators. Thanks to it, we find the spin Hall conductivity in the particular good metal limit ($\varepsilon\tau \gg 1$) and we recover the suppression of the SHE due to the presence of the vertex corrections, as expected. In the end we discuss in details the algebra used for this calculation and the connection with the well-known diagrammatic evaluation.

7.1 The clean case

In this section we evaluate the spin Hall conductivity in the simple stationary case of the clean Hamiltonian in the presence of Rashba SOC given by the Eq.(3.1). It is evident that we expect the same result found in the Section 4.2, i.e. the spin Hall conductivity given by the Eq.(4.37), but the manipulation here is quite different. We show this calculation because it is useful to understand the algebra in the presence of disorder that we will discuss in the Section 7.2. From the Dyson equation, as already mentioned, one can recover the equation for the density matrix function or for the quasiclassical Green's function. The difference lives in the type of integration one performs. Having said that, we start from LR subtrcted Dyson equation Eq.(2.56) with no disorder $\Sigma = 0$. In a stationary system, the kinetic equation can be written as follows (we set $e = 1$ for simplicity)

$$i[h(\mathbf{k}), G] = \mathcal{Y}, \tag{7.1}$$

where $\mathcal{Y} = \boldsymbol{\sigma} \cdot \mathbf{E} \partial_\omega G_{eq}$ is the vector of the known terms that comes from the equilibrium Green's function and $h(\mathbf{k})$ is the density 2D Dirac-Rashba Hamiltonian Eq.(4.24). At this stage we define the matrix $\mathcal{M}$ as

$$\mathcal{M} \doteq i[h(\mathbf{k}), G], \tag{7.2}$$

i.e. the commutator of matrix G with the Hamiltonian. The matrix is in principle 16 by 16. However, each element of the matrix is obtained by the trace of the commutator between two elements of the algebra[1] multiplied by the Hamiltonian (it is clear that each element of the algebra commutes with the identity matrix), i.e.

$$\mathcal{M}^{ab} = \frac{i}{4} \mathrm{Tr}[h(\mathbf{k})(t^a t^b - t^b t^a)] \qquad with \quad a, b = 1, ..., 16 \quad , \tag{7.3}$$

where the Clifford's matrices are ordered as reported in the Table. C.1. The resulting matrix is showed in the Appendix F. In the Eq.(7.2), the part of G which commutes with the Hamiltonian is in the null-space of the linear system. To find the solution of G which is not in the null-space, we take the commutator with $h(\mathbf{k})$ of both the terms[2], i.e.

$$[h(\mathbf{k}), [h(\mathbf{k}), G]] = [h(\mathbf{k}), \mathcal{Y}]. \tag{7.4}$$

---

[1] As already pointed out several times, for the system under study we refer to the Clifford's algebra $t^a \equiv \gamma_{ij} = \sigma_i \otimes s_j$.

[2] We note that the commutation operation selects automatically the perpendicular component of G.

The linear operation of commutation with $h(\mathbf{k})$ is described by the matrix $\mathcal{M}$. Hence the double commutator is given by the square of the matrix $M = \mathcal{M}^2$ (also reported in the Appendix F). In order to solve the equation in the presence of an electric field such as the Eq.(4.2), we must invert the matrix M. To do that, we investigate the null space of this matrix. In particular, the matrix M has four vectors in this subspace that means M^{-1} does not exist. This suggests that we need to manipulate this matrix in order to solve the linear system Eq.(7.1). In the following, we use the density matrix approach first and then the quasiclassical Green's function to solve the kinetic equation. For both, we recover the well-know spin Hall conductivity but the algebra used below helps us to discuss the effect of disorder.

7.1.1 The density matrix evaluation

We start from the kinetic equation Eq.(7.1). After ω integration, we obtain an equation for the density matrix function. As discussed in the Chapter 4, we are looking for the linearized BTE with $f = f_{eq} + \delta f$. We assume as usual that f vanishes at $\pm\infty$. According to what we learned so far, one has to select only the perpendicular component of f_{eq} that does not commute with the Hamiltonian. It has the form[3]

$$\partial_{k_x} f_{eq} = \sum_{ln} (\partial_{k_x} P_{ln}) f_{FD} \equiv y_{ln}, \tag{7.5}$$

where we use the field choice Eq.(4.2). We also underline that $\mathcal{Y} = E_x \partial_{k_x} f_{eq}$ with $e = v = \hbar = 1$ in the Eq.(7.1). Now, we concentrate on the projector of the third-band first (P_{1-1}), and then on the one of the fourth one (P_{11}). To simplify the discussion, we call $y^{eff}_{ln} = \mathcal{M} \cdot y_{ln}$. When only one band crosses the Fermi level, i.e. the regime I, the RHS of the Eq.(7.4) is the vector

$$\begin{aligned} y^{eff}_{1-1} = \Big\{ & 0, 0, \frac{\lambda}{2\sqrt{\lambda^2 + k^2}}, \frac{1}{2k^2}\Big(\frac{\lambda {k_x}^2}{\sqrt{\lambda^2 + k^2}} - {k_y}^2\Big), 0, 0, 0, \\ & \frac{1}{2k^2} k_x k_y \left(\frac{\lambda}{\sqrt{\lambda^2 + k^2}} + 1\right), -\frac{k_y}{2\sqrt{\lambda^2 + k^2}}, 0, 0, 0, 0, 0, 0, 0 \Big\}, \end{aligned} \tag{7.6}$$

where we use the plane waves definition $\mathbf{k}_{ln} = k_{ln}(cos(\theta), sin(\theta)) \equiv (k_x, k_y)$ with here $k_{ln} = k_{1-1}$ and $k^2 = k_x^2 + k_y^2$. On the contrary, the LHS of the kinetic equation Eq.(7.2) is described by $M-$matrix. The latter has a quite complicated structure (as showed in the Appendix F) and, as already mentioned, its inverse doesn't exist. After a careful analysis, one can observe that the sub-block defined by the rows and columns 3 and 7 decouples from the others. We stress that the third element of the Clifford's algebra is connected to the spin Hall observable, i.e. $t^3 = \sigma_y \otimes s_z$, we are interested in (look at the Table C.1). For this reason we define a two by two matrix M_{eff} with the elements of this sub-block, i.e.

---

[3] Here we refer to the expression Eq.(4.27).

$$M^{eff}_{(3,7)} = \begin{pmatrix} -4\left({k_x}^2+\lambda^2\right) & 4k_x k_y \\ 4k_x k_y & -4\left({k_y}^2+\lambda^2\right) \end{pmatrix} \equiv \mathscr{M}. \tag{7.7}$$

Now, the system becomes easier to manipulate. In fact, one can solve the restricted problem for the density matrix δf, i.e. the linear system can be written as

$$\delta f = \mathscr{M}^{-1} \cdot x_{eff}, \tag{7.8}$$

where

$$x_{eff} = (y^{eff}_{1-1}[3], y^{eff}_{1-1}[7]) \tag{7.9}$$

is the restricted vector of the known terms. Solving the Eq.(7.8), the solution for the non equilibrium density matrix in the one-band regime reads

$$\delta f_{1-1} = \left\{ \frac{-\lambda^2 - {k_y}^2}{8\lambda\left(\lambda^2+k^2\right)^{3/2}}, -\frac{k_x k_y}{8\lambda\left(\lambda^2+k^2\right)^{3/2}} \right\}. \tag{7.10}$$

The angle average selects only the first component of δf_{1-1} that is linked to the physical observable of the spin Hall effect. Performing the integration over the angle θ, one obtains the following relation ($k_{1-1} \equiv k$)

$$\delta f^{sH}_{1-1} = \frac{-\frac{k^2}{2} - \lambda^2}{8\lambda\left(k^2+\lambda^2\right)^{3/2}}. \tag{7.11}$$

After the integration over the momentum, according to the Eq.(2.12) and taking into account with what was done in the Chapter 4, one can write the spin Hall conductivity in the well-know form for the third band (here we reintroduce the electrical charge e)

$$\sigma^{sH}_{1-1} = -\frac{e}{16\pi\lambda}\left(\frac{\varepsilon(\varepsilon+2\lambda)}{\varepsilon+\lambda}\right). \tag{7.12}$$

At this stage, one can perform the same calculation for the fourth band. Of course, the matrices $\mathcal{M}$ and $\mathscr{M}$ are the same while now the projector is P_{11}. One can manipulate the linear system in the same way done above so that the result for the spin Hall observable is (the reader can verify the result performing the same calculation)

$$\sigma^{sH}_{11} = \frac{e}{16\pi\lambda}\left(\frac{\varepsilon(\varepsilon-2\lambda)}{\varepsilon-\lambda}\right). \tag{7.13}$$

It is evident that the results Eqs.(7.12) and (7.13) agree with the expression Eq.(4.37). In fact, the total spin Hall conductivity in the two-band regime (regime II) is the sum of both terms, i.e. the contribution of the third and the fourth band. It reads

$$\sigma^{sH} = \sigma^{sH}_{1-1} + \sigma^{sH}_{11} = -\frac{e}{8\pi}\left(\frac{\varepsilon^2}{\varepsilon^2-\lambda^2}\right), \tag{7.14}$$

according to what reported in the literature Ref.[127, 128]. We stress that the integration over the energy ω captures both contributions to the conductivity (σ^I and σ^{II}), as already discussed in the Section 4.2. We recall here that the $far-$contribution to the conductivity vanishes, i.e. $\sigma^{II}_{1-1}+\sigma^{II}_{11}=0$. So, in the Eq.(7.14) only the terms $at-$ the Fermi surfaces appear. In the following, we evaluate the spin Hall observable with the help of the quasiclassical Green's function. We use the same algebra here discussed that prepares the basis for the next calculation in the presence of disorder.

7.1.2 The quasiclassical Green's function evaluation

We now turn to the ξ-integration and focus on the Keldysh component $g^K \equiv g$. Again, we focus in the clean and stationary 2D Dirac-Rashba system. We want to check if the linear operators manipulation discussed in the previous section gives us the proper result. Of course this calculation is preparatory for the more interesting model with the disorder effect. In the two-band regime, one has to take into account the presence of the two Fermi surfaces. In particular, the definition given in the Eq.(2.62) is not obvious. The problem is that the ξ-variable measures the distance from the Fermi energy, as already discussed for the one-band regime. In this case we have two Fermi energies, so evidently the problem must be faced in an another way. In the rest of this section, we go beyond this problem using the expansion in the basis of the Clifford's algebra. As painted in the Chapter 4 and from what discussed above, the kinetic equation has the same form of the Eq.(7.1) but $f \longrightarrow g$. Using $g = g_{eq}+\delta g$, one has the following equation

$$i[h(\mathbf{k}_F), \delta g] = \mathcal{Y}, \tag{7.15}$$

where, as before, $\mathcal{Y}$ is the known term linked to the equilibrium Green's function. In particular, from the Eq.(2.63), it reads

$$\mathcal{Y} = \frac{1}{2}\{\sigma_x \otimes s_0, g_{eq}\} \equiv \frac{1}{2}\mathrm{y}_{ln}, \tag{7.16}$$

with the field choice Eq.(4.2). Furthermore, in the Clifford's language $t^1 = \sigma_x \otimes s_0$. One can use the spectral theorem to write the equilibrium Green's function and expand the anticommutator in the Clifford's algebra, i.e.

$$\mathrm{y}^b_{ln} = \frac{1}{4}\mathrm{Tr}[(P_{ln}t^1 + t^1 P_{ln})t^b] \qquad with \quad b = 1, ..., 16, \tag{7.17}$$

with t^b the Clifford's matrices, as usual. We report the resulting matrix in the Appendix F. Again to solve the Eq.(7.15), one can take the commutator of both sides of the equation to select only the perpendicular component. The $h(\mathbf{k})$-commutation means to use the same matrices $\mathcal{M}$ and M found in the previous section. Similarly, we denote with y^{eff}_{ln} the vector that comes from the product $\mathcal{M} \cdot \mathrm{y}_{ln}$. We focus on the third band first (y^{eff}_{1-1}) and then on the fourth one (y^{eff}_{11}). The reader can find their explicit expressions in the Appendix F. As for the density matrix function -since the matrices are the same- we can solve the restricted problem for δg. The linear system is quite similar to the Eq.(7.8), in fact it reads

$$\delta g = \mathscr{M}^{-1} \cdot x_{eff}, \tag{7.18}$$

but now the restricted vector of the known term is

$$x_{eff} = \frac{1}{2}\left(\mathrm{y}^{eff}_{1-1}[3], \mathrm{y}^{eff}_{1-1}[7]\right). \tag{7.19}$$

In the end, solving the Eq.(7.18), the solution for the Green's function is[4]

$$\delta g_{1-1} = \left\{ \frac{\left(\sqrt{k^2+\lambda^2}+\lambda\right)\sin^2(\theta) - \lambda}{4\,(k^2+\lambda^2)}, \frac{\left(\sqrt{k^2+\lambda^2}+\lambda\right)\sin(2\theta)}{8\,(k^2+\lambda^2)} \right\}. \tag{7.20}$$

According to the Eq.(2.69), after the integration over the angle θ and using the DOS given by the Eq.(5.21), the corresponding contribution to the spin Hall conductivity is

$$\sigma^{sH}_{1-1} = -\frac{\varepsilon}{16\pi(\varepsilon+\lambda)}. \tag{7.21}$$

As expected, this is the contribution due to processes "at" the Fermi surface for the third band, i.e. when the chemical potential is positive and less than 2λ. If we want to consider also the fourth band, we have to do the same calculation done before but for the projector P_{11} and with the DOS given by the Eq.(5.20). Of course the reader can verify this statement. The obtained result reads

---

[4] Here we use the relation $k^2 = k_x^2 + k_y^2$.

$$\sigma_{11}^{sH} = -\frac{\varepsilon}{16\pi(\varepsilon - \lambda)}. \tag{7.22}$$

This contribution describes the processes $at-$ the Fermi surface when the chemical potential is positive and bigger than 2λ. These agree with the result Eq.(4.37). It is evident that the sum of the Eqs.(7.21) and (7.22) reproduces the total σ^I contribution to the spin Hall conductivity Eq.(4.41). In the next section we discuss the presence of disorder for the 2D Dirac-Rashba system in the two-band regime. What has been done so far helps us to manipulate the kinetic equation with a non-zero self-energy.

7.2 The disorder effect

In this section we want to take into account also the presence of disorder in the 2D Dirac-Rashba system, this means $\Sigma \neq 0$. As already mentioned, the definition of the quasiclassical Green's function is not obvious in the regime II so that the Eilenberger equation is not easy to derive. The presence of two Fermi surfaces makes difficult the definition of the $\xi-$variable that measures the distance with respect to the Fermi energy. For the reasons here exposed, we need to start from the kinetic equation before the integration over the variable ξ. Let us consider as usual the field choice Eq.(4.2). Having in mind the Eqs.(2.57) and (2.58), for the Keldysh component we have the following kinetic equation ($G^K \equiv G$ and $e = 1$ for simplicity)

$$\begin{aligned} -E_x\partial_{k_x}G_{eq}(\mathbf{k}) - E_x\frac{1}{2}\Big\{\sigma_x, \partial_\omega G_{eq}(\mathbf{k})\Big\} + i\,[h(\mathbf{k}), G(\mathbf{k})] = \\ -i\Big\{\Sigma^R, G(\mathbf{k})\Big\} + i\left(G^R(\mathbf{k})\Sigma^K - \Sigma^K G^A(\mathbf{k})\right). \end{aligned} \tag{7.23}$$

As already mentioned in the previous section, $h(\mathbf{k})$ is the density 2D Dirac-Rashba Hamiltonian Eq.(4.24). In the regime II the retarded/advanced self-energy in the Born approximation is given by the relation Eq.(5.19), so the above equation can be rewritten as

$$\mathcal{L}(\mathbf{k})G(\mathbf{k}) = E\partial_{k_x}G_{eq}(\mathbf{k}) + E\frac{1}{2}\Big\{\sigma_x, \partial_\omega G_{eq}(\mathbf{k})\Big\} + i\left(G^R(\mathbf{k})\Sigma^K - \Sigma^K G^A(\mathbf{k})\right), \tag{7.24}$$

with the linear operator $\mathcal{L}(\mathbf{k})$ defined as follows (see Appendix F for its explicit form)

$$\frac{1}{\tau}G(\mathbf{k}) + i\,[h(\mathbf{k}), G(\mathbf{k})] \equiv \mathcal{L}(\mathbf{k})G(\mathbf{k}). \tag{7.25}$$

It is important to stress that the presence of disorder makes the matrix $\mathcal{L}(\mathbf{k})$ non-singular. This means that $\mathcal{L}(\mathbf{k})^{-1}$ exists and the kinetic equation can be solved. Formally the Eq.(7.24) for the Green's function can be written as

$$G(\mathbf{k}) = \mathcal{L}^{-1}(\mathbf{k})\left(E\partial_{k_x}G_{eq}(\mathbf{k}) + E\frac{1}{2}\Big\{\sigma_x,\partial_\omega G_{eq}(\mathbf{k})\Big\} + i\left(G^R(\mathbf{k})\Sigma^K - \Sigma^K G^A(\mathbf{k})\right)\right). \tag{7.26}$$

Here we use an alternative trick to rewrite the above equation, i.e. the integration over the momentum $\mathbf{k}$ instead of the variable ξ. Using the following notation

$$\int_{\mathbf{k}} \equiv \int \frac{d\mathbf{k}}{(2\pi)^2}, \tag{7.27}$$

one can integrate both members of the Eq.(7.26) and obtain[5]

$$\begin{aligned}\int_{\mathbf{k}} G(\mathbf{k}) = E\int_{\mathbf{k}}\mathcal{L}^{-1}(\mathbf{k})\frac{1}{2}\Big\{\sigma_x,\partial_\omega G_{eq}(\mathbf{k})\Big\} + \\ + iu_0^2\int_{\mathbf{k}}\mathcal{L}^{-1}(\mathbf{k})\left(G^R(\mathbf{k})\int_{\mathbf{k}'}G(\mathbf{k}') - \int_{\mathbf{k}'}G(\mathbf{k}')G^A(\mathbf{k})\right).\end{aligned} \tag{7.28}$$

Here the Keldysh self-energy is defined as follows

$$\Sigma^K = u_0^2\int_{\mathbf{k}'}G(\mathbf{k}'), \tag{7.29}$$

with u_0 the strength of the well-known scalar potential Eq.(2.3). By a careful analysis of the Eq.(7.28) one may notice that by defining the quantity

$$X \equiv \int_{\mathbf{k}} G(\mathbf{k}), \tag{7.30}$$

the kinetic equation can be rewritten as[6]

$$X = Y + \Big\{R, X\Big\}. \tag{7.31}$$

Above we have introduced the quantities Y and R as follows

$$Y \equiv E\int_{\mathbf{k}}\mathcal{L}^{-1}(\mathbf{k})\frac{1}{2}\Big\{\sigma_x,\partial_\omega G_{eq}(\mathbf{k})\Big\} \tag{7.32}$$

and[7]

---

[5] Here we use the expression Eq.(2.46), so that the first term on the RHS of the Eq.(7.26) vanishes.

[6] Note that the retarded and advanced component of the Green's function has different sign.

[7] Here we use the relation $u_0^2 = 1/\tau\varepsilon$.

$$R \equiv iu_0^2 \int_{\mathbf{k}} \mathcal{L}^{-1}(\mathbf{k}) G^R(\mathbf{k}) = \frac{i}{\tau\varepsilon} \int_{\mathbf{k}} \mathcal{L}^{-1}(\mathbf{k}) G^R(\mathbf{k}). \tag{7.33}$$

Now we assume that the poles, as function of momentum $\mathbf{k}$, are only in the retarded Green's function $G^R(\mathbf{k})$. Having in mind the Eq.(5.19), by considering the two Fermi surfaces and performing the integration, one has

$$R = \frac{\pi}{\tau\varepsilon} \langle \Big(\mathcal{L}^{-1}(k_{1-1}) N_{1-1} P_{1-1}(k_{1-1}) + \mathcal{L}^{-1}(k_{11}) N_{11} P_{11}(k_{11}) \Big) \rangle, \tag{7.34}$$

where the two DOS are given by the Eqs.(5.21) and (5.20). Furthermore $k_{1-1}^2 + \lambda^2 = (\varepsilon + \lambda)^2$ and $k_{11}^2 + \lambda^2 = (\varepsilon - \lambda)^2$. In a similar way, the reader can verify that the Eq.(7.32) becomes

$$Y = E \langle \Big(\mathcal{L}^{-1}(k_{1-1}) N_{1-1} \Big\{ \sigma_x, P_{1-1}(k_{1-1}) \Big\} + \mathcal{L}^{-1}(k_{11}) N_{11} \Big\{ \sigma_x, P_{11}(k_{11}) \Big\} \Big) \rangle, \tag{7.35}$$

where the Keldysh equilibrium Green's function is in the form given by the Eq.(2.46). To proceed further, the idea is to expand all the matrices in the Clifford's basis t^a. So, the linear system Eq.(7.31) becomes

$$X^a = Y^a + R^{ab} X^b, \tag{7.36}$$

where

$$Y^a = \frac{1}{4} \mathrm{Tr}(t^a Y), \qquad R^{ab} = \frac{1}{4} \mathrm{Tr}\Big(R \Big\{ t^a, t^b \Big\} \Big) \quad with \quad a, b = 1, ..., 16. \tag{7.37}$$

We stress that the term Y^a in the RHS represents the "bare bubble" in the presence of disorder, whereas the term $R^{ab} X^b$ are the vertex corrections. In the next section we discuss and comment in details this significant result. We report the explicit form of the vector Y and the operator R in the Appendix F. It is important to underline here that the linear operator R shows the 4 by 4 sub-blocks structure according to the symmetries of the system (see Appendix C for details). At this stage one can introduce the operator Q^{ab} as (in the Appendix F we report explicitly its matrix structure)

$$Q^{ab} = \delta^{ab} - R^{ab}, \tag{7.38}$$

so that the final system becomes

$$Q^{ab} X^b = Y^a. \tag{7.39}$$

One can notice that the matrix Q has the same sub-block structure of R, as expected. As already pointed out, this stresses the symmetries of the system. The linear equation Eq.(7.39) is a closed system and describes the entire model, so one can solve it without any approximation. To proceed further, we focus on the first sub-block of the operator Q, i.e. the sub-block linked to the Γ_1-group of matrices (see Appendix C). Furthermore, the vector Y has only the first four components non vanishing (the explicit form is reported in the Appendix F). We recall here that the third line in the matrix structure is connected to the spin Hall observable and we expect to see the suppression of the SH conductivity, as pointed out several times. The linear system in the Γ_1-subspace reads

$$Q_{\Gamma_1} X_{\Gamma_1} = Y_{\Gamma_1} \tag{7.40}$$

with

$$Q_{\Gamma_1} = \begin{pmatrix} \frac{\left(\varepsilon^2-2\lambda^2\right)}{2(\lambda^2-\varepsilon^2)}+1 & -\frac{\lambda\varepsilon}{2\lambda^2-2\varepsilon^2} & -\frac{\varepsilon}{4\varepsilon\tau(\lambda^2-\varepsilon^2)} & \frac{\lambda\varepsilon}{4\varepsilon\tau(\lambda^2-\varepsilon^2)} \\ -\frac{\lambda\varepsilon}{2(\lambda^2-\varepsilon^2)} & \frac{\left(\varepsilon^2-2\lambda^2\right)}{2(\lambda^2-\varepsilon^2)}+1 & -\frac{\varepsilon^3}{4\varepsilon\tau(\lambda^3-\lambda\varepsilon^2)} & \frac{\varepsilon^2}{4\varepsilon\tau(\lambda^2-\varepsilon^2)} \\ \frac{\varepsilon^2}{4\varepsilon\tau(\lambda^2-\varepsilon^2)} & \frac{\varepsilon^3}{4\varepsilon\tau(\lambda^3-\lambda\varepsilon^2)} & 1 & 0 \\ -\frac{\lambda\varepsilon}{4\varepsilon\tau(\lambda^2-\varepsilon^2)} & -\frac{\varepsilon^2}{4\varepsilon\tau(\lambda^2-\varepsilon^2)} & 0 & 1 \end{pmatrix}. \tag{7.41}$$

The linear system Eq.(7.40) can be solved by first looking at leading terms in $\varepsilon\tau \gg 1$ (good metal condition) and for strong SOC ($\lambda\tau \gg 1$). In fact, in the weak-disorder limit, the vector of the known terms can be rewritten as

$$Y_{\Gamma_1} = \Big(-\frac{\varepsilon\tau\left(\varepsilon^2-2\lambda^2\right)}{4\pi\left(\varepsilon^2-\lambda^2\right)},\quad -\frac{\varepsilon\tau(\lambda\varepsilon)}{4\pi(\lambda^2-\varepsilon^2)},\quad -\frac{\varepsilon^2}{8\pi\left(\varepsilon^2-\lambda^2\right)},\quad \frac{\lambda\varepsilon}{8\pi(\lambda^2-\varepsilon^2)} \Big). \tag{7.42}$$

From the above expression, it is easy to note that the first two elements of the vector Y_{Γ_1} are of order $(\varepsilon\tau)^1$, while the others of order $(\varepsilon\tau)^0$. One can notice that the third element of the Eq.(7.42) is exactly the SH conductivity (σ^I) at leading order in the expansion of the inverse relaxation time τ^{-1}, i.e. the "empty bubble" solution without disorder Eq.(4.41). If one has a look at the matrix Eq.(7.41), it is immediately possible to notice that the 2 by 2 sub-blocks are independent from each others. Furthermore, the off-diagonal 2 by 2 sub-blocks are of order $(\varepsilon\tau)^{-1}$, while the others of the order of the unity. In particular, the 2 by 2 sub-block at the bottom right is the identity matrix. This means that the problem can be decoupled and one can control the dominant terms in $\varepsilon\tau$ and the sub-leading ones. Solving the linear system Eq.(7.40) with these ingredients, one easily obtains

$$X_{\Gamma_1} = \left(\frac{\varepsilon\tau}{2}, \quad -\lambda\tau, \quad 0, \quad 0\right). \tag{7.43}$$

In other words we recover the suppression of the spin Hall effect ($X^3_{\Gamma_1} = 0$), as expected. This happens thanks to the vertex corrections that are of order $(\varepsilon\tau)^0$ and cancel out the "empty bubble" spin Hall conductivity. This result agrees with what reported in the Ref.[127]. The empty bubble SH conductivity is precisely counteracted by the corresponding empty bubble for the spin density-charge current response function ($\sigma_{SG} \propto \sigma_0 \otimes s_y$). This means that the absence of the SHE is linked to the onset of a current-induced in-plane spin polarization, i.e. the spin-galvanic effect. This manipulation is very compact and powerful. In fact, if one considers an electric field along a different direction (instead of the x one), the problem is reduced to solve the linear system in the another subspace or sub-block. Finally, if we consider only the "bare bubble" solution in the presence of disorder without the vertex corrections, i.e.

$$X_{\Gamma_1} = Y_{\Gamma_1}, \tag{7.44}$$

in the good metal limit and for $\lambda\tau$ arbitrary, the spin Hall conductivity reads

$$\sigma^{sH} = -\frac{1}{8\pi}\left(\frac{\varepsilon^2}{\varepsilon^2 - \lambda^2} - \frac{1}{1 + 4\lambda^2\tau^2}\right), \tag{7.45}$$

according to what reported in the Ref.[127]. Here it is important to emphasize that, while the good metal condition constrains $\varepsilon\tau$, the quantity $\lambda\tau$ is completely arbitrary. Of course, this is possible only in the regime II. In the following, we discuss better the meaning of the linear system here discussed and we stress the connection with the diagrammatic evaluation.

7.2.1 About the ladder diagrams

Here we want to discuss about the manipulation done in the previous section to solve the problem in the presence of disorder. The interesting result that needs a comment concerns the linear operator R^{ab} (reported in the Appendix F). The matrix shows a block structure that reflects the symmetries of the system [132]. The 2D Dirac-Rashba model is invariant under the group $C_{\infty v}$, which is an emergent symmetry of the continuum long-wavelength theory (see Appendix C for more details). For example, the rotation of π around the $\hat{z}-$axis exchanging sublattice and valley (C_2) or the reflection over the $\hat{x}-$axis (R_x) are relevant. One has also the pseudospin (valley) rotation $\Lambda_{x,y,z}$ [146, 147]. From the expansion Eq.(7.37), it is clear that under the symmetry transformations only the Clifford's algebra elements can change sign[8]. If $t^a \longrightarrow \pm t^a$ and $t^b \longrightarrow \pm t^b$, the result is not zero. Otherwise, when $t^a \longrightarrow \pm t^a$ and $t^b \longrightarrow \mp t^b$ the element R^{ab} vanishes. The 4 by 4 sub-block structure of the $R-$matrix makes this property manifest. Another important result of this work is that while we cannot define a proper quasiclassical Green's function, all bubble diagrams can be taken into account thanks to this manipulation. We shortly explain how this happens. Before each manipulation, one can write the following relation

$$R \equiv i \int_{\mathbf{k}} \mathcal{L}^{-1}(\mathbf{k}) \Big(G^R(\mathbf{k}) \Sigma^K - \Sigma^K G^A(\mathbf{k}) \Big) = \int_{\mathbf{k}} \mathcal{L}^{-1}(\mathbf{k}) \Big(G^R(\mathbf{k}) \Sigma^K G^A(\mathbf{k}) \Big), \tag{7.46}$$

that is easy to verify in the scalar case. Writing the $(ij)-$element of the linear operator R and using a simple algebra, one can prove the above relation in the matrix case (we let the reader to verify it). If one neglects for the moment the known term in the Eq.(7.28), the kinetic equation in the Clifford's basis becomes

$$X^a = u_0^2 \frac{1}{4} \mathrm{Tr} \Big(t^a \int_{\mathbf{k}} \mathcal{L}^{-1}(\mathbf{k}) G^R(\mathbf{k}) t^b G^A(\mathbf{k}) \Big) X^b, \tag{7.47}$$

where we use the definition Eq.(7.30). This result tells us that R is the summation of non-crossing two-particle ladder diagrams. In other words, the Eq.(7.47) represents the linear response theory where R has the same form of the susceptibility reported in the Ref.[132], i.e.

$$\chi_i^{ab} \propto \sum_{\mathbf{k}} \mathrm{Tr}\{ \gamma_{0i} \mathcal{G}^R(\mathbf{k}) \bar{\gamma}_{ab} \mathcal{G}^A(\mathbf{k}) \}, \tag{7.48}$$

where $i = x, y, z$ is a generic component and $\bar{\gamma}_{ab}$ is the dressed vertex. Of course, in our case, the operator $\mathcal{L}^{-1}(\mathbf{k})$ takes into account the the presence of disorder that gives rise to the vertex corrections. Summing up briefly, using the trick of integration over the momentum $\mathbf{k}$ one can solves the problem of the two Fermi energies in the regime II. Furthermore, since the effect of disorder makes the operator $\mathcal{L}(\mathbf{k})$ not singular, one can evaluate all terms in the kinetic equation and, in particular, is able to take into account all the ladder diagrams.

---

[8] The Green's function is invariant under symmetry transformations because is a function of the system Hamiltonian.

Conclusion

In this Chapter we studied the two-band regime for the 2D Dirac-Rashba Hamiltonian. The spin Hall observable obtained with the kinetic equation for the density matrix function and for the quasiclassical Green's function confirms what already discussed about the "two" contributions of the conductivity, i.e. the Kubo-Streda formula. From the $\omega-$integration we obtained both terms, while the $\xi-$one captures only the processes $at-$ the Fermi surface, as expected. These results are well-known, but the matrix manipulation of the kinetic equation sheds new light on the problem. As mentioned, the quasiclassical Green's function can not be defined in the ordinary way due to the presence of the two Fermi surfaces. We showed that although we are unable to write g, the kinetic equation can be manipulated in an innovative way. The trick of the integration over the momentum $\mathbf{k}$, makes the equation easy to solve (apart the complicated 16 by 16 matrix structure). However, the linear operators show the correct symmetries of the system, as expected. This makes all the problem easier to manipulate. In fact, the 4 by 4 sub-block structure helps us to solve the system. Furthermore, we proved that the power of this manipulation lies in the fact that one can take into account all the non-crossing ladder diagrams. In fact, the linear operator R has the same matrix structure of the susceptibility that comes from the linear response theory. In particular, in the limit of a good metal and for strong SOC, we recovered the suppression of SH conductivity, as expected. This cancellation is due to the presence of vertex corrections linked to the spin density-charge current response. In the end, we recovered the well-know result for the "empty bubble" spin Hall conductivity reported in the recent literature.

Conclusions

In this thesis we have studied the coupled charge/spin dynamics in the 2D honeycomb layers with strong proximity-induced spin-orbit interactions. Our system of interest is one of the most promising for the next generation of spintronics nanodevices and nanoelectronics. The multiple $spin-like$ DOFs in 2D graphene-layers (pseudospin, spin and valley) offer unprecedented possibilities to explore unconventional spin dynamics and charge-to-spin conversion. The innovative approach in the work of this thesis consists in the derivation of the Eilenberger equation for the quasiclassical Green's function for such a system. To make that, we stressed first the equivalence between the Boltzmann kinetic equation end the quasiclassical approximation. After the short derivation of the kinetic transport equation for the density matrix and quasiclassical Green's function, we went deeper in the calculation. For the simple system of the massive Dirac fermions with no static disorder, we proved the consistency of the two methods performing the calculation of the (anomalous) Hall conductivity. We showed how only selecting the $perpendicular$ component of the density function we can obtain the correct linear relation between the current and the applied electric field. This result helped us to manipulate the quasiclassical Green's function in the proper way. The expression obtained for the Hall conductivities with both approaches overlap and this confirms the consistency of the quasiclassical approximation. Using what has been discovered about the simple massive Dirac fermions, we were able to write the Boltzmann equation for the 2D Dirac-Rashba model and evaluate the spin Hall observable. This result agrees with what reported in the literature and shows the two contributions $"far"$ and $"at"$ the Fermi surface according to the Kubo-Streda equation. This allowed us to immediately point out that the $\xi-$integration in the quasiclassical approximation captures only the processes $"at"$ the Fermi surface by definition. Furthermore, the $\sigma^{sH} \neq 0$ is not in contradiction with the conservation law for the spin current. In fact, the suppression of the SHE occurs in the presence of an arbitrary small concentration of scalar impurities which allow for a stationary.

After the clean cases, we went in details about the effect of disorder for the system under study. We discussed how to treat the presence of disorder via the $\mathrm{T}-$matrix approximation. In particular we concentrated on the static scalar impurity scattering in order to perform the disordered-average of the Green's function. Here we found one of the main result of the work of this thesis that is the completely generic expression for the collision integral of the kinetic equation in terms of $\mathrm{T}-$matrix. After a careful analysis of this expression, we proved that the microscopic reversibility of the scattering probability is preserved, as expected. Depending on which approximation one performs for the $\mathrm{T}-$matrix, one can write the collision integral for the system which is interested in. In fact, we studied the 2D Dirac-Rashba system first and, then, we added the $spin-valley$ coupling. In the first case, two regimes exist: regime I when $|\epsilon| < 2|\lambda|$ and regime II for $|\epsilon| > 2|\lambda|$. In the stationary case at the Born level (only the first term in the $\mathrm{T}-$matrix expansion), we found the corresponding self-energy for both regimes. We stressed that the matrix structure of the disordered averaged self-energy in the regime II is simpler than the one in regime I. However the presence of two Fermi surfaces makes the mathematical description quite complex. For this reason we focused on the one-band regime first. For such a regime, we derived the Eilenberger equation at the Born level and the physical observables. To do that, we used an $ansatz$ regarding the matrix structure of the quasiclassical Green's function. The latter can be justified by the argument that the physical observables we are interested in, like the spin Hall or Edelstein effect, are of order of the relaxation time. The results found for the spin density along the $y-$direction and the charge current along $x-$direction coincide exactly with what reported in the recent literature obtained via the Kubo linear response theory. Furthermore, in this case, the spin Hall response vanishes as expected.

After the results found for the 2D Dirac-Rashba Hamiltonian, we were confident to go further and study the skew-scattering mechanism in the more interesting model with the presence of spin-valley coupling. For such a system, we introduced a very compact notation for its eigenstates that helped us to derive the Eilenberger kinetic equation. To do that, we first went beyond the Born approximation including higher-order terms in the $\mathrm{T}-$matrix expansion and we used again the ansatz for the quasiclassical Green's function. In the end, we were able to write the kinetic equation and its analytic solution for the quasiclassical Green's function. Thanks to this result, we performed a numerical analysis of the physical quantities. In particular, one of the most interesting result concerns how much the skew-scattering affects the observables. For this purpose, we defined a skew-scattering coupling useful to perform the numerical analysis. We showed that the behaviour of the Edelstein response does not change significantly. This is also evident from a deeper analysis of its analytic formula in the limit of small skew-scattering. On the contrary, the spin Hall effect is affected by the presence of the skew-scattering mechanism. In particular, for small values of skew-scattering coupling the SHE is relevant only in the high range of spin-valley coupling.

In the last part of our work, we focused on the two-band regime (regime II). From the definition of the quasiclassical Green's function and the $\xi-$variable, it is evident that in this case the definition of the distance from the Fermi energy is not trivial due to the presence of two Fermi surfaces. We started from the manipulation of the kinetic equation in the clean case for the density matrix first and the quasiclassical Green's function after. For both cases we recovered the well-know results for the spin Hall conductivity but with a different matrix-manipulation. This helped us to understand how perform the calculation in the presence of disorder. In fact, although we were not able to define the $\xi-$variable, we found a different and powerful way to solve the kinetic equation. We reduced it to a "simple" and closed linear system from which we recovered the (empty bubble) spin Hall observable in the limit of a good metal and for arbitrary SOC, according to what reported in the literature. Furthermore, thanks to the symmetries of the system, we reduced the problem to the first sub-block, i.e. the sub-block that contains the spin Hall observable. Solving the reduced problem, we found the cancellation of SH conductivity due to the presence of the vertex corrections, as expected. The power of such a manipulation lies in the compactness of the algebra used and, at the same time, in the control of the dominant and the sub-leading terms. The most important feature here is the fact that the integration over momentum $\mathbf{k}$ (instead of ξ) helped us to rewrite the kinetic equation in terms of two linear operators (Y and R). These represent the "bare bubble" in the presence of disorder and the vertex corrections, respectively. We discussed in details this concept stressing the equivalence between the linear response theory and the diagrammatic evaluation. The main result here is that R represents the summation of non-crossing two-particle ladder diagrams and has the same structure of the susceptibility which comes from the linear response theory. This tells us that, with the trick of $\mathbf{k}-$integration instead of the $\xi-$one, we automatically can take into account all the "bubble" diagrams.

A

The Dirac equation and the SOC

Here we recall the derivation of spin-orbit coupling starting from the Dirac equation. The latter one reads

$$i\hbar\partial_t\psi = (c\boldsymbol{\alpha}\cdot\mathbf{k}+\beta mc^2+V)\psi \tag{A.1}$$

with

$$\boldsymbol{\alpha}=\begin{pmatrix}0 & \boldsymbol{\sigma}\\ \boldsymbol{\sigma} & 0\end{pmatrix},\quad \beta=\begin{pmatrix}1 & 0\\ 0 & -1\end{pmatrix},\quad V=eV\begin{pmatrix}1 & 0\\ 0 & 1\end{pmatrix},\quad \psi=\begin{pmatrix}\psi_1\\ \psi_2\end{pmatrix},$$

where we consider the presence of a static electric field described by eV, ψ_1 and ψ_2 are the upper and lower components of the bispinor ψ. While $\boldsymbol{\sigma}$ are the Pauli matrices linked to the spin of the electron $\boldsymbol{\sigma}=2\mathrm{S}/\hbar$. Taking mc^2 as the zero of energy, the Dirac equation becomes

$$\begin{aligned} i\hbar\partial_t\psi_1 &= eV\psi_1+c\boldsymbol{\sigma}\cdot\mathbf{k}\psi_2, \\ i\hbar\partial_t\psi_2 &= c\boldsymbol{\sigma}\cdot\mathbf{k}\psi_1+(eV-2mc^2)\psi_2, \end{aligned} \tag{A.2}$$

which shows that when eV and ck are small compared to the so-called Dirac gap $2mc^2$ (the non-relativistic limit), $\psi_1\sim e^{-imc^2t/\hbar}$ and $\psi_2\sim e^{imc^2t/\hbar}$. Now we want to derive an equation for the upper component ψ_1 when the Dirac gap is the largest energy scale. To this end we use the second equation in the Eq.(A.2) expressing ψ_2 in terms of ψ_1 and we make an expansion in the parameter $1/(2mc^2)$

$$\psi_2 \simeq \frac{1}{2mc}\Big(1-\frac{i\hbar\partial_t}{2mc^2}+\frac{eV}{2mc^2}\Big)\boldsymbol{\sigma}\cdot\mathbf{k}\psi_1. \tag{A.3}$$

In this way we can eliminate ψ_2 in the equation for ψ_1. The normalization condition for the original wave function $\langle\psi|\psi\rangle = 1$ implies

$$\langle\psi|\psi\rangle = \langle\psi_1|\psi_1\rangle + \langle\psi_2|\psi_2\rangle = 1. \tag{A.4}$$

Therefore, if we define

$$\tilde{\psi} = \left(1 + \frac{(\boldsymbol{\sigma}\cdot\mathbf{k})^2}{8m^2c^2}\right)\psi_1, \tag{A.5}$$

$\tilde{\psi}$ satisfies $\langle\tilde{\psi}|\tilde{\psi}\rangle = 1$ at order $1/(2mc^2)$. The equation for $\tilde{\psi}$ then reads

$$i\hbar\partial_t\tilde{\psi} = \left(1 - \frac{k^2}{8m^2c^2}\right)\left[eV + \frac{k^2}{2m} + \boldsymbol{\sigma}\cdot\mathbf{k}\frac{eV}{4m^2c^2}\boldsymbol{\sigma}\cdot\mathbf{k}\right]\left(1 + \frac{k^2}{8m^2c^2}\right)\tilde{\psi}. \tag{A.6}$$

By calculating the product up to terms of order $1/c^2$, we get

$$H_{eff} = eV + \frac{k^2}{2m} - \frac{k^4}{8m^3c^2} + \frac{e\hbar\Delta V}{8m^3c^2} + \frac{e\hbar}{4m^2c^2}\boldsymbol{\sigma}\cdot\nabla V \times \mathbf{k}, \tag{A.7}$$

where the first two terms represent the classical non-relativistic hamiltonian, the third term is the first relativistic correction to the kinetic energy while the fourth term is the so-called Darwin term. The last term is the so-called spin-orbit interaction we are interested in. Using the relation $\mathbf{k} = -i\hbar\nabla$ with $\hbar = 1$, one obtains the Eq.(1.1).

B

The Tight-Binding Low-Energy Model of Graphene

Here we discuss the low-energy continuum limit of pure graphene. Graphene is a 2D allotrope of carbon, with atoms arranged in a honeycomb lattice configuration. This structure stems from the sp^2 hybridisation of the electron orbitals of carbon producing three new orbitals: sp^2_1, sp^2_2 and sp^2_3. In the binding process, three out of four valence electrons per carbon atom are involved in the formation of a strongly covalent $\sigma-$bond, determining the energetic stability and the elastic properties of graphene. The remaining electron involved is a $\pi-$bond. While $\sigma-$electrons form bands far away from the Fermi energy, $\pi-$electrons are responsible for the electron properties at low energy [148–150]. The honeycomb structure can be seen as a bipartite lattice (sublattices A and B) spanned by the basis vectors

$$\mathbf{a}_1 = \sqrt{3}a\hat{x}, \qquad \mathbf{a}_2 = \frac{\sqrt{3}}{2}a(\hat{x}+\sqrt{3}\hat{y}), \tag{B.1}$$

with $a \simeq 0.142nm$. The inequality of the two sublattices is readily seen by looking at the position of the nearest neighbours for two inequivalent sites. While, say, a site on the A sublattice has nearest neighbours in the north, south-east and south-west directions, a site on the B sublattice has them in the south, north-east and north-west directions. The reciprocal Bravais lattice [see Fig.B.1] is spanned by the vectors:

$$\mathbf{a}^*_1 = \frac{2\pi}{\sqrt{3}a}\left(\hat{x}-\frac{\hat{y}}{\sqrt{3}}\right), \qquad \mathbf{a}^*_2 = \frac{4\pi}{3a}\hat{y}. \tag{B.2}$$

The corners of the Brillouin zone of inequivalent K and $\mathrm{K}' = -\mathrm{K}$ (*Dirac points*), explicitly

$$\pm\mathrm{K} = \pm\frac{4\pi}{3\sqrt{3}a}\hat{x}. \tag{B.3}$$

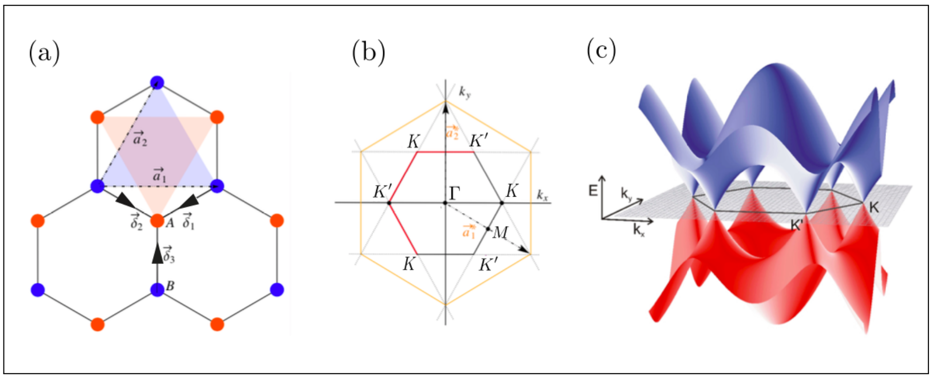

Figure B.1: *Lattice structure and band dispersion of bare graphene. (a) The honeycomb structure with penetrating inequivalent Bravais lattices made up of A, B carbon atoms (red and blue respectively) with lattice vectors* a_1 *and* a_2*. (b) In reciprocal space, two inequivalent corners* K, K' *appear, with the low-energy physics of this material being descried by excitations around those points. The Brillouin zone of graphene has the highest symmetry point* Γ*. (c) Visualisation of graphene band structure, where the linear dispersion (Dirac cone) in the vicinity of* K, K' *can be recognised. Ref.[15, 81].*

To study the low-energy properties of graphene we take into account a tight-binding (TB) model for the π-electrons [151, 152]. Restricting our focus to nearest-neighbours interaction only, the Hamiltonian reads

$$H_G = -t \sum_{\langle i,j \rangle} (a_i^\dagger b_j + h.c.), \tag{B.4}$$

where $a_i^\dagger$ (a_i) and $b_i^\dagger$ (b_i) creates (annihilates) a electron on a site i belonging to the A or B sublattice respectively, while $t \simeq 2.7eV$ is the nearest-neighbours hopping-integral energy between inequivalent sites. Expressing the creation-annihilation operators into their Fourier components and substituting in the Eq.(B.4) one obtains

$$H_G = \sum_{\mathbf{q}} F_{\mathbf{q}}^* a_{\mathbf{q}}^\dagger b_{\mathbf{q}} + h.c., \tag{B.5}$$

with

$$F_{\mathbf{q}} = -t \sum_{\alpha=1,2,3} e^{i\mathbf{q}\delta_\alpha}, \tag{B.6}$$

and

$$\delta_1 = -\frac{a}{2}(\sqrt{3}, 1), \quad \delta_2 = \frac{a}{2}(\sqrt{3}, -1), \quad \delta_3 = a(0, 1). \tag{B.7}$$

Simplifying the notation, one can write

$$H_G = \sum_{\mathbf{q}} (a^\dagger_{\mathbf{q}} b^\dagger_{\mathbf{q}}) \begin{pmatrix} 0 & F^+_{\mathbf{q}} \\ F_{\mathbf{q}} & 0 \end{pmatrix} \begin{pmatrix} a_{\mathbf{q}} \\ b_{\mathbf{q}} \end{pmatrix}, \tag{B.8}$$

from which, by analysing the Schrödinger equation, the dispersion relation is found as

$$\epsilon_{\mathbf{q}} = \pm |F_{\mathbf{q}}| = \sigma t \sqrt{3 + \sum_{\alpha \neq \beta} cos[\mathbf{q} \cdot (\delta_\alpha - \delta_\beta))]}, \tag{B.9}$$

where $\sigma = \pm 1$ is a band index denoting the positive and negative branch of the spectrum respectively. We can hence derive a low-energy continuum Hamiltonian describing excitations around K and K' points. Defining the relative momentum $\mathbf{q} \equiv \pm \mathbf{k} \mp \mathbf{K}$, we can write $F_{\pm \mathbf{q}}$ in terms of $\mathbf{q}$. When $\mathbf{q} \longrightarrow 0$, one has

$$F_{\pm \mathbf{k}} \simeq \frac{3ta}{2} (\pm k_x + i k_y). \tag{B.10}$$

Around the Dirac points, the matrix Hamiltonian becomes

$$H_{G,\mathbf{k}} = \hbar v \begin{pmatrix} 0 & k_x - i k_y & 0 & 0 \\ k_x + i k_y & 0 & 0 & 0 \\ 0 & 0 & 0 & -k_x - i k_y \\ 0 & 0 & -k_x + i k_y & 0 \end{pmatrix}, \tag{B.11}$$

with $v = 3ta/2\hbar$. The matrix Eq.(B.11) acts on the spinor $\Psi_{\mathbf{k}} = (\Psi_{\mathrm{K}A\mathbf{k}}, \Psi_{\mathrm{K}B\mathbf{k}}, \Psi_{\mathrm{K}'A\mathbf{k}}, \Psi_{\mathrm{K}'B\mathbf{k}})^t$. Therefore we see in the low-energy continuum model, sublattices (A,B) and valleys (K, K′) are treated as SU(2) DOFs similar to electrons' spin. In the end, being $H_{G,\mathbf{k}}$ diagonal in the valley DOF, we introduce a valley index $\tau_z = \pm 1$ for the K, K′ valley respectively, writing

$$H_{G,\tau_z \mathbf{k}} = \hbar v (\tau_z \sigma_x k_x + \sigma_y k_y), \tag{B.12}$$

with $\sigma = (\sigma_x, \sigma_y)$ being x, y Pauli matrices associated the sublattice two-fold space and with the Fermi velocity of graphene $v \simeq 10^6 m/s$.

C

Symmetry Point Group of Graphene

The 2D Dirac-Rahsba Hamiltonian Eq.(3.2) is invariant under the group $C_{\infty v}$, which is an emergent symmetry of the continuum (long-wavelength) theory. A lattice point group is commonly defined as the collection of the set of symmetry operations about a lattice point which is invariant under the applied symmetry operations. A hexagon is a regular polygon of six sides [see Fig.B.1]. The inner angle between any two faces is $60°$. If one looks at the hexagon figure from a symmetry point of view, one can count a total of 12 symmetry operations. The symmetry operations of this hexagon consist of six rotation and six reflection operations. The six rotation operations correspond respectively to rotations by $720°$, $120°$, $240°$, $360°$, $480°$ and $600°$. The six reflection operations include three mirror planes bisecting the opposite faces of the hexagon, and three mirror planes bisecting the opposite vertices of the hexagon. The unit cell of graphene in reciprocal space called the first Brillouin zone is also highly symmetric. The highest symmetry point in the first Brillouin zone is the Γ point [see Fig.B.1] which is isomorphic to the point group D_{6h}. It is clear that for any symmetry $\mathcal{S}$, we have

$$\mathcal{S}^{-1} G_0^{R(A)} \mathcal{S} = G_0^{R(A)} \qquad and \qquad \mathcal{S}^{\dagger}\mathcal{S} = 1. \tag{C.1}$$

We consider two symmetry operations: the reflection over the $\hat{x}$ and $\hat{y}$ axis respectively, i.e.

$$R_x \equiv \Sigma_v^{xy} = \sigma_x \otimes s_y, \tag{C.2}$$

$$R_y \equiv \Sigma_v^{yx} = \sigma_y \otimes s_x. \tag{C.3}$$

For all the elements of Clifford's algebra γ_{ab}, we can perform these operations. The idea is the following (for more details we refer the reader to other references as [127, 128, 132]). Under a symmetry operation, one has

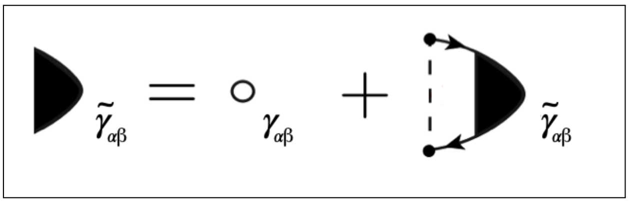
$\tilde{\gamma}_{\alpha\beta}$
=
$\gamma_{\alpha\beta}$
+
$\tilde{\gamma}_{\alpha\beta}$

Figure C.1: *Equation for the vertex renormalization. The empty dot represents the bare vertex while the black dots represent the scattering potential insertions. Ref.[127, 128].*

$$\mathcal{S}^{-1}\gamma_{ab}\mathcal{S} = \varepsilon_{ab}\gamma_{ab}, \tag{C.4}$$

with $\varepsilon_{ab} = \pm 1$. In the diagrammatic language, the susceptibility is written in terms of the dressed vertex [15, 51]. As shown in the Fig.[C.1], the equation for the dressed vertex $\tilde{\gamma}_{\alpha\beta}$ can be written as [127, 128]

$$\tilde{\gamma}_{\alpha\beta} = \gamma_{\alpha\beta} + \frac{4}{2\pi\tau N_0}\sum_{\mathbf{k}} \mathcal{G}^R_{\mathbf{k}}\tilde{\gamma}_{\alpha\beta}\mathcal{G}^A_{\mathbf{k}}, \tag{C.5}$$

where $\gamma_{\alpha\beta}$ is the bare vertex and $\frac{1}{2\pi\tau N_0} = u_0^2$. Projecting the above equation onto the elements of the Clifford's algebra $\gamma_{ab} = \sigma_a \otimes s_b$, one has

$$\tilde{\gamma}_{\alpha\beta ab} = \delta_{\alpha a}\delta_{\beta b} + \sum_{\mu\nu=0,x,y,z} M_{\mu\nu ab}\cdot\tilde{\gamma}_{\alpha\beta\mu\nu}, \tag{C.6}$$

where

$$M_{\mu\nu ab} = \frac{4}{2\pi\tau N_0}\sum_{\mathbf{k}} \mathrm{Tr}\{\gamma_{\mu\nu}\mathcal{G}^R\gamma_{ab}\mathcal{G}^A\}. \tag{C.7}$$

To understand the properties of symmetry transformations, one has a look at the coefficient $M_{\mu\nu ab}$. Under symmetry transformations it becomes

$$M_{\mu\nu ab} = \varepsilon_{\mu\nu}\varepsilon_{ab}M_{\mu\nu ab}. \tag{C.8}$$

The above expression means only when $\varepsilon_{\mu\nu}\varepsilon_{ab} = 1$ the coefficients does not vanish. Furthermore, it is possible to divide the 16 elements of Clifford's algebra in four groups where the element in each group transform in the same way for both symmetry operation. We report the result in the Table C.1. The four-block structure found is a very interesting feature of our system. We find again these symmetries in the matrix structure of the linear operator obtained in the Chapter 7.

γ_{ab}	R_x	R_y
σ_x	+	-
s_y	+	-
$\sigma_y\ s_z$	+	-
$\sigma_z\ s_x$	+	-
σ_y	-	+
s_x	-	+
$\sigma_x\ s_z$	-	+
$\sigma_z\ s_y$	-	+
σ_z	-	-
$\sigma_x\ s_x$	-	-
$\sigma_y\ s_y$	-	-
s_z	-	-
$\sigma_0\ s_0$	+	+
$\sigma_x\ s_y$	+	+
$\sigma_y\ s_x$	+	+
$\sigma_z\ s_z$	+	+

Table C.1: Symmetry operations of all the elements of Clifford's algebra. Four groups of four matrices transform in the same way, i.e. with same sign, under reflection transformation over $\hat{x}$ and $\hat{y}$ axis.

For a easier visualization, we call the four sub-blocks in the following way

$$\begin{aligned}
\Gamma_1 &= \{\sigma_x \otimes s_0, \quad \sigma_0 \otimes s_y, \quad \sigma_y \otimes s_z, \quad \sigma_z \otimes s_x\}, \\
\Gamma_2 &= \{\sigma_y \otimes s_0, \quad \sigma_0 \otimes s_x, \quad \sigma_x \otimes s_z, \quad \sigma_z \otimes s_y\}, \\
\Gamma_3 &= \{\sigma_z \otimes s_0, \quad \sigma_x \otimes s_x, \quad \sigma_y \otimes s_y, \quad \sigma_0 \otimes s_z\}, \\
\Gamma_4 &= \{\sigma_0 \otimes s_0, \quad \sigma_x \otimes s_y, \quad \sigma_y \otimes s_x, \quad \sigma_z \otimes s_z\}
\end{aligned}$$

and note that Γ_1 contains the elements linked to the charge ($\sigma_x \otimes s_0$), inverse-spin galvanic ($\sigma_0 \otimes s_y$) and spin Hall ($\sigma_y \otimes s_z$) response. This is true when $\mathbf{E}$ is along the $x-$direction, as in the our case. If the electric field is along another direction, one has to change the sub-block. We underline that all matrices found in the work of this thesis are projected onto the Clifford's algebra ordered as shown in the Table C.1.

D

From the Kubo to the Streda formula

In the linear response approximation, Kubo has shown that the conductivity tensor is related to a two-currents correlation function [115]

$$\sigma_{ij}(\omega) = \Omega \lim_{x\to 0^+} \int_0^\beta d\lambda \int dt e^{\frac{it}{\hbar}(-\hbar\omega+is)} \mathrm{Tr}\langle \rho_0 j_j(0) j_i(t+i\hbar\lambda)\rangle_c, \tag{D.1}$$

where it is assumed that the applied field leads to a time-dependent perturbation of the form $H_i(t) = H_0 exp(\frac{it}{\hbar}(-\hbar\omega+is))$. Ω is the volume of the sample, $\beta = 1/k_B T$, ρ_0 is the density matrix in equilibrium in absence of perturbation, j_i is the $i-$component of the current density operator in the Heisenberg representation and $\langle ...\rangle_c$ denotes the configurational average. Following the Ref.[153], one can use the independent electrons approximation. Introducing the Fermi-Dirac distribution function $f_0(\epsilon)$, the Eq.(D.1) becomes

$$\sigma_{ij}(\omega) = \Omega \lim_{x\to 0^+} \int_0^\beta d\lambda e^{-\lambda(\delta\mu)} \int dt \sum_{mn} \left\langle f_0(\epsilon_m)(1-f_0(\epsilon_m)) e^{\frac{it}{\hbar}(-\hbar\omega+is+\delta\mu)} A_{ij} \right\rangle_c, \tag{D.2}$$

with $\delta\epsilon = \epsilon_n - \epsilon_m$ and $A_{ij} = \langle m|\bar{j}_j|n\rangle\langle n|\bar{j}_i|m\rangle$. Here $\epsilon_{n(m)}$ is the eigenvalue associated to the $n(m)-$eigenstate, while $\bar{j}$ is the current density operator in the Schr$\ddot{o}$dinger representation. After the integration over λ (that simply the factor $f_0(\epsilon_m)(1-f_0(\epsilon_m))$ and performing the $t-$integration one obtains

$$\sigma_{ij}(\omega) = i\hbar\Omega \lim_{x\to 0^+} \sum_{nm} \left\langle \frac{f_0(\epsilon_n) - f_0(\epsilon_m)}{(\epsilon_n - \epsilon_m)(\epsilon_n - \epsilon_m - \hbar\omega + is)} A_{ij} \right\rangle_c. \tag{D.3}$$

Now, at zero frequency, after some manipulation the Eq.(D.3) reduces to the Bastin formula. This one can be expressed as

$$\sigma_{ij} = \frac{ie^2\hbar}{\Omega}\int d\epsilon f_0(\epsilon)\mathrm{Tr}\Big\langle v_i\frac{dG^R(\epsilon)}{d\epsilon}v_i\delta(\epsilon-H) - v_i\delta(\epsilon-H)v_j\frac{dG^A(\epsilon)}{d\epsilon}\Big\rangle_c, \tag{D.4}$$

where we have introduced the Green's function $G^{R(A)}(\epsilon) = \lim_{x\to 0^+}(\epsilon - H \pm is)^{-1}$ and the velocity through the relation $\mathbf{j} = -e\mathbf{v}/\Omega$. This expression for the conductivity was first obtained by Bastin et al. [154] but in the particular case of a Schröodinger Hamiltonian and made explicit use of the form taken by the velocity operator in the Schröodinger case. This formula is interesting because it expresses the conductivity as a product of velocities and Green's functions. However, it is still difficult to calculate because of the integration over the energy ϵ. By making an integration by parts, a factor $df_0(\epsilon)/d\epsilon$ appears instead of the factor $f_0(\epsilon)$ and the integration interval will be thus reduced. We express the delta function in terms of Green's functions using $\delta(\epsilon-H) = -(G^R(\epsilon)-G^A(\epsilon))/2i\pi$. We keep one half of the expression Eq.(D.4) and make an integration by parts on the second half then we get the Eqs.(2.24)-(2.25). Using the relations $dG^{R(A)}(\epsilon)/d\epsilon = -(G^{R(A)}(\epsilon))^2$ and $i\hbar v_i = [r_i, H] = -[r_i, G^{-1}]$ and by performing one more integration by parts, the conductivity can be written as a sum of two terms $\sigma_{ij} = \sigma^I_{ij} + \sigma^{II}_{ij}$ where

$$\sigma^I_{ij} = -\frac{e^2\hbar}{4\pi\Omega}\int d\epsilon\frac{df(\epsilon)}{d\epsilon}\mathrm{Tr}\Big\langle v_i(G^R(\epsilon)-G^A(\epsilon))v_jG^A(\epsilon) - v_iG^R(\epsilon)v_j(G^R(\epsilon)-G^A(\epsilon))\Big\rangle_c \tag{D.5}$$

and

$$\sigma^{II}_{ij} = \frac{e^2\hbar}{4i\pi\Omega}\int d\epsilon f(\epsilon)\mathrm{Tr}\Big\langle (G^R(\epsilon)-G^A(\epsilon))(r_iv_j - r_jv_i)\Big\rangle_c. \tag{D.6}$$

The Eqs.(D.5)-(D.6) correspond to the formula obtained by Streda [117, 142] in the Schrödinger case. The present brief discussion shows that it holds also in the Pauli and Dirac cases. At zero temperature, the factor $df(\epsilon)/d\epsilon$ is equal to $-\delta(\epsilon-\varepsilon)$, only electrons at the Fermi level contribute to the conductivity (for both diagonal and off-diagonal components). In conclusion, at $\omega = 0$ and $T = 0$, the conductivity tensor can be expressed as a sum of these two contributions

$$\sigma^I_{ij} = \frac{e^2\hbar}{4\pi\Omega}\mathrm{Tr}\Big\langle v_i(G^R - G^Av_jG^A - v_iG^Rv_j(G^R-G^A)\Big\rangle_c \tag{D.7}$$

and

$$\sigma^{II}_{ij} = -\frac{e^2\hbar}{4i\pi\Omega}\int d\epsilon f(\epsilon)\mathrm{Tr}\Big\langle (G^R-G^A)(r_iv_j - r_jv_i)\Big\rangle_c, \tag{D.8}$$

where we have dropped the energy reference ε by introducing the Green's functions at the Fermi level $G^{R(A)} = G(\varepsilon \pm i0) = (\varepsilon \pm i0 - H))$.

E

The diagrammatic evaluation of skew-scattering

Here we want to consider the additional contribution to the self-energy reported also in the Fig.[5.1]. The evaluation here reported takes into account the well-know Feynmann rules of the diagram technique. The simplest term arises in the third order, i.e. the self-energy graph with three legs, is (we omit other arguments for brevity)

$$\check{\Sigma}_{ss} = u_0^3 \int d\mathbf{k}' d\mathbf{k}'' \check{G}\left(\mathbf{k}'\right) \check{G}\left(\mathbf{k}''\right), \tag{E.1}$$

where $\mathbf{k}'$ and $\mathbf{k}''$ are the integration variables according to the diagrammatic rules. By using the triangular structure of the Keldysh technique one has the following expression for the retarded (advanced) components ($a = R(A)$)

$$\Sigma_{ss}^{a} = u_0^3 \int d\mathbf{k}' d\mathbf{k}'' G^{a}\left(\mathbf{k}'\right) G^{a}\left(\mathbf{k}''\right), \tag{E.2}$$

whereas the Keldysh component becomes

$$\Sigma_{ss} = u_0^3 \int d\mathbf{k}' d\mathbf{k}'' \left(G^{R}\left(\mathbf{k}'\right) G\left(\mathbf{k}''\right) + G\left(\mathbf{k}'\right) G^{A}\left(\mathbf{k}''\right)\right). \tag{E.3}$$

From these expressions, it is easy to see that now the relations between the components of self-energy and Green's function are

$$g^{R} = -g^{A} \qquad \Sigma^{R} = \Sigma^{A}. \tag{E.4}$$

Now, we need to start from L-R subtracted Dyson equation for the Keldysh component Eq.(2.57) before all kind of manipulation, i.e.

$$-eE\partial_{k_x}G^K_{eq}-eE\frac{1}{2}\left\{\sigma_x,\partial_\omega G^K_{eq}\right\}+i\left[h(\mathbf{k}),G^K\right]=-i(\Sigma^R G^K+\Sigma^K G^A-G^R\Sigma^K-G^K\Sigma^A),$$

where G^K_{eq} is the equilibrium Keldysh Green's function. We focus on RHS term only for the additive contribution due to skew-scattering. Writing $\Sigma \longrightarrow \Sigma+\delta\Sigma$ and using the relation Eq.(E.4), the additive term to the collision integral becomes

$$\delta I=i\{\delta\Sigma^K,G^R\}-i[\delta\Sigma^R,G^K]=-i(\delta\Sigma^R G^K-G^K\delta\Sigma^R)+i(\delta\Sigma^K G^R+G^R\delta\Sigma^K). \tag{E.5}$$

After the integration over ξ and introducing the scattering time Eq.(5.22) as done in the Chapter 6, we can define the skew-scattering coupling given by the Eq.(6.5). At this point we rewrite the Eq.(E.5) as $(g^K\equiv g)$

$$\delta\mathcal{I}=ig_{ss}\frac{N_F}{N_0}\frac{1}{\tau}\Big([\langle g^R(k')\rangle\langle g^R(k'')\rangle,g]-\{\langle g^R(k')\rangle\langle g^K(k'')\rangle-\langle g^K(k')\rangle\langle g^R(k'')\rangle,g^R\}\Big).$$

Now, as done for the calculation of the kinetic equation in the Chapter 5, using the definition of retarded component g^R and the ansatz Eq.(5.26), we rewrite the additional contribution in terms of function g_0 as (we omit the dependence from the Fermi momentum k_F for simplicity)

$$\begin{aligned}\delta\mathcal{I}=ig_{ss}\frac{N_F}{N_0}\frac{1}{\tau}\Big([\langle P_{1-1}(\theta')\rangle\langle P_{1-1}(\theta'')\rangle,g_0(\theta)P_{1-1}(\theta)]+\\-\{\langle P_{1-1}(\theta')\rangle\langle g_0(\theta'')P_{1-1}(\theta'')\rangle-\langle g_0(\theta'')P_{1-1}(\theta')\rangle\langle P_{1-1}(\theta'')\rangle,P_{1-1}(\theta)\}\Big).\end{aligned} \tag{E.6}$$

After the integration over angles, the final total L-R subtracted Dyson equation for g_0 reads[1]

---

[1] Here we reintroduce the contribute due to the Born approximation to write the total kinetic equation.

$$
\begin{aligned}
-eE\partial_\omega f\{\sigma_x, P_{1-1}(\theta)\} = &-\frac{N_F}{N_0}\frac{1}{2\pi\tau}\int_0^{2\pi} d\theta'(g_0(\theta)-g_0(\theta'))\{P_{1-1}(\theta'),P_{1-1}(\theta)\}\\
&+ig_{ss}\frac{N_F}{N_0}\frac{1}{(2\pi)^2\tau}\int_0^{2\pi} d\theta' d\theta''\Big(g_0(\theta)[P_{1-1}(\theta_1)P_{1-1}(\theta''),P_{1-1}(\theta)]+\\
&\qquad+(g_0(\theta')-g_0(\theta''))\{P_{1-1}(\theta')P_{1-1}(\theta''),P_{1-1}(\theta)\}\Big).
\end{aligned}
$$

By taking the trace of the equation, we may get a scalar equation for $g_0(\theta)$ with total scattering kernel in the form $\mathcal{W} = W + \Omega$. At this stage we obtain the following relations[2]

$$
W(\theta,\theta') = \frac{N_F}{N_0} Tr\{P_{1-1}(\theta'),P_{1-1}(\theta)\}, \tag{E.7}
$$

$$
\Omega(\theta,\theta',\theta'') = ig_{ss}\frac{N_F}{N_0} Tr\{P_{1-1}(\theta')P_{1-1}(\theta''),P_{1-1}(\theta)\}. \tag{E.8}
$$

Now we focus on $\Omega(\theta,\theta',\theta'')-$ contribution to the scattering kernel. We immediately note the dependence on two different scattering angles (θ',θ'') is dummy because, changing the variable name $\theta''\to\theta'$, we can rewrite it as

$$
\int_0^{2\pi} d\theta' d\theta''\Omega(\theta,\theta',\theta'')(g_0(\theta')-g_0(\theta'')) = \int_0^{2\pi} d\theta' d\theta''[\Omega(\theta,\theta',\theta'')-\Omega(\theta,\theta'',\theta')]g_0(\theta').
$$

Using the $\Omega-$potential definition Eq.(E.8), we note that

$$
\begin{aligned}
&[\Omega(\theta,\theta',\theta'')-\Omega(\theta,\theta'',\theta')]\frac{N_0}{ig_{ss}N_F} =\\
&\quad= [Tr\{P_{1-1}(\theta')P_{1-1}(\theta'')P_{1-1}(\theta)+P_{1-1}(\theta)P_{1-1}(\theta_1)P_{1-1}(\theta'')+\\
&\qquad -P_{1-1}(\theta'')P_{1-1}(\theta')P_{1-1}(\theta)-P_{1-1}(\theta)P_{1-1}(\theta'')P_{1-1}(\theta')\}].
\end{aligned}
$$

After some manipulation we can rewrite the difference of $\Omega-$ potential as

---

[2] Note that W is the same scattering kernel at the Born level, while Ω is the additional term due to skew-scattering.

$$\begin{aligned}
&\Omega(\theta,\theta',\theta'')-\Omega(\theta,\theta'',\theta')=\\
&=ig_{ss}\frac{N_F}{N_0}Tr\Big(\{P_{1-1}(\theta),[P_{1-1}(\theta'),P_{1-1}(\theta'')]\}\Big)\\
&=ig_{ss}\frac{N_F}{N_0}2Tr\Big(P_{1-1}(\theta)[P_{1-1}(\theta'),P_{1-1}(\theta'')]\Big).
\end{aligned}$$

In the end, one can use the properties of the trace to manipulate this object. Using the identity $\mathrm{Tr}\{\mathrm{A}\,[\mathrm{B},\mathrm{C}]\}=\mathrm{Tr}\{\mathrm{C}\,[\mathrm{A},\mathrm{B}]\}$, one may rewrite the additive term to the collision integral as

$$\delta\mathcal{I}=ig_{ss}\frac{N_F}{N_0}\frac{1}{2\pi}\int_0^{2\pi}d\theta'\frac{1}{2\pi}\int_0^{2\pi}d\theta'' g(\theta')2\mathrm{Tr}\Big(P_{1-1}(\theta'')\left[P_{1-1}(\theta),P_{1-1}(\theta')\right]\Big). \tag{E.9}$$

One can then integrate on the angle θ'' before the trace operation

$$\delta I=ig_{ss}\frac{N_F}{N_0}\frac{1}{2\pi}\int_0^{2\pi}d\theta' g(\theta')\mathrm{Tr}\Big(\langle P_{1-1}\rangle\left[P_{1-1}(\theta),P_{1-1}(\theta')\right]\Big), \tag{E.10}$$

where

$$\langle P_{1-1}\rangle=\frac{1}{2\pi}\int_0^{2\pi}d\theta'' P_{1-1}(\theta''). \tag{E.11}$$

In such a way the quantity

$$\Omega(\theta,\theta')=ig_{ss}\frac{N_F}{N_0}2\mathrm{Tr}\Big\{\langle P_{1-1}\rangle\left[P_{1-1}(\theta),P_{1-1}(\theta')\right]\Big\} \tag{E.12}$$

only depends on θ and θ'. This is exactly the same contribution to the scattering kernel obtained with the $\mathrm{T}-$matrix approximation Eq.(6.2).

F Calculation details in the regime II

F.1 On the clean case

Here we report the details on the matrix calculation for the double-band regime discussed in the Section 7.1. We stress that t^a $(a = 1, ..., 16)$ are the Clifford's algebra elements in the same order reported in the Table C.1. As already mentioned, we select this matrix ordering in order to verify the system symmetries. The resulting $\mathcal{M}$ matrix from the Eq.(7.3) is

$$\begin{pmatrix}
0 & 0 & 0 & -2\lambda & 0 & 0 & 0 & 0 & 2k_y & 0 & 0 & 0 & 0 & 0 & 0 & 0 \\
0 & 0 & 2\lambda & 0 & 0 & 0 & 0 & 0 & 0 & 0 & 0 & 0 & 0 & 0 & 0 & 0 \\
0 & -2\lambda & 0 & 0 & 0 & 0 & 0 & 0 & 0 & 0 & 0 & 0 & 0 & 0 & 0 & -2k_x \\
2\lambda & 0 & 0 & 0 & 0 & 0 & 0 & 0 & 0 & -2k_y & 0 & 0 & 0 & 0 & 2k_x & 0 \\
0 & 0 & 0 & 0 & 0 & 0 & 0 & -2\lambda & -2k_x & 0 & 0 & 0 & 0 & 0 & 0 & 0 \\
0 & 0 & 0 & 0 & 0 & 0 & 2\lambda & 0 & 0 & 0 & 0 & 0 & 0 & 0 & 0 & 0 \\
0 & 0 & 0 & 0 & 0 & -2\lambda & 0 & 0 & 0 & 0 & 0 & 0 & 0 & 0 & 0 & 2k_y \\
0 & 0 & 0 & 0 & 2\lambda & 0 & 0 & 0 & 0 & 0 & 2k_x & 0 & 0 & -2k_y & 0 & 0 \\
-2k_y & 0 & 0 & 0 & 2k_x & 0 & 0 & 0 & 0 & 2\lambda & 2\lambda & 0 & 0 & 0 & 0 & 0 \\
0 & 0 & 0 & 2k_y & 0 & 0 & 0 & 0 & -2\lambda & 0 & 0 & 2\lambda & 0 & 0 & 0 & 0 \\
0 & 0 & 0 & 0 & 0 & 0 & 0 & -2k_x & -2\lambda & 0 & 0 & 2\lambda & 0 & 0 & 0 & 0 \\
0 & 0 & 0 & 0 & 0 & 0 & 0 & 0 & 0 & -2\lambda & -2\lambda & 0 & 0 & 0 & 0 & 0 \\
0 & 0 & 0 & 0 & 0 & 0 & 0 & 0 & 0 & 0 & 0 & 0 & 0 & 0 & 0 & 0 \\
0 & 0 & 0 & 0 & 0 & 0 & 0 & 2k_y & 0 & 0 & 0 & 0 & 0 & 0 & 0 & 0 \\
0 & 0 & 0 & -2k_x & 0 & 0 & 0 & 0 & 0 & 0 & 0 & 0 & 0 & 0 & 0 & 0 \\
0 & 0 & 2k_x & 0 & 0 & 0 & -2k_y & 0 & 0 & 0 & 0 & 0 & 0 & 0 & 0 & 0
\end{pmatrix}.$$

While the matrix $M = \mathcal{M}^2$ reads

$$\left(\begin{array}{cccccccccccccccc}
-4\left(k_y{}^2+\lambda^2\right) & 0 & 0 & 0 & 4k_xk_y & 0 & 0 & 0 & 0 & 8k_y\lambda & 4k_y\lambda & 0 & 0 & 0 & -4k_x\lambda & 0 \\
0 & -4\lambda^2 & 0 & 0 & 0 & 0 & 0 & 0 & 0 & 0 & 0 & 0 & 0 & 0 & 0 & -4k_x\lambda \\
0 & 0 & -4\left(k_x{}^2+\lambda^2\right) & 0 & 0 & 0 & 4k_xk_y & 0 & 0 & 0 & 0 & 0 & 0 & 0 & 0 & 0 \\
0 & 0 & 0 & -4\left(k_x{}^2+k_y{}^2+\lambda^2\right) & 0 & 0 & 0 & 0 & 8k_y\lambda & 0 & 0 & -4k_y\lambda & 0 & 0 & 0 & 0 \\
4k_xk_y & 0 & 0 & 0 & -4\left(k_x{}^2+\lambda^2\right) & 0 & 0 & 0 & 0 & -4k_x\lambda & -8k_x\lambda & 0 & 0 & 4k_y\lambda & 0 & 0 \\
0 & 0 & 0 & 0 & 0 & -4\lambda^2 & 0 & 0 & 0 & 0 & 0 & 0 & 0 & 0 & 0 & 4k_y\lambda \\
0 & 0 & 4k_xk_y & 0 & 0 & 0 & -4\left(k_y{}^2+\lambda^2\right) & 0 & 0 & 0 & 0 & 0 & 0 & 0 & 0 & 0 \\
0 & 0 & 0 & 0 & 0 & 0 & 0 & -4\left(k_x{}^2+k_y{}^2+\lambda^2\right) & -8k_x\lambda & 0 & 0 & 4k_x\lambda & 0 & 0 & 0 & 0 \\
0 & 0 & 0 & 8k_y\lambda & 0 & 0 & 0 & -8k_x\lambda & -4\left(k_x{}^2+k_y{}^2+2\lambda^2\right) & 0 & 0 & 8\lambda^2 & 0 & 0 & 0 & 0 \\
8k_y\lambda & 0 & 0 & 0 & -4k_x\lambda & 0 & 0 & 0 & 0 & -4\left(k_y{}^2+2\lambda^2\right) & -8\lambda^2 & 0 & 0 & 0 & 4k_xk_y & 0 \\
4k_y\lambda & 0 & 0 & 0 & -8k_x\lambda & 0 & 0 & 0 & 0 & -8\lambda^2 & -4\left(k_x{}^2+2\lambda^2\right) & 0 & 0 & 4k_xk_y & 0 & 0 \\
0 & 0 & 0 & -4k_y\lambda & 0 & 0 & 0 & 4k_x\lambda & 8\lambda^2 & 0 & 0 & -8\lambda^2 & 0 & 0 & 0 & 0 \\
0 & 0 & 0 & 0 & 0 & 0 & 0 & 0 & 0 & 0 & 0 & 0 & 0 & 0 & 0 & 0 \\
0 & 0 & 0 & 0 & 4k_y\lambda & 0 & 0 & 0 & 0 & 0 & 4k_xk_y & 0 & 0 & -4k_y{}^2 & 0 & 0 \\
-4k_x\lambda & 0 & 0 & 0 & 0 & 0 & 0 & 0 & 0 & 4k_xk_y & 0 & 0 & 0 & 0 & -4k_x{}^2 & 0 \\
0 & -4k_x\lambda & 0 & 0 & 0 & 4k_y\lambda & 0 & 0 & 0 & 0 & 0 & 0 & 0 & 0 & 0 & -4\left(k_x{}^2+k_y{}^2\right).
\end{array}\right).$$

The anticommutator expansion Eq.(7.17) we call y_{ln} is

$$\left(\begin{array}{cccccccccccccccc}
\frac{1}{2} & -\frac{\lambda\left(\lambda+\sqrt{\lambda^2+k_x{}^2+k_y{}^2}\right)+k_x{}^2}{2\left(\lambda\left(\lambda+\sqrt{\lambda^2+k_x{}^2+k_y{}^2}\right)+k_x{}^2+k_y{}^2\right)} & 0 & 0 & 0 & \frac{k_xk_y}{2\left(\lambda\left(\lambda+\sqrt{\lambda^2+k_x{}^2+k_y{}^2}\right)+k_x{}^2+k_y{}^2\right)} & 0 & 0 & 0 & -\frac{k_y}{2\sqrt{\lambda^2+k_x{}^2+k_y{}^2}} & 0 & 0 & -\frac{k_x}{2\sqrt{\lambda^2+k_x{}^2+k_y{}^2}} & \frac{k_x}{2\sqrt{\lambda^2+k_x{}^2+k_y{}^2}} & 0 & 0 \\
\frac{1}{2} & \frac{k_x{}^2-\frac{\lambda k_y{}^2}{\sqrt{\lambda^2+k_x{}^2+k_y{}^2}}}{2\left(k_x{}^2+k_y{}^2\right)} & 0 & 0 & 0 & -\frac{k_xk_y}{2\left(\lambda\left(\lambda-\sqrt{\lambda^2+k_x{}^2+k_y{}^2}\right)+k_x{}^2+k_y{}^2\right)} & 0 & 0 & 0 & \frac{k_y}{2\sqrt{\lambda^2+k_x{}^2+k_y{}^2}} & 0 & 0 & -\frac{k_x}{2\sqrt{\lambda^2+k_x{}^2+k_y{}^2}} & -\frac{k_x}{2\sqrt{\lambda^2+k_x{}^2+k_y{}^2}} & 0 & 0 \\
\frac{1}{2} & \frac{\frac{\lambda k_y{}^2}{\sqrt{\lambda^2+k_x{}^2+k_y{}^2}}-k_x{}^2}{2\left(k_x{}^2+k_y{}^2\right)} & 0 & 0 & 0 & \frac{k_xk_y}{2\left(\lambda\left(\lambda-\sqrt{\lambda^2+k_x{}^2+k_y{}^2}\right)+k_x{}^2+k_y{}^2\right)} & 0 & 0 & 0 & \frac{k_y}{2\sqrt{\lambda^2+k_x{}^2+k_y{}^2}} & 0 & 0 & \frac{k_x}{2\sqrt{\lambda^2+k_x{}^2+k_y{}^2}} & -\frac{k_x}{2\sqrt{\lambda^2+k_x{}^2+k_y{}^2}} & 0 & 0 \\
\frac{1}{2} & \frac{\frac{\lambda k_y{}^2}{\sqrt{\lambda^2+k_x{}^2+k_y{}^2}}+k_x{}^2}{2\left(k_x{}^2+k_y{}^2\right)} & 0 & 0 & 0 & -\frac{k_xk_y}{2\left(\lambda\left(\lambda+\sqrt{\lambda^2+k_x{}^2+k_y{}^2}\right)+k_x{}^2+k_y{}^2\right)} & 0 & 0 & 0 & -\frac{k_y}{2\sqrt{\lambda^2+k_x{}^2+k_y{}^2}} & 0 & 0 & \frac{k_x}{2\sqrt{\lambda^2+k_x{}^2+k_y{}^2}} & \frac{k_x}{2\sqrt{\lambda^2+k_x{}^2+k_y{}^2}} & 0 & 0
\end{array}\right).$$

The y^{eff} vectors from the relation $\mathcal{M}\cdot\mathrm{y}_{ln}$ for the two bands are explicitly (for simplicity we call $\mathrm{k} = k_x + ik_y$ and $\bar{\mathrm{k}} = k_x - ik_y$)

$$\begin{aligned}
\mathrm{y}^{eff}_{1-1} = \{0,0,&-\frac{\lambda}{k^2}\left(\frac{\lambda k_y{}^2}{\sqrt{\lambda^2+k^2}} - k_x{}^2\right), \lambda - \frac{ik_y(4\bar{\mathrm{k}}-4\mathrm{k})}{8\sqrt{\lambda^2+k^2}}, 0, 0, \\
&-\frac{\lambda k_x k_y}{\lambda\left(\lambda-\sqrt{\lambda^2+k^2}\right)+k^2}, \frac{ik_x(4\bar{\mathrm{k}}-4\mathrm{k})}{8\sqrt{\lambda^2+k^2}}, \\
&\frac{\lambda k_y}{\sqrt{\lambda^2+k^2}} - \frac{1}{8}i(4\bar{\mathrm{k}}-4\mathrm{k}), 0, 0, -\frac{\lambda k_y}{\sqrt{\lambda^2+k^2}}, 0, 0, 0, 0\}
\end{aligned}$$

and

$$\begin{aligned}
\mathrm{y}^{eff}_{11} = \{0,0,&-\frac{\lambda}{k^2}\left(\frac{\lambda k_y{}^2}{\sqrt{\lambda^2+k^2}} + k_x{}^2\right), \lambda + \frac{ik_y(4\bar{\mathrm{k}}-4\mathrm{k})}{8\sqrt{\lambda^2+k^2}}, 0, 0, \\
&\frac{\lambda k_x k_y}{\lambda\left(\lambda+\sqrt{\lambda^2+k^2}\right)+k^2}, -\frac{ik_x(4\bar{\mathrm{k}}-4\mathrm{k})}{8\sqrt{\lambda^2+k^2}}, \\
&-\frac{\lambda k_y}{\sqrt{\lambda^2+k^2}} - \frac{1}{8}i(4\bar{\mathrm{k}}-4\mathrm{k}), 0, 0, \frac{\lambda k_y}{\sqrt{\lambda^2+k^2}}, 0, 0, 0, 0\}.
\end{aligned}$$

F.2 The disorder case

Here we report the calculation details in the presence of disorder discussed in the Section 7.2. The linear operator $\mathcal{L}$ from the expression Eq.(7.25) is

$$\begin{pmatrix}
-4\left(\lambda^2+{k_y}^2\right) & 0 & 0 & -\frac{2\lambda}{\tau} & 4k_xk_y & 0 & 0 & 0 & \frac{2k_y}{\tau} & 8\lambda k_y & 4\lambda k_y & 0 & 0 & 0 & -4\lambda k_x & 0 \\
0 & -4\lambda^2 & \frac{2\lambda}{\tau} & 0 & 0 & 0 & 0 & 0 & 0 & 0 & 0 & 0 & 0 & 0 & 0 & -4\lambda k_x \\
0 & -\frac{2\lambda}{\tau} & -4\left(\lambda^2+{k_x}^2\right) & 0 & 0 & 0 & 4k_xk_y & 0 & 0 & 0 & 0 & 0 & 0 & 0 & 0 & -\frac{2k_x}{\tau} \\
\frac{2\lambda}{\tau} & 0 & 0 & -4\left(\lambda^2+{k_x}^2+{k_y}^2\right) & 0 & 0 & 0 & 0 & 8\lambda k_y & -\frac{2k_y}{\tau} & 0 & -4\lambda k_y & 0 & 0 & \frac{2k_x}{\tau} & 0 \\
4k_xk_y & 0 & 0 & 0 & -4\left(\lambda^2+{k_x}^2\right) & 0 & 0 & -\frac{2\lambda}{\tau} & -\frac{2k_x}{\tau} & -4\lambda k_x & -8\lambda k_x & 0 & 0 & 4\lambda k_y & 0 & 0 \\
0 & 0 & 0 & 0 & 0 & -4\lambda^2 & \frac{2\lambda}{\tau} & 0 & 0 & 0 & 0 & 0 & 0 & 0 & 0 & 4\lambda k_y \\
0 & 0 & 4k_xk_y & 0 & 0 & -\frac{2\lambda}{\tau} & -4\left(\lambda^2+{k_y}^2\right) & 0 & 0 & 0 & 0 & 0 & 0 & 0 & 0 & \frac{2k_y}{\tau} \\
0 & 0 & 0 & 0 & \frac{2\lambda}{\tau} & 0 & 0 & -4\left(\lambda^2+{k_x}^2+{k_y}^2\right) & -8\lambda k_x & 0 & \frac{2k_x}{\tau} & 4\lambda k_x & 0 & -\frac{2k_y}{\tau} & 0 & 0 \\
-\frac{2k_y}{\tau} & 0 & 0 & 8\lambda k_y & \frac{2k_x}{\tau} & 0 & 0 & -8\lambda k_x & -4\left(2\lambda^2+{k_x}^2+{k_y}^2\right) & \frac{2\lambda}{\tau} & \frac{2\lambda}{\tau} & 8\lambda^2 & 0 & 0 & 0 & 0 \\
8\lambda k_y & 0 & 0 & \frac{2k_y}{\tau} & -4\lambda k_x & 0 & 0 & 0 & -\frac{2\lambda}{\tau} & -4\left(2\lambda^2+{k_y}^2\right) & -8\lambda^2 & \frac{2\lambda}{\tau} & 0 & 0 & 4k_xk_y & 0 \\
4\lambda k_y & 0 & 0 & 0 & -8\lambda k_x & 0 & 0 & -\frac{2k_x}{\tau} & -\frac{2\lambda}{\tau} & -8\lambda^2 & -4\left(2\lambda^2+{k_x}^2\right) & \frac{2\lambda}{\tau} & 0 & 4k_xk_y & 0 & 0 \\
0 & 0 & 0 & -4\lambda k_y & 0 & 0 & 0 & 4\lambda k_x & 8\lambda^2 & -\frac{2\lambda}{\tau} & -\frac{2\lambda}{\tau} & -8\lambda^2 & 0 & 0 & 0 & 0 \\
0 & 0 & 0 & 0 & 0 & 0 & 0 & 0 & 0 & 0 & 0 & 0 & 0 & 0 & 0 & 0 \\
0 & 0 & 0 & 0 & 4\lambda k_y & 0 & 0 & \frac{2k_y}{\tau} & 0 & 0 & 4k_xk_y & 0 & 0 & -4{k_y}^2 & 0 & 0 \\
-4\lambda k_x & 0 & 0 & -\frac{2k_x}{\tau} & 0 & 0 & 0 & 0 & 0 & 4k_xk_y & 0 & 0 & 0 & 0 & -4{k_x}^2 & 0 \\
0 & -4\lambda k_x & \frac{2k_x}{\tau} & 0 & 0 & 4\lambda k_y & -\frac{2k_y}{\tau} & 0 & 0 & 0 & 0 & 0 & 0 & 0 & 0 & -4\left({k_x}^2+{k_y}^2\right).
\end{pmatrix}.$$

While the linear operator R from the Eq.(7.37) has the form

$$R = \begin{pmatrix} R_{\Gamma_1} & 0 & 0 & 0 \\ 0 & R_{\Gamma_2} & 0 & 0 \\ 0 & 0 & R_{\Gamma_3} & 0 \\ 0 & 0 & 0 & R_{\Gamma_4} \end{pmatrix}, \tag{F.1}$$

where the 4 sub-blocks are respectively

$$R_{\Gamma_1} = \begin{pmatrix}
\frac{\varepsilon\tau\left(\varepsilon^2-2\lambda^2\right)}{2(\varepsilon^2-\lambda^2)} & \frac{\lambda\varepsilon^2\tau}{2\lambda^2-2\varepsilon^2} & \frac{\varepsilon^2}{4\lambda^2-4\varepsilon^2} & -\frac{\lambda\varepsilon}{4(\lambda^2-\varepsilon^2)} \\
\frac{\lambda\varepsilon^2\tau}{2\lambda^2-2\varepsilon^2} & \frac{\varepsilon\tau\left(\varepsilon^2-2\lambda^2\right)}{2(\varepsilon^2-\lambda^2)} & \frac{\varepsilon^3}{4\lambda^3-4\lambda\varepsilon^2} & \frac{\varepsilon^2}{4(\varepsilon^2-\lambda^2)} \\
\frac{\varepsilon^2}{4(\varepsilon^2-\lambda^2)} & -\frac{\varepsilon^3}{4\lambda^3-4\lambda\varepsilon^2} & 0 & 0 \\
\frac{\lambda\varepsilon}{4\lambda^2-4\varepsilon^2} & \frac{\varepsilon^2}{4\lambda^2-4\varepsilon^2} & 0 & 0
\end{pmatrix},$$

$$R_{\Gamma_2} = \begin{pmatrix}
\frac{\varepsilon\tau\left(\varepsilon^2-2\lambda^2\right)}{2(\varepsilon^2-\lambda^2)} & -\frac{\lambda\varepsilon^2\tau}{2(\lambda^2-\varepsilon^2)} & \frac{\varepsilon^2}{4(\varepsilon^2-\lambda^2)} & -\frac{\lambda\varepsilon}{4(\lambda^2-\varepsilon^2)} \\
-\frac{\lambda\varepsilon^2\tau}{2(\lambda^2-\varepsilon^2)} & \frac{\varepsilon\tau\left(\varepsilon^2-2\lambda^2\right)}{2(\varepsilon^2-\lambda^2)} & \frac{\varepsilon^3}{4\lambda^3-4\lambda\varepsilon^2} & \frac{\varepsilon^2}{4\lambda^2-4\varepsilon^2} \\
\frac{\varepsilon^2}{4\lambda^2-4\varepsilon^2} & -\frac{\varepsilon^3}{4\lambda^3-4\lambda\varepsilon^2} & 0 & 0 \\
\frac{\lambda\varepsilon}{4\lambda^2-4\varepsilon^2} & \frac{\varepsilon^2}{4(\varepsilon^2-\lambda^2)} & 0 & 0
\end{pmatrix},$$

$$R_{\Gamma_3} = \begin{pmatrix}
0 & 0 & 0 & 0 \\
\frac{\varepsilon^3\tau}{8(\varepsilon^2-\lambda^2)} & \frac{\varepsilon^3\tau}{8\lambda^2-8\varepsilon^2} & -\frac{\varepsilon}{4\lambda} & \\
\frac{\varepsilon^3\tau}{8\lambda^2-8\varepsilon^2} & \frac{\varepsilon^3\tau}{8(\varepsilon^2-\lambda^2)} & -\frac{\varepsilon}{4\lambda} & \\
\frac{\varepsilon}{4\lambda} & \frac{\varepsilon}{4\lambda} & 0 & 0
\end{pmatrix},$$

$$R_{\Gamma_4}=\begin{pmatrix}\varepsilon\tau & 0 & 0 & 0\\ 0 & \frac{3\varepsilon^3\tau}{8(\varepsilon^2-\lambda^2)} & \frac{\varepsilon^3\tau}{8\lambda^2-8\varepsilon^2} & \frac{\lambda\varepsilon^2\varepsilon}{2\lambda^2-2\varepsilon^2}\\ 0 & \frac{\varepsilon^3\tau}{8\lambda^2-8\varepsilon^2} & \frac{3\varepsilon^3\tau}{8(\varepsilon^2-\lambda^2)} & \frac{1}{4}\lambda\tau\left(\frac{\lambda\sqrt{k^2+\lambda^2}}{(\lambda-\varepsilon)^2}+\frac{\varepsilon}{\lambda+\varepsilon}+1\right)\\ 0 & \frac{\lambda\varepsilon^2\tau}{2\lambda^2-2\varepsilon^2} & -\frac{\lambda\varepsilon^2\tau}{2(\lambda^2-\varepsilon^2)} & -\frac{\lambda^2\varepsilon\tau}{\lambda^2-\varepsilon^2}\end{pmatrix}.$$

The matrix structure of the linear operator R shows the 4 by 4 sub-block-structure as we expected from the symmetries of the system (Appendix C).

The linear operator Q given by the Eq.(7.39) has the form

$$Q=\begin{pmatrix}Q_{\Gamma_1} & 0 & 0 & 0\\ 0 & Q_{\Gamma_2} & 0 & 0\\ 0 & 0 & Q_{\Gamma_3} & 0\\ 0 & 0 & 0 & Q_{\Gamma_4}\end{pmatrix}, \tag{F.2}$$

where the 4 sub-blocks are respectively

$$Q_{\Gamma_1}=\begin{pmatrix}\frac{\varepsilon\tau\left(\varepsilon^2-2\lambda^2\right)}{2\varepsilon\tau(\lambda^2-\varepsilon^2)}+1 & -\frac{\lambda\varepsilon^2\tau}{2\lambda^2\varepsilon\tau-2\varepsilon^2\varepsilon\tau} & -\frac{\varepsilon^2}{4\lambda^2\varepsilon\tau-4\varepsilon^2\varepsilon\tau} & \frac{\lambda\varepsilon}{4\lambda^2\varepsilon\tau-4\varepsilon^2\varepsilon\tau}\\ -\frac{\lambda\varepsilon^2\tau}{2\lambda^2\varepsilon\tau-2\varepsilon^2\varepsilon\tau} & \frac{\varepsilon\tau\left(\varepsilon^2-2\lambda^2\right)}{2\varepsilon\tau(\lambda^2-\varepsilon^2)}+1 & -\frac{\varepsilon^3}{4\lambda^3\varepsilon\tau-4\lambda\varepsilon^2\varepsilon\tau} & \frac{\varepsilon^2}{4\lambda^2\varepsilon\tau-4\varepsilon^2\varepsilon\tau}\\ \frac{\varepsilon^2}{4\lambda^2\varepsilon\tau-4\varepsilon^2\varepsilon\tau} & \frac{\varepsilon^3}{4\lambda^3\varepsilon\tau-4\lambda\varepsilon^2\varepsilon\tau} & 1 & 0\\ -\frac{\lambda\varepsilon}{4\lambda^2\varepsilon\tau-4\varepsilon^2\varepsilon\tau} & -\frac{\varepsilon^2}{4\lambda^2\varepsilon\tau-4\varepsilon^2\varepsilon\tau} & 0 & 1\end{pmatrix},$$

$$Q_{\Gamma_2}=\begin{pmatrix}\frac{\varepsilon\tau\left(\varepsilon^2-2\lambda^2\right)}{2\varepsilon\tau(\lambda^2-\varepsilon^2)}+1 & \frac{\lambda\varepsilon^2\tau}{2\lambda^2\varepsilon\tau-2\varepsilon^2\varepsilon\tau} & \frac{\varepsilon^2}{4\lambda^2\varepsilon\tau-4\varepsilon^2\varepsilon\tau} & \frac{\lambda\varepsilon}{4\lambda^2\varepsilon\tau-4\varepsilon^2\varepsilon\tau}\\ \frac{\lambda\varepsilon^2\tau}{2\lambda^2\varepsilon\tau-2\varepsilon^2\varepsilon\tau} & \frac{\varepsilon\tau\left(\varepsilon^2-2\lambda^2\right)}{2\varepsilon\tau(\lambda^2-\varepsilon^2)}+1 & -\frac{\varepsilon^3}{4\lambda^3\varepsilon\tau-4\lambda\varepsilon^2\varepsilon\tau} & -\frac{\varepsilon^2}{4\lambda^2\varepsilon\tau-4\varepsilon^2\varepsilon\tau}\\ -\frac{\varepsilon^2}{4\lambda^2\varepsilon\tau-4\varepsilon^2\varepsilon\tau} & \frac{\varepsilon^3}{4\lambda^3\varepsilon\tau-4\lambda\varepsilon^2\varepsilon\tau} & 1 & 0\\ -\frac{\lambda\varepsilon}{4\lambda^2\varepsilon\tau-4\varepsilon^2\varepsilon\tau} & \frac{\varepsilon^2}{4\lambda^2\varepsilon\tau-4\varepsilon^2\varepsilon\tau} & 0 & 1\end{pmatrix},$$

$$Q_{\Gamma_3}=\begin{pmatrix}1 & 0 & 0 & 0 & \\ 0 & \frac{\varepsilon^3\tau}{8\lambda^2\varepsilon\tau-8\varepsilon^2\varepsilon\tau}+1 & -\frac{\varepsilon^3\tau}{8\lambda^2\varepsilon\tau-8\varepsilon^2\varepsilon\tau} & \frac{\varepsilon}{4\lambda\varepsilon\tau} & 0\\ 0 & -\frac{\varepsilon^3\tau}{8\lambda^2\varepsilon\tau-8\varepsilon^2\varepsilon\tau} & \frac{\varepsilon^3\tau}{8\lambda^2\varepsilon\tau-8\varepsilon^2\varepsilon\tau}+1 & \frac{\varepsilon}{4\lambda\varepsilon\tau} & 0\\ 0 & -\frac{\varepsilon}{4\lambda\varepsilon\tau} & -\frac{\varepsilon}{4\lambda\varepsilon\tau} & 1 & \end{pmatrix},$$

$$Q_{\Gamma_4}=\begin{pmatrix}0 & 0 & 0 & 0\\ 0 & \frac{3\varepsilon^3\tau}{8\lambda^2\varepsilon\tau-8\varepsilon^2\varepsilon\tau}+1 & -\frac{\varepsilon^3\tau}{8\lambda^2\varepsilon\tau-8\varepsilon^2\varepsilon\tau} & -\frac{\lambda\varepsilon^2\tau}{2\lambda^2\varepsilon\tau-2\varepsilon^2\varepsilon\tau}\\ 0 & -\frac{\varepsilon^3\tau}{8\lambda^2\varepsilon\tau-8\varepsilon^2\varepsilon\tau} & \frac{3\varepsilon^3\tau}{8\lambda^2\varepsilon\tau-8\varepsilon^2\varepsilon\tau}+1 & -\frac{\lambda\tau\left(\frac{\lambda\sqrt{k^2+\lambda^2}}{(\lambda-\varepsilon)^2}+\frac{\varepsilon}{\lambda+\varepsilon}+1\right)}{4\varepsilon\tau}\\ 0 & -\frac{\lambda\varepsilon^2\tau}{2\lambda^2\varepsilon\tau-2\varepsilon^2\varepsilon\tau} & \frac{\lambda\varepsilon^2\tau}{2\lambda^2\varepsilon\tau-2\varepsilon^2\varepsilon\tau} & \frac{\lambda^2\varepsilon\tau}{\lambda^2\varepsilon\tau-\varepsilon^2\varepsilon\tau}+1\end{pmatrix}.$$

Of course, the 4 by 4 sub-block-structure in the operator Q is preserved.
In the end, the vector Y from the Eq.(7.37) reads

$$Y = \begin{pmatrix} Y_{\Gamma_1} \\ Y_{\Gamma_2} \\ Y_{\Gamma_3} \\ Y_{\Gamma_4} \end{pmatrix}, \tag{F.3}$$

with the following sub-block elements

$$Y_{\Gamma_1} = \begin{pmatrix} \frac{\varepsilon\tau\left(128\lambda^6\left(2\varepsilon^2\tau^8+\tau^6\right)-64\lambda^4\tau^4\left(6\varepsilon^4\tau^4+2\varepsilon^2\tau^2-1\right)+4\lambda^2\tau^2\left(2\varepsilon^2\tau^2+1\right)\left(16\varepsilon^4\tau^4+3\right)+\left(2\varepsilon^2\tau^2+1\right)\left(4\varepsilon^2\tau^2+1\right)^2\right)}{2(4\lambda^2\tau^2+1)(4\varepsilon^2\tau^2+1)\left(8\tau^2\left(2\tau^2(\lambda^2-\varepsilon^2)^2+\lambda^2+\varepsilon^2\right)+1\right)} \\ \frac{4\lambda^3\varepsilon^2\tau^5\left(4\tau^2(\lambda-\varepsilon)(\lambda+\varepsilon)-3\right)}{4\tau^2\left(16\tau^4(\lambda^3-\lambda\varepsilon^2)^2+4\tau^2(3\lambda^4+\varepsilon^4)+3\lambda^2+2\varepsilon^2\right)+1} \\ \frac{2\lambda^2\varepsilon^2\tau^4\left(3-4\tau^2(\lambda-\varepsilon)(\lambda+\varepsilon)\right)}{4\tau^2\left(16\tau^4(\lambda^3-\lambda\varepsilon^2)^2+4\tau^2(3\lambda^4+\varepsilon^4)+3\lambda^2+2\varepsilon^2\right)+1} \\ \frac{4\lambda^3\varepsilon\left(\tau^6\left(4\lambda^2-6\varepsilon^2\right)+8\varepsilon^2\tau^8(\lambda-\varepsilon)(\lambda+\varepsilon)+\tau^4\right)}{(4\lambda^2\tau^2+1)(4\varepsilon^2\tau^2+1)\left(8\tau^2\left(2\tau^2(\lambda^2-\varepsilon^2)^2+\lambda^2+\varepsilon^2\right)+1\right)} \end{pmatrix},$$

$$Y_{\Gamma_2} = Y_{\Gamma_3} = Y_{\Gamma_4} = \begin{pmatrix} 0 \\ 0 \\ 0 \\ 0 \end{pmatrix}.$$

It is important to stress here that only the first sub-block of the vector Y, i.e. the subspace linked to the Γ_1-group of matrices, has non zero elements. This is a consequence of having chosen the electric field along the $x-$axis. Y_{Γ_1} is the vector of the "bare bubble" that we use in the Section 7.2 to solve the linear system Eq.(7.40).

Bibliography

[1] S. A. Wolf, D. D. Awschalom, R. A. Buhrman, J. M. Daughton, S. von Molnar, M. L. Roukes, A. Y. Chtchelkanova, D. M. Treger. "*Spintronics: A Spin-Based Electronics Vision for the Future*". *Science*, **294**:1488–1495, 2001.

[2] D. D. Awschalom and M. E. Flattè. "*Challenges for semiconductor spintronics*". *Nature Physics*, **3**:153, 2007.

[3] I. Žutić, J. Fabian, and S. Das Sarma. "*Spintronics: Fundamentals and applications*". *Rev. Mod. Phys*, **76**:323, 2004.

[4] G. A. Prinz. *Magnetoelectronics.*, volume **282**. Science, 1998.

[5] D. Kochan, S. Irmer, and J. Fabian. "*Model spin–orbit coupling Hamiltonians for graphene systems*". *Phys.Rev. B*, **95**:165415, 2017.

[6] M. N. Baibich, J. M. Broto, A. Fert, F. Nguyen Van Dau, F. Petroff, P. Etienne, G. Creuzet, A. Friederich, and J. Chazelas. "*Giant Magnetoresistance of (001)Fe/(001)Cr Magnetic Superlattices*". *Phys. Rev. Lett.*, **61**:2472, 1988.

[7] G. Binasch, P. Grunberg, F. Saurenbach, and W. Zinn. "*Enhanced magnetoresistence in layered magnetic structures with antiferromagnetic interlayer exchange*". *Phys. Rev. B.*, **39**:4828(R), 1989.

[8] E. Y. Tsymbal and D. G. Pettifor. "*Perspectives of Giant Magnetoresistance*". *Solid State Physics*, **56**:113–237, 2001.

[9] S. Yuasa, T. Nagahama, A. Fukushima, Y. Suzuki, and K. Ando. "*Giant room-temperature magnetoresistance in single-crystal Fe/MgO/Fe magnetic tunnel junctions*". *Nature Materials*, **3**:868–871, 2004.

[10] D.D. Djayaprawiraa, K. Tsunekawa, M. Nagai, H. Maehara, S. Yamagata, N. Watanabe, S. Yuasa, T. Suzuki, and K. Ando. "*230% room-temperature magnetoresistance in CoFeB/MgO/CoFeB magnetic tunnel junctions*". *Appl. Phys. Lett.*, **86**:092502, 2005.

[11] J. C. Sankey, Y. T. Cui, J. Z. Sun, J. C. Slonczewski, R. A. Buhrman, and Daniel C. Ralph. "*Measurement of the spin-transfer-torque vector in magnetic tunnel junctions*". *Nature Physics*, **4**:67–71, 2008.

[12] Z. Diao, Z. Li, S. Wang, Y. Ding, A. Panchula, E. Chen, L. C. Wang, and Y. Huai. "*Spin-transfer torque switching in magnetic tunnel junctions and spin-transfer torque random access memory*". *Journal of Physics Condensed Matter*, **19**:16, 2007.

[13] P. Upadhyaya. *"Spin-orbitronics: Electrical control of magnets via spin- orbit interaction"*. PhD Thesis, California Digital Library, University of California, 2015.

[14] E. Chen, D. Apalkov, Z. Diao, A. Driskill-Smith, D. Druist, D. Lottis, V. Nikitin, X. Tang, S. Watts, S. Wang, S. A. Wolf, A. W. Ghosh, J. W. Lu, S. J. Poon, M. Stan, W. H. Butler, S. Gupta, C. K. Mewes, T. Mewes, , and P. B. Visscher. "*Advances and Future Prospects of Spin-Transfer Torque Random Access Memory*". *IEEE Transactions on Magnetics*, **46**:6, 2010.

[15] Manuel Offidani. *"PhD Thesis: Coupled Charge-Spin Transport and Spin–Orbit Phenomena in 2D Dirac Materials"*. University of York, Department of Physics, 2018.

[16] A.H. Compton. "*The magnetic electron*". **192**:145, 1921.

[17] J. Schwinger. "*On Quantum-Electrodynamics and the Magnetic Moment of the Electron*". *Phys. Rev.*, **73**:416, 1948.

[18] M. I. Dyakonov, and V. I. Perel. "*Possibility of Orienting Electron Spins with Current*". *Soviet Journal of Experimental and Theoretical Physics Letters*, **13**:467, 1971.

[19] M. I. Dyakonov, and V. I. Perel. "*Current-induced spin orientation of electrons in semiconductors*". *Phys. Lett. A*, **35**:459, 1971.

[20] J. E. Hirsch. "*Spin Hall Effect*". *Phys. Rev. Lett.*, **83**:9, 1999.

[21] S. Murakami, N. Nagaosa, and S. C. Zhang. "*Dissipationless quantum spin current at room temperature*". *Science*, **301**:1348, 2003.

[22] J. Sinova, D. Culcer, Q. Niu, N. A. Sinitsyn, T. Jungwirth, and A. H. Mac Donald. "*Universal intrinsic spin Hall effect*". *Phys. Rev. Lett.*, **92**:126603, 2004.

[23] E. Hall. "*On a New Action of the Magnet on Electric Currents*". *American J. of Mathematics*, **2**:287–292, 1879.

[24] N. F. Mott. "*The scattering of fast electrons by atomic nuclei*". *Proceeding of the Royal Society A*, **124**:794, 1929.

[25] Y. K. Kato, R. C. Myers, A. C. Gossard, and D. D. Awschalom. "*Observation of the Spin Hall effect in Semiconductors*". *Science*, **306**:1910, 2004.

[26] J. Wunderlich, B. Kaestner, J. Sinova, and T. Jungwirth. "*Experimental Observation of the Spin- Hall Effect in a Two-Dimensional Spin-Orbit Coupled Semiconductor System*". *Phys. Rev. Lett.*, **94**:047204, 2005.

[27] J. Wunderlich, B. Kaestner, J. Sinova, and T. Jungwirth. "*Reciprocal Relations in Irreversible Processes*". *Phys. Rev.*, **37**:405–426, 1931.

[28] E. Saitoh, M. Ueda, H. Miyajima, and G. Tatara. "*Conversion of spin current into charge current at room temperature: Inverse spin-Hall effect*". *Appl. Phys. Lett.*, **88**:182509, 2006.

[29] S. O. Valenzuela and M. Tinkham. "*Direct electronic measurement of the spin Hall effect*". *Nature*, **442**:176, 2006.

[30] E. Saitoh, M. Ueda, H. Miyajima, and G. Tatara. "*Coherence Control of Hall Charge and Spin Currents*". *Phys. Rev. Lett.*, **96**:246601, 2006.

[31] C.Herschbach, D. V. Fedorov, I. Mertig, M. Gradhand, K. Chadova, H. Ebert, and D. Ködderitzsch. "*Insight into the skew-scattering mechanism of the spin Hall effect: Potential scattering versus spin-orbit scattering*". *Phys. Rev. B*, **88**:205102, 2013.

[32] M. Gradhand, D. V. Fedorov, P. Zahn and I. Mertig. "*Skew Scattering Mechanism by an Ab Initio Approach: Extrinsic Spin Hall Effect in Noble Metals*". *Solid State Phenomena*, **88**:168–169, 2010.

[33] J. Schwinger. "*Brownian motion of a quantum particle*". *J. Math. Phys.*, **2**:407, 1961.

[34] E. Ivchenko, and G. Pikus. "*New photogalvanic effect in gyrotropic crystals*". *Soviet Journal of Experimental and Theoretical Physics Letters*, **27**:604–608, 1978.

[35] L. E. Vorobev, E. L. Ivchenko, G. E. Pikus, I. I. Farbshtein, V. A. Shalygin and V. A. Shturbin. "*Optical activity in tellurium induced by a current*". *Soviet Journal of Experimental and Theoretical Physics Letters*, **29**:441, 1979.

[36] A. Aronov, and Y. B. Lyanda-Geller. "*Nuclear electric resonance and orientation of carrier spins by an electric field*". *Soviet Journal of Experimental and Theoretical Physics Letters*, **50**:431, 1989.

[37] V. Edelstein. "*Spin polarization of conduction electrons induced by electric current in two- dimensional asymmetric electron systems*". *Solid State Communications*, **73**:3, 1990.

[38] S. D. Ganichev, E. L. Ivchenko, V. V. Belkov, S. A. Tarasenko, M. Sollinger, D. Weiss, W. Wegscheider and W. Prettl. "*Spin-galvanic effect*". *Nature*, **417**:153–156, 2002.

[39] A. Maleki, and R. Raimondi. "*Inverse spin galvanic effect in the presence of impurity spin-orbit scattering: a diagrammatic approach*". *MDPI Condensed Matter*, **2**:17, 2017.

[40] Th. Sch$\ddot{a}$pers. *"Virtual Institue of Topological Insulators"*. Forschungszentrum J$\ddot{u}$lich.

[41] M. Z. Hasan, C. L. Kane. "*Topological Insulators*". *Rev. Mod. Phys.*, **82**:3045, 2010.

[42] J. C. Rojas-Sánchez, S. Oyarzun, Y. Fu, A. Marty, C. Vergnaud, S. Gambarelli, L. Vila, M. Jamet, Y. Ohtsubo, A. Taleb-Ibrahimi, P. Le Fèvre, F. Bertran, N. Reyren, J. M. George, A. Fert. "*Spin-pumping into surface states of topological insulator α-Sn, spin to charge conversion at room temperature*". *Phys. Rev. Lett.*, **116**:096602, 2016.

[43] C. L. Kane and E. J. Mele. "*Quantum Spin Hall Effect in Graphene*". *Phys.Rev. Lett.*, **95**:226801, 2005.

[44] J. E. Moore . "*The birth of topological insulators*". *Nature*, **464**:7286, 2010.

[45] M. Z. Hasan and J. E. Moore. "*Three-Dimensional Topological Insulators*". *Annual Review of Condensed Matter Physics*, **2**:55–78, 2011.

[46] Liang Fu and C. L. Kane. "*Topological insulators with inversion symmetry*". *Phys. Rev. B*, **76**:045302, 2007.

[47] A. Soumyanarayanan, N. Reyren, A. Fert, and C. Panagopoulos. "*Emergent phenomena induced by spin– orbit coupling at surfaces and interfaces*". *Nature*, **539**:509–517, 2016.

[48] M. Heide, G. Bihlmayer, and S. Blugel. "*Dzyaloshinskii–Moriya interaction accounting for the orientation of magnetic domains in ultrathin films: Fe/W(110)*". *Phys. Rev. B*, **78**:140403, 2008.

[49] N. Nagaosa, and Y. Tokura. "*Topological properties and dynamics of magnetic skyrmions*". *Nature Nanotechnology*, **8**:899–911, 2013.

[50] Z. Qiao, H. Jiang, X. Li, Y. Yao and Q. Niu. "*Microscopic theory of quantum anomalous Hall effect in graphene*". *Phys. Rev. B*, **85**:115439, 2013.

[51] M. Offidani, and A. Ferreira. "*Anomalous Hall Effect in 2D Dirac Materials*". *Phys. Rev. Lett.*, **121**:126802, 2018.

[52] N. D. Mermin. "*Crystalline order in two dimensions*". *Phys. Rev.*, **176**:250–254, 1968.

[53] A. J Huh, and Y. J. Kwon. "*Nanoantibiotics": A new paradigm for treating infectious diseases using nanomaterials in the antibiotics resistant era*". *Journal of Controlled Release*, **156**:2, 2011.

[54] A. Schindler, J. Brill, N. Fruehauf, J. P. Novak, Z. Yaniv. "*Solution-deposited carbon nanotube layers for flexible display applications*". *Physica E*, **37**:119–123, 2007.

[55] Y. Kim, S. Cook, S. M. Tuladhar, S. A. Choulis, J. Nelsnon, J. R. Durrant, D. D. C. Bradley M. Giles, I. McCulloch, C. Ha and, M. Ree. "*A strong regioregularity effect in self-organizing conjugated polymer films and high-efficiency polythiophene: fullerene solar cells*". *Nature Materials*, **5**:197–2013, 2006.

[56] K. S. Novoselov, A. K. Geim, S. V. Morozov, D. Jiang, Y. Zhang, S. V. Dubonos, I. V. Grigorieva, and A. A. Firsov. "*Electric field effect in atomically thin carbon films*". *Science*, **306**:666–669, 2004.

[57] R. Mas-Balleste, C. Gomez-Navarro, J. Gomez-Herrero, and F. Zamora. "*D materials: to graphene and beyond*". *Nanoscale*, **3**:20, 2011.

[58] J. N. Coleman, M. Lotya, A. O'Neill, S. D. Bergin, P. J. King, U. Khan, K. Young, A. Gaucher, S. De, R. J. Smith, I. V. Shvets, K. Arora, G. Stanton, H.-Y. Kim, K. Lee, G. T. Kim, G. S. Duesberg, T. Hallam, J. J. Boland, J. J. Wang, J. F. Donegan, J. C. Grunlan, G. Moriarty, A. Shmeliov, R. J. Nicholls, J. M. Perkins, E. M. Grieveson, K. Theuwissen, D. W. McComb, P. D. Nellist, and V. Nicolosi. "*Two-Dimensional Nanosheets Produced by Liquid Exfoliation of Layered Materials*". *Science*, **331**:568–571, 2011.

[59] V. Nicolosi, M. Chhowalla, M. G. Kanatzidis, M. S. Strano, and J. N. Coleman. "*Liquid exfoliation of layered materials*". *Science*, **340**:1226419, 2013.

[60] P. Mirò, M. Audiffred, and T. Heine. "*An atlas of two-dimensional materials*". *Chem. Soc. Rev.*, **43**:6537, 2014.

[61] Y. Zhang, L. Zhang, and C. Zhou. "*Review of Chemical Vapor Deposition of Graphene and Related Applications*". *Acc. Chem. Res.*, **46**:2329–2339, 2013.

[62] Wei Han, K. Pi, K. M. McCreary, Yan Li, Jared J. I. Wong, A. G. Swartz, and R. K. Kawakami. "*Tunneling Spin Injection into Single Layer Graphene*". *Phys. Rev. Lett.*, **105**:167202, 2010.

[63] Wei Han and R. K. Kawakami. "*Spin Relaxation in Single-Layer and Bilayer Graphene*". *Phys. Rev. Lett.*, **107**:047207, 2011.

[64] Nikolaos Tombros, Csaba Jozsa, Mihaita Popinciuc, Harry T. Jonkman and Bart J. van Wees . "*Electronic spin transport and spin precession in single graphene layers at room temperature*". *Nature*, **448**:571–574, 2006.

[65] Wei Han, Roland K. Kawakami, Martin Gmitra and Jaroslav Fabian . "*Graphene spintronics*". *Nature Nanotechnology*, **9**:794–807, 2014.

[66] Dmytro Pesin and Allan H. MacDonald. "*Spintronics and pseudospintronics in graphene and topological insulators*". *Nature Materials*, **11**:409–416, 2012.

[67] Pedram Roushan, Jungpil Seo, Colin V. Parker, Y. S. Hor, D. Hsieh, Dong Qian, Anthony Richardella, M. Z. Hasan, R. J. Cava and Ali Yazdani. "*Topological surface states protected from backscattering by chiral spin texture*". *Nature*, **460**:1106–1109, 2009.

[68] Wang-Kong Tse, Zhenhua Qiao, Yugui Yao, A. H. MacDonald, and Qian Niu. "*Quantum anomalous Hall effect in single-layer and bilayer graphene*". *Phys. Rev. B*, **83**:155447, 2011.

[69] WA. Geim, and I. Grigorieva. "*Van der Waals heterostructures*". *Nature*, **499**:419–425, 2013.

[70] K. S. Novoselov, A. Mischenko, A. Carvalho, and A. H. Castro Neto. "*2D materials and van der Waals heterostructures*". *Science*, **353**:6298, 2016.

[71] M. Yankowitz, J. Xue, D. Cormode, J. D. Sanchez-Yamagishi, K. Watanabe, T. Taniguchi, P. Jarillo-Herrero, P. Jacquod, and B. J. LeRoy. "*Emergence of superlattice Dirac points in graphene on hexagonal boron nitride*". *Nature Physics*, **8**:382–386, 2012.

[72] C. R. Woods, L. Britnell, A. Eckmann, R. S. Ma, J. C. Lu, H. M. Guo, X. Lin, G. L. Yu, Y. Cao, R. V. Gorbachev, A. V. Kretinin, J. Park, L. A. Ponomarenko, M. I. Katsnelson, Yu. N. Gornostyrev, K. Watanabe, T. Taniguchi, C. Casiraghi, H-J. Gao, A. K. Geim, and K. S. Novoselov. "*Commensurate-incommensurate transition in graphene on hexagonal boron nitride*". *Nature Physics*, **10**:451–456, 2014.

[73] B. Hunt, J. D. Sanchez-Yamagishi, , A. F. Young, , M. Yankowitz, B. J. LeRoy, K. Watanabe, T. Taniguchi, P. Moon, M. Koshino, P. Jarillo-Herrero, and R. C. Ashoori. "*Massive Dirac Fermions and Hofstadter Butterfly in a van der Waals Heterostructure*". *Science*, **340**:6139, 2013.

[74] T. Kuschel, and G. Reiss. "*Spin orbitronics: Charges ride the spin wave*". *Nature Nanotech.*, **10**:22–24, 2015.

[75] K. Roy, M. Padmanabhan, S. Goswami, T. P. Sai, G. Ramalingam, S. Raghavan, A. Ghosh. "*Graphene–MoS2 hybrid structures for multifunctional photoresponsive memory devices*". *Nature Nanotech.*, **8**:826–830, 2013.

[76] M. Gmitra, and J. Fabian. "*Graphene on transition-metal dichalcogenides: A platform for proxim- ity spin-orbit physics and optospintronics*". *Phys. Rev. B*, **92**:155403, 2015.

[77] Y. K. Luo, J. Xu, T. Zhu, G. Wu, E. J. McCormick, W. Zhan, M. R. Neupane and R. K. Kawakam. "*Opto-Valleytronic Spin Injection in Monolayer MoS2/Few-Layer Graphene Hybrid SpinValves*". *Nano Lett.*, **17**:3877, 2013.

[78] H. Fang, C. Battaglia, C. Carraro, S. Nemsak, B. Ozdol, J. S. Kang, H. A. Bechtel, S. B. Desai, F. Kronast, A. A. Unal, G. Conti, C. Conlon, G. K. Palsson, M. C. Martin, A. M. Minor, C. S. Fadley, E. Yablonovitch, R. Maboudian, and A. Javey. "*GStrong interlayer coupling in van der Waals heterostructures built from single-layer chalcogenides*". *PNAS*, **111**:6198–6202, 2014.

[79] V. W. Brar, M. S. Jang, M. Sherrott, S. Kim, J. J. Lopez, L. B. Kim, M. Choi, H. Atwater. "*Hybrid surface-phonon-plasmon polariton modes in graphene/monolayer h-BN heterostructures*". *ACS Nano Lett.*, **14**:3876–3880, 2014.

[80] Z. Qiao, S. A. Yang, W. Feng, W. K. Tse, J. Ding, Y. Yao, J. Wang, and Q. Niu. "*Quantum anomalous Hall effect in graphene from Rashba and exchange effects*". *Phys. Rev. B*, **82**:161414(R), 2010.

[81] A. H. Castro Neto, and F. Guinea. "*Impurity-induced spin–orbit coupling in graphene*". *Phys. Rev. Lett.*, **103**:026804, 2009.

[82] U. Chandni, E. A. Henriksen, and J. P. Eisenstein. "*Transport in indium-decorated graphene*". *Phys. Rev. B.*, **91**:245402, 2015.

[83] Y. Wang, S. Xiao, X. Cai, W. Bao, J. R. Robey, and M. S. Fuhrer. "*Electronic transport properties of Ir-decorated graphene*". *Scientific Rep.*, **5**:15764, 2015.

[84] Z. Jia, B. Yan, J. Niu, Q. Han, R. Zhu, D. Yu, and X. Wu. "*Transport study of graphene adsorbed with indium adatoms*". *Phys. Rev. B*, **91**:085411, 2015.

[85] Y. Wang, X. Cai, J. Reutt-Robey, and M. S. Fuhrer. "*Neutral-current Hall effects in disordered graphene*". *Phys. Rev. B*, **92**:161411(R), 2015.

[86] J. A. Elias, and E. A. Henriksen. "*Electronic transport and scattering times in tungsten-decorated graphene*". *Phys. Rev. B*, **95**:075405, 2017.

[87] M. Chhowalla, H. S. Shin, G. Eda, L. Li, K. Ping, and H. Zhang. "*The chemistry of two- dimensional layered transition metal dichalcogenide nanosheets*". *Nature Chem.*, **5**:263–275, 2013.

[88] S. Manzeli, D. Ovchinnikov, D. Pasquier, O. V. Yazyev, and A. Kis. "*2D transition metal dichalcogenides*". *Nature Rev. Mat.*, **2**:17033, 2017.

[89] L. Ruitao, J. A. Robinson, R. E. Schaak, D. Sun, Y. Sun, T. E. Mallouk, and M. Terrones. "*Transition Metal Dichalcogenides and Beyond: Synthesis, Properties, and Applications of Single- and Few-Layer Nanosheets*". *Accounts of Chem. Research*, **48**:1, 2014.

[90] Q. Li, L. Tang, C. Zhang, D. Wang, Q. Chen, Y. Feng, L. Tang, and K. Chen. "*Seeking the Diraccones in the MoS2/WSe2 van der Waals heterostructure*". *Appl. Phys. Lett.*, **111**:171602, 2017.

[91] J. H. Garcia, M. Vila, A. W. Cummings and Stephan Roche. "*Spin transport in graphene/transitionmetal dichalcogenide heterostructures*". *Chemical Society Reviews*, **47**:3359, 2017.

[92] T. Völkl,T. Rockinger, M. Drienovsky, K. Watanabe, T. Taniguchi, D. Weiss and J. Eroms. "*Magnetotransport in heterostructures of transition metal dichalcogenides and graphene*". *Phys. Rev. B*, **96**:125405, 2013.

[93] J. Fabian. "*Proximity physics in graphene: spin-orbit coupling,exchange, field effects, and pseudohelical states*". *APS - March Meeting*, 2018.

[94] C. Tang, B. Cheng, M. Aldosary, Z. Wang, Z. Jiang, K. Watanabe, T. Taniguchi, M. Bockrath and J. Shi. "*Approaching quantum anomalous Hall effect in proximity-coupled YIG/graphene/h-BN sandwich structure*". *APL Materials*, **6**:026401, 2018.

[95] M. Ben Shalom, M. J. Zhu, V. I. Falko, A. Mishchenko, A. V. Kretinin, K. S. Novoselov, C. R. Woods, K. Watanabe, T. Taniguchi, A. K. Geim, and J. R. Prance. "*Quantum oscillations of the critical current and high-field superconducting proximity in ballistic graphene*". *APL Materials*, **12**:318–322, 2016.

[96] L. A. Benítez, W. S. Torres, J. F. Sierra, M. Timmermans, J. H. Garcia, S. Roche, M. V. Costache and S. O. Valenzuela . "*Tunable room-temperature spin galvanic and spin Hall effects in van der Waals heterostructures*". *Nature Materials*, **19**:170–175, 2020.

[97] J. Rammer. *Quantum Field Theory of Non-equilibrium States.* Cambridge University Press, 2007.

[98] J. Rammer and H. Smith. "*Quantum field-theoretical methods in transport theory of metals*". *Rev. Mod. Phys.*, **58**:323, 1986.

[99] P. Schwab and R. Raimondi. "*Quasiclassical theory of charge transport in disordered interacting electron systems*". *Ann. Phys.*, **12**:471, 2003.

[100] J. Rammer. *Quantum Transport Theory.* Perseus Books, 1998.

[101] A. Kamenev. "*Keldysh technique and nonlinear σ-model: basic principles and applications*". *arXiv:cond-mat.s/0901.3586*, 2009.

[102] E. Calzetta and B. I. Hu. "*Closed-time-path functional formalism in curved spacetime: application to cosmological back-reaction problems*". *Phys. Rev. D*, **35**:495, 1994.

[103] A. J. Niemi and G. W. Semenoff. *Nonequilibrium problems in quantum field theory and Schwinger's closed time path formalism.* arXiv:hep-th/9504073, 1995.

[104] D. Culcer, Y. Yao, and Q. Niu. "*Coherent wave-packet evolution in coupled bands*". *Phys. Rev. B*, **72**:085110, 2005.

[105] N. A. Sinitsyn, A. H. MacDonald, T. Jungwirth, V. K. Dugaev and Jairo Sinova. "*Anomalous Hall effect in a two-dimensional Dirac band: The link between the Kubo-Streda formula and the semiclassical Boltzmann equation approach*". *Phys. Rev. B*, **75**:045315, 2007.

[106] H. J. W. Haug, and A. P. Jahuo. *"Quantum Kinetics in Transport and Optics of Semiconductors - 2nd Edition."*. Springer-Verlag Berlin Heidelberg., 2008.

[107] J. M. Ziman. *Principles of the Theory of Solids.* Cambridge University Press., 1972.

[108] E. Fermi. *Nuclear Physics.* University of Chicago Press ISBN 978-0226243658., 1950.

[109] E. Adams, and E. Blount. "*Energy bands in the presence of an external force field*". *J. Phys. Chem. Solids*, **10**:286, 1959.

[110] N. A. Sinitsyn, Q. Niu, J. Sinova, and Kentaro Nomura. "*Disorder effects in the anomalous Hall effect induced by Berry curvature*". *Phys. Rev. B*, **72**:045346, 2005.

[111] N. A. Sinitsyn, Q. Niu, and A. H. MacDonald. "*Coordinate shift in the semiclassical Boltzmann equation and the anomalous Hall effect*". *Phys. Rev. B*, **73**:075318, 2006.

[112] N.D. Mermin. "*Lindhard Dielectric Function in the Relaxation-Time Approximation*". *Phys. Rev. B*, **1**:2362, 1970.

[113] R. Kragler and H. Thomas. "*Dielectric Function in the Relaxation-Time Approximation Generalized to Electronic Multiple-Band Systems*". *Z. Phys. B*, **39**:99, 1980.

[114] C. Huang, Y. D. Chong, G. Vignale, and M. A. Cazalilla. "*Graphene electrodynamics in the presence of the extrinsic spin Hall effect*". *Phys. Rev. B*, **93**:165429, 2016.

[115] R.Kubo. "*Statistical-Mechanical Theory of Irreversible Processes. I. General Theory and Simple Applications to Magnetic and Conduction Problems*". *Journal of Japanese Phys. Soc.*, **12**:570–586, 1957.

[116] G. D. Mahan. *Many-particle physics.* Springer Science & Business Media., 2013.

[117] P. Streda. "*Theory of quantised Hall conductivity in two dimensions*". *J.P.C.*, **15**:L717, 1982.

[118] A. Crépieux and P. Bruno. "*Theory of the anomalous Hall effect from the Kubo formula and the Dirac equation*". *Phys. Rev. B*, **64**:014416, 2001.

[119] L. V. Keldysh. "*Diagram technique for nonequilibrium processes*". *JETP*, **20**:1018, 1965.

[120] Ashok Das. "*Topics in Finite Temperature Field Theory*". *arXiv:hep-ph/0004125*, 2000.

[121] L. D. Landau and E. M. Lifshitz. *Course of theoretical physics - Volume 9, Statistical Physics (Part 2).* Pergamon International Library of Science, Technology, Engineering and Social Studies - Robert Maxwell, M. C., 1980.

[122] A.I.Larkin and Yu.N.Ovchinnnikov. "*Non linear conductivity of superconductors in the mixed state". JETP*, **41**:960, 1975.

[123] Y. A. Bychkov, and E. I. Rashba. "*Properties of a 2D electron gas with lifted spectral degeneracy*". *Soviet Journal of Experimental and Theoretical Physics Letters*, **39**:71, 1984.

[124] R. Raimondi, C. Gorini and S. Tölle. "*Spin-charge coupling effects in a two-dimensional electron gas*". *arXiv:1611.07210v1*, 2016.

[125] G. Eilenberger . "*Transformation of Gorkov's equation for type II superconductors into transport-like equations*". *EPL*, **214**:195–213, 1968.

[126] L. P. Kadanoff and G. Baym. *Green's Function Methods in Equilibrium and Nonequilibrium Problems.* Addison-Wesley Publishing Co., 1962.

[127] M. Offidani, M. Milletarì, R. Raimondi and A. Ferreira. "*Covariant Conservation Laws and Spin Hall Effect in Dirac-Rashba Systems*". *Phys. Rev. Lett.*, **119**:246801, 2017.

[128] M. Offidani, M. Milletarì, R. Raimondi and A. Ferreira. "*Optimal Charge-to-Spin Conversion in Graphene on Transition-Metal Dichalcogenide*". *Phys. Rev. Lett.*, **119**:196801, 2017.

[129] P. Schwab, R. Raimondi, and C. Gorini. "*Spin-charge locking and tunneling into a helical metal*". *EPL*, **93**:67004, 2011.

[130] D. Hsieh, Y. Xia, D. Qian, L. Wray, J. H. Dil, F. Meier, J. Osterwalder, L. Patthey, J. G. Checkelsky, N. P. Ong, A. V. Fedorov, H. Lin, A. Bansil, D. Grauer, Y. S. Hor, R. J. Cava, and M. Z. Hasan. "*A tunable topological insulator in the spin helical Dirac transport regime*". *Nature*, **460**:1101, 2009.

[131] M. Gmitra, D. Kochan, P. Hogl, and J. Fabian. "*Trivial and inverted Dirac bands and the emergence of quantum spin Hall states in graphene on transition-metal dichalcogenides*". *Phys.Rev. B*, **93**:155104, 2016.

[132] Manuel Offidani and Aires Ferreira. "*Microscopic theory of spin relaxation anisotropy in graphene with proximity-induced spin-orbit coupling*". *Phys.Rev. B*, **98**:245408, 2018.

[133] Tarik P. Cysne, Aires Ferreira, and Tatiana G. Rappoport. "*Crystal-field effects in graphene with interface-induced spin-orbit coupling*". *Phys.Rev. B*, **98**:045407, 2018.

[134] I. A. Ado, I. A. Dmitriev, P. M. Ostrovsky, and M. Titov. "*Anomalous Hall effect with massive Dirac fermions*". *EPL*, **111**:3, 2015.

[135] Carlo Cercignani. *The Linearized Boltzmann Equation.* Mathematical Methods in Kinetic Theory, 1969.

[136] G. Seibold, S. Caprara, M. Grilli and R. Raimondi. "*Intrinsic spin Hall effect in systems with striped spin-orbit coupling*". *EPL*, **112**:17004, 2015.

[137] A. Dyrdal, V. K. Dugaev, and J. Barnas. "*Spin Hall effect in a system of Dirac fermions in the honeycomb lattice with intrinsic and Rashba spin-orbit interaction*". *Phys. Rev. B*, **80**:155444, 2009.

[138] Ol'ga V. Dimitrova. "*Spin-Hall conductivity in a two-dimensional Rashba electron gas*". *Phys. Rev. B*, **71**:245327, 2005.

[139] J. Inoue, Gerrit E. W. Bauer, and Laurens W. Molenkamp. "*Suppression of the persistent spin Hall current by defect scattering*". *Phys. Rev. B*, **70**:041303(R), 2004.

[140] E. G. Mishchenko, A. V. Shytov, and B. I. Halperin. "*Spin Current and Polarization in Impure Two-Dimensional Electron Systems with Spin-Orbit Coupling*". *Phys. Rev. Lett.*, **93**:226602, 2004.

[141] Roberto Raimondi and Peter Schwab. "*Spin-Hall effect in a disordered two-dimensional electron system*". *Phys. Rev. B.*, **71**:033311, 2005.

[142] P. Streda. "*Quantised Hall effect in a two-dimensional periodic potential*". *J.P.C.*, **15**:L1299, 1982.

[143] M. Milletarì, and A. Ferreira. "*Quantum Diagrammatic Theory of the Extrinsic Spin Hall Effect in Graphene*". *Phys. Rev. B*, **94**:134202, 2016.

[144] Walter Tarantino, Pina Romaniello, J. A. Berger, and Lucia Reining. "*The self-consistent Dyson equation and self-energy functionals: failure or new opportunities?*". *Phys. Rev. B.*, **96**:045124, 2017.

[145] Joel L. Lebowitz. "*Mathematical methods in solid state and superfluid theory*". *25 Years of Non-Equilibrium Statistical Mechanics, Springer*, **442**:1–20, 1995.

[146] E. McCann, K. Kechedzhi, Vladimir I. Fal'ko, H. Suzuura, T. Ando, and B. L. Altshuler. "*Weak-Localization Magnetoresistance and Valley Symmetry in Graphene*". *Phys. Rev. Lett.*, **97**:146805, 2006.

[147] P. M. Ostrovsky, I. V. Gornyi, and A. D. Mirlin. "*Electron transport in disordered graphene*". *Phys. Rev. B.*, **74**:235443, 2006.

[148] A. H. Castro Neto, F. Guinea, N. M. R. Peres, K. S. Novoselov, and A. K. Geim. "*The electronic properties of graphene*". *Phys. Mod. Phys.*, **81**:109, 2009.

[149] N. H. Shon and T. Ando. "*Quantum Transport in Two-Dymensional Graphite System*". *Journal of Physical Society of Japan*, **67**:7, 1998.

[150] T. Ando. "*Anomaly of Optical Phonon in Monolayer Graphene*". *Journal of Physical Society of Japan*, **75**:12, 2006.

[151] C. Kittel. *Solid State Physics.* Hoboken, NJ: John Wiley and Sons, Inc., 1996.

[152] R. Saito, G. Dresselhaus, and M. S. Dresselhaus. *Physical Properties of Carbon Nanotubes*. London: Imperial College Press, 1998.

[153] J.M. Luttinger. "*Mathematical methods in solid state and superfluid theory*". *Oliver and Boyd, Edinburgh*, **214**:157, 1968.

[154] A. Bastin, C. Lewiner, O. Betbeder-Matibet, and P. Nozières. "*Quantum oscillations of the hall effect of a fermion gas with random impurity scattering*". *J. Phys. Chem. Solids*, **32**:1811–1824, 1971.